FISCHER TROPSCH SYNTHESIS OVER SUPPORTED COBALT CATALYSTS: EFFECT OF ETHANOL ADDITION, PRECURSORS AND GOLD DOPING

Kalala Jalama

A thesis submitted to the Faculty of Engineering and the Built Environment, University of the Witwatersrand, Johannesburg, in fulfilment of the requirements for the degree of Doctor of Philosophy.

Johannesburg, 2007

DECLARATION

I declare that this thesis is my own, unaided work. It is being submitted to the Degree of Doctor of Philosophy to the University of the Witwatersrand, Johannesburg. It has not been submitted before for any degree or examination to any other University.

_____

(Signature of candidate)

27th day of July 2007

ABSTRACT

The effect of the addition of ethanol (2% and 6%) during the Fischer-Tröpsch (FT) synthesis has been investigated using a 10%Co/TiO_2 catalyst in a stirred basket reactor (T = 220°C, P = 8 bar, H_2/CO = 2). The transformation of ethanol vapour (2% and 6% in nitrogen) over the Co/TiO_2 catalyst was also studied in the absence of the synthesis gas under FT reaction conditions. Ethanol was observed to be incorporated in the growing chain and was found to (i) increase the selectivity to light products, (ii) increase the olefin to paraffin ratio and (iii) significantly decrease the catalyst activity. These effects were almost completely reversed when the ethanol in the feed was removed. Thermodynamic predictions, TPR and XRD analysis have shown that cobalt metal particles were oxidised to CoO by ethanol but that re-reduction to Co metal was possible when ethanol was removed from the feed stream allowing the catalyst to recover most of its initial performance, in particular when high flow rates were used.

The effect of the cobalt carboxylate chain length (C2, C5 and C9) used in the preparation of alumina supported cobalt catalysts has been studied by TPR, XRD and hydrogen chemisorption techniques. The activity and selectivity of the prepared catalysts have been evaluated for the Fischer-Tröpsch (FT) reaction in a stirred basket reactor. It is shown that for catalysts with Co content of 10 wt.% the activity increases as the carboxylate chain length increases while the selectivity towards methane and

light hydrocarbons decreases with the carboxylate chain length. The catalyst prepared using cobalt acetate was found to present the highest metal-support interaction and the poorest performance for the Fischer-Tröpsch reaction. When the metal content was increased to 15 wt.% Co and 20 wt.% Co respectively, the metal-support interaction for the catalyst prepared from cobalt acetate significantly decreased making it a better catalyst for the FT reaction compared to the catalysts prepared from C5 and C9 cobalt carboxylates.

The effect of the addition of Au to a Co FT catalyst supported on titania, alumina and silica respectively, has been investigated by varying the amount of Au (0.2 to 5 wt.%) added to the catalyst. The catalysts were characterized by atomic absorption spectroscopy, XRD, XPS and TPR analysis. The catalyst evaluation for the Fischer-Tröpsch reaction activity and selectivity was achieved in a fixed bed micro-reactor (H_2:CO = 2; 20 bar; 220°C). Addition of Au to supported Co catalysts improved the catalyst reduction and the cobalt dispersion on the catalyst surface. The catalyst activity for the FT reaction and the methane and light product selectivity increased with Au loading in the catalyst.

To my parents, my wife and my children

ACKNOWLEDGEMENTS

I wish to express my deep gratitude to the following for their various contributions:

My supervisors, Prof. Diane Hildebrandt, Prof. Neil J. Coville and Prof. David Glasser for their guidance and enthusiasm;

Dr Linda L. Jewell for her assistance and co-supervision;

Prof Graham J. Hutchings for guidance and supervision during my work in his research group at Cardiff University, Wales, UK;

Basil Chassoulas for technical support in the laboratory;

Dr Albert Carley and Dr Stuart Taylor at Cardiff University for assistance with the XPS studies;

My colleagues in the Catalysis, Organo-metallic and Ceramic (CATOMCER) group and the Centre of Materials and Process Synthesis (COMPS) group for creating a supportive and friendly working environment;

My wife, Guyguy Haliyamtu Kalala and my son Manel Kalambay Kalala for their support during the project;

The National Research Foundation (NRF), the DST/NRF Centre of Excellence in Catalysis and the Molecular Sciences Institute, the Centre of Materials and Process Synthesis (COMPS), the Canon Collins Trust and the University of the Witwatersrand for financial support.

PUBLICATIONS

1 Kalala Jalama, Neil J. Coville, Diane Hildebrandt, David Glasser, Linda L. Jewell, Fischer-Tröpsch synthesis over Co/TiO_2: Effect of ethanol addition, *Fuel* 86 (2007) 73.

2 Kalala Jalama, Diane Hildebrandt, David Glasser, Linda L. Jewell, Jim A. Anderson, Stuart Taylor, Neil J. Coville, Graham J. Hutchings, Effect of the addition of Au on a Co/TiO_2 catalyst for use in the Fischer-Tröpsch reaction, *Topics in Catalysis* 44 (2007) 129.

3 Kalala Jalama, Neil J. Coville, Diane Hildebrandt, David Glasser, Linda L. Jewell, Effect of cobalt carboxylate precursor chain length on Fischer-Tröpsch cobalt/alumina catalysts, *Applied Catalysis* 326 (2007) 164.

4 Kalala Jalama, Diane Hildebrandt, David Glasser, Linda L. Jewell, Jim A. Anderson, Stuart Taylor, Neil J. Coville, Graham J. Hutchings, Effect of the addition of Au on a Co/SiO_2 catalyst for use in the Fischer-Tröpsch reaction, in preparation.

5 Kalala Jalama, Diane Hildebrandt, David Glasser, Linda L. Jewell, Jim A. Anderson, Stuart Taylor, Neil J. Coville, Graham J. Hutchings, Effect of the addition of Au on a Co/Al_2O_3 catalyst for use in the Fischer-Tröpsch reaction, in preparation.

CONTENTS

LIST OF FIGURES

CHAPTER 1

CHAPTER 2

CHAPTER 3

CHAPTER 6

CHAPTER 7

CHAPTER 8

LIST OF TABLES

CHAPTER 3

CHAPTER 4

CHAPTER 5

CHAPTER 6

CHAPTER 7

CHAPTER 8

LIST OF ABBREVIATION AND SYMBOLS

AA: Atomic absorption

ASF: Anderson-Schulz-Flory

BET: Brunnauer, Emmett and Teller

CFB: Circulating Fluidised Bed

CSTR: Continuous Stirred Tank Reactor

CTL: Coal-To-Liquid

EDS: Energy Dispersive Spectroscopy

EDTA: ethylenediamine tetraacetic acid

e.V: electron volt

EXAFS: Extended X-ray Absorption Fine Structure

FFB: Fixed Fluidised Bed

FID: Flame Ionisation Detector

FT: Fischer-Tröpsch

FT/IR: Fourier Transform/Infrared spectroscopy

FTS: Fischer-Tröpsch Synthesis

GC: Gas Chromatograph

$\mathbf{g_{cat}}$: gram of catalyst

$\mathbf{g_{Co}}$: gram of cobalt in the catalyst

MCM-41: Mobil Catalytic Material number 41

PFR: Plug Flow Reactor

PPQ: Poropak-Q

RPM: Rounds Per Minute

SA: Specific surface Area

SBA-15: Santa Barbara 15

SCO: Selective Catalytic Oxidation

SMSI: Strong Metal-Support Interactions

SSITKA: Steady State Isotopic Transcient Kinetic Analysis

STM: Scanning Tunneling Microscopy

Syngas: Synthesis gas ($CO + H_2$)

TCD: Thermal Conductivity Detector

TGA: Thermo-gravimetric Analysis

TOF: Turnover frequency (s^{-1})

TOS: Time-On-Stream

TPD: Temperature Programmed Desorption

TPR: Temperature Programmed Reduction

Vol.%: Percentage by volume

WGS: Water-Gas-Shift

$\mathbf{W_n}$: Weight fraction of hydrocarbon with carbon number n

Wt.%: Percentage by weight

XANES: X-ray Absorption Near Edge Structure

XAS: X-ray Absorption Spectroscopy

XPS: X-ray Photoelectron Spectroscopy

XRD: X-ray Diffraction

α: Chain growth probability

∞: Infinite

Chapter 1

Introduction

1.1 History of the Fischer-Tröpsch Synthesis (FTS)

The Fischer-Tröpsch Synthesis (FTS) is essentially a polymerisation reaction in which carbon bonds are formed from carbon atoms derived from carbon monoxide, under the influence of hydrogen in the presence of a metal catalyst. The reaction leads to a range of products which depend on the reaction conditions and catalysts employed [1]. Sabatier and Senderens [2] were the first to report on CO hydrogenation in 1902 when they observed methane formation over cobalt and nickel catalysts. In 1913 and 1914 Badische Anilin and Soda Fabrick (BASF) was awarded patents for the production of hydrocarbons and mainly oxygenated derivatives (synthol) from syngas using alkali promoted osmium and cobalt catalysts at high pressure [3 a-c]. In the 1920's Fischer and Tröpsch [4] reported the formation of a product similar to the synthol product over alkalised iron shavings at 100 atm and 400°C. They also synthesized small amounts of ethane and higher hydrocarbons at atmospheric pressure and at 370°C over Fe_3O_4 – ZnO catalysts [5, 6]. Because of the rapid deactivation exhibited by iron-based catalysts, further studies focused on the use of cobalt and nickel catalysts. Fischer and Meyer developed Ni-ThO_2-Kieselguhr and Co-ThO_2-Kieselguhr catalysts in the early 1930's [7]. Due to limited supply of cobalt, initial studies used nickel catalyst but the high yields of methane over the latter

catalyst shifted the attention to cobalt. The application of FTS at an industrial level started in Germany and by 1938 nine plants with a combined production capacity of about 660 X 10^3 t per year were in operation using cobalt catalysts at medium pressures [8]. From 1937 research focused on use of iron as FTS catalyst and Fischer and Pichler found improved product yields and longer catalyst lifetime when using alkalised iron catalysts at medium pressures (5 – 30 atm) [1]. The use of ruthenium based catalysts was also reported in 1938 by Pichler who observed the formation of high boiling waxes over these catalysts [9]. Even though the nine FT plants in Germany ceased to operate after World War II, the fear of an impending shortage of petroleum kept the interest in the FT process alive. An FT plant with a capacity of 360 X 10^3 t per year was built and operated in Brownsville, TX, during the 1950s. This plant was based on syngas produced from methane but a sharp increase in the price of methane caused the plant to be shut down [10, 11]. During the same time period, based on the world-wide prediction of increasing crude oil prices, the South Africa Coal Oil and Gas cooperation (SASOL) commissioned an FT plant based on coal in Sasolburg in South Africa. Research on FTS has continued ever since at SASOL [11]. Due to the oil crises of the mid 1970s, Sasol constructed two much larger coal-based FT plants which came on-line in 1980 and 1982 respectively. The combined capacity of the three Sasol plants was about 6000 X 10^3 t per year. Some commercial ventures in FTS by Shell international in Malaysia for the production of waxes [12 a], the Norway Statoil GMD slurry process [12 b] and the Mossgas project in South Africa have also been described. Based on methane, the Mossgas plant in South Africa and the Shell plant at Bantuli, Malaysia, came on stream in 1992 and

1993, respectively [10]. In the last few years the interest for FTS has significantly grown due to the increase in oil prices as well as the high demand for energy. Recent commercial ventures include the development of a GTL plant, Oryx GTL, in a joint venture of Sasol with Qatar Petroleum at Ras Laffan in Qatar. Sasol is also developing a GTL plant at Escravos in Nigeria. With demand for energy expected to grow 5 % a year to 2020 (according to the Carbon Sequestration Leadership Forum: www.cslforum.org/china.htm), China has been looking at exploiting its abundant coal reserves to meet its energy requirements. Pre-feasibility studies focusing on exploring the potential of developing two Coal-To-Liquid (CTL) plants, using Sasol's low-temperature Fischer-Tröpsch technology, each with a capacity of about 80000 barrels per day were concluded in November 2005.

1.2 FT reactors

The FTS is operated in two modes. The high-temperature (300 -350°C) process with iron-based catalysts is used for the production of gasoline and linear low molecular mass olefins. The low-temperature (200 - 240°C) process with either iron or cobalt catalysts is used for the production of high molecular mass linear waxes [10]. Efficient and rapid removal of heat from the highly exothermic FT reaction from the catalyst particles is an important factor for the design of an FT reactor. An overheating of the

catalyst would adversely affect product selectivity and catalyst lifetime. Three main types of reactor are used for FT reaction:

i) Fixed bed reactors which are used by Sasol to produce high value linear waxes at low temperatures (225°C). The catalyst is loaded in 5 cm i.d. tubes. Heat removal is achieved by converting water, circulating outside of the tubes [11];

ii) Fluidised bed reactors with either a fixed or a circulating bed. The main difference between the two types of reactor is that in the fixed fluidised bed reactor (FFD) the catalyst bed remains stationary and the gases pass upward through the bed while in the circulating fluidised bed reactor (CFB) the catalyst is entrained in the fast moving stream. The FT plant in the Brownsville, TX [13] which was later shut down for economic reasons, used the FFB reactor while the CFB reactor was developed by The Kellogg Company and was used in the first Sasol plat at Sasolburg [14]. The improved version of these CFB reactors was named Synthol reactors. The two new Sasol plants constructed in Secunda used the same type of reactors but with improved heat exchangers and the capacity per reactor was increased three-fold. The Mossgas FT complex also used the same larger type of CFB reactors with further improved heat exchangers. From 1995 to 1999 the 16 second generation CFB reactors at Secunda were replaced by eight FFB reactors, four of 8 m i.d. with capacities of 470 X 10^3 t per year each and four of 10.7 m i.d. each with a capacity of 850 X

10^3 t per year. These reactors were named Sasol Advanced Synthol (SAS) reactors [10]. The main advantages of FFB over CFB reactors include low construction cost, increase in cooling capacity, low overall catalyst consumption because of a lower rate of on-line catalyst removal and replacement with fresh catalyst to maintain high conversions.

iii) Slurry bed reactors in which gas is bubbled through a suspension of finely divided catalyst in a liquid which has a low vapour pressure at the temperature of operation. The use of slurry bed reactors for FT synthesis was studied by several investigators in the 1950s [10]. A 1.5 m i.d. unit was developed and operated by Kolbel [15]. In the 1970s Sasol R&D found similar conversions and selectivities when comparing the performance of fixed and slurry bed reactors in their 5 cm i.d pilot plants [16]. A 5 m i.d. commercial unit with a capacity of about 100 x 10^3 t per year was commissioned in 1993 and has been in operation ever since [17]. Exxon also operated a slurry bed reactor for wax production. This reactor with 1.2 m i.d used cobalt-based catalyst and the unit's capacity was about 8.5 x 10^3 t per year [18]. The advantages of slurry over multitubular reactors are low cost of reactor train, lower gas compression costs, lower catalyst consumption per tonne of product, ability to operate at a higher average temperature resulting in higher conversions and on-line removal/addition of catalyst allows longer reactor runs. The disadvantage of this type of reactor is that in the case of catalyst poising, all the catalyst is deactivated whereas in the case of a fixed bed reactor the poisoning substance is

adsorbed by the top layers of catalyst, leaving the balance of the bed essentially untouched [10].

1.4 FT selectivity

FT synthesis is characterised by non-selectivity to products. A wide range of olefins, paraffins and oxygenated products is usually obtained. The FT product distribution is explained by a stepwise growth process occurring on the catalyst surface [10]. The CH_2 units [figure 1.1], formed by the hydrogenation of CO are taken as the "monomers" in a stepwise oligomerization process. At each stage of growth the adsorbed hydrocarbon species has the option of desorbing or being hydrogenated to form the primary FT products or of adding another monomer to continue the chain growth. The probability of chain growth (α) is assumed to be independent of the chain length. A product distribution model known as the Anderson-Schulz-Flory (ASF) model [19 – 22] is usually used to obtain the relationship between the weight fraction of formed hydrocarbons and the chain growth probability. This model is described by the following equation:

$$W_n = n(1-\alpha)^2\alpha^{n-1} \qquad 1.1$$

where W_n is the weight fraction of hydrocarbons with carbon number n and α is the probability that one hydrocarbon will link to another hydrocarbon. Equation 1.1 is usually linearised as equation 1.2 and used to determine the α value from experimental data.

$$\log (W_n/n) = n \log (\alpha) + \log ((1-\alpha)/\alpha)^2 \qquad 1.2$$

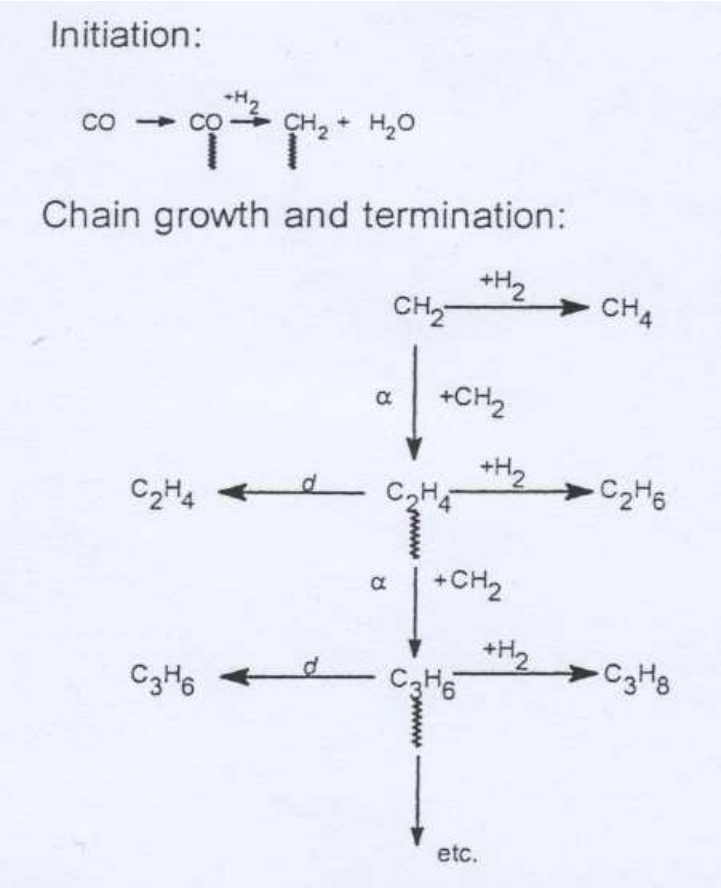

Figure 1.1 *FT stepwise growth process* [10]

A plot of log (W_n/n) versus carbon number (n), should be linear and the chain growth probability is obtained from the slope as log (α) or from the intercept as log $((1-\alpha)/\alpha)^2$ at n = 1. However some deviations from the ASF plot are usually observed:

1. A typical deviation from the ASF distribution plot is a very high methane value. It is proposed that methane can be formed by more than one pathway [23].
2. Very low ethane, ethene and in some cases propane are also observed in the product. It is suggested that this could be due to the re-insertion of these very reactive species back into the growing chain.
3. Some negative [19, 22, 24-26] and positive [8, 22, 27-33] deviations especially when the carbon number is greater than 8 have also been reported. Various theories accounting for chain-length related phenomena have been proposed. These theories include a vapor-liquid equilibrium phenomena [22], diffusion-enhanced olefin readsorption model [32], different physisorption strength of the olefins [33] and the two-active-site model [29, 31]. Shi and Davis [34] have accounted for chain-length related phenomena by proposing that the apparent products of the FTS reaction is a mixture of freshly produced FTS products and the products left in the reactor. They concluded that in order to obtain correct product distribution of a FTS reaction, it is necessary to find a way to evaluate or eliminate the contribution from the products left in the reactor.

Calculated product selectivities versus probability of chain growth are illustrated in figure 1.2 [35]. This plot shows that only the light ($\alpha \rightarrow 0$) or heavy ($\alpha \rightarrow \infty$) products can have a high selectivity. All other products go through a maximum yield.

The product distribution is influenced by operating conditions (temperature, pressure, feed gas composition, space velocity) and catalyst type and promoters.

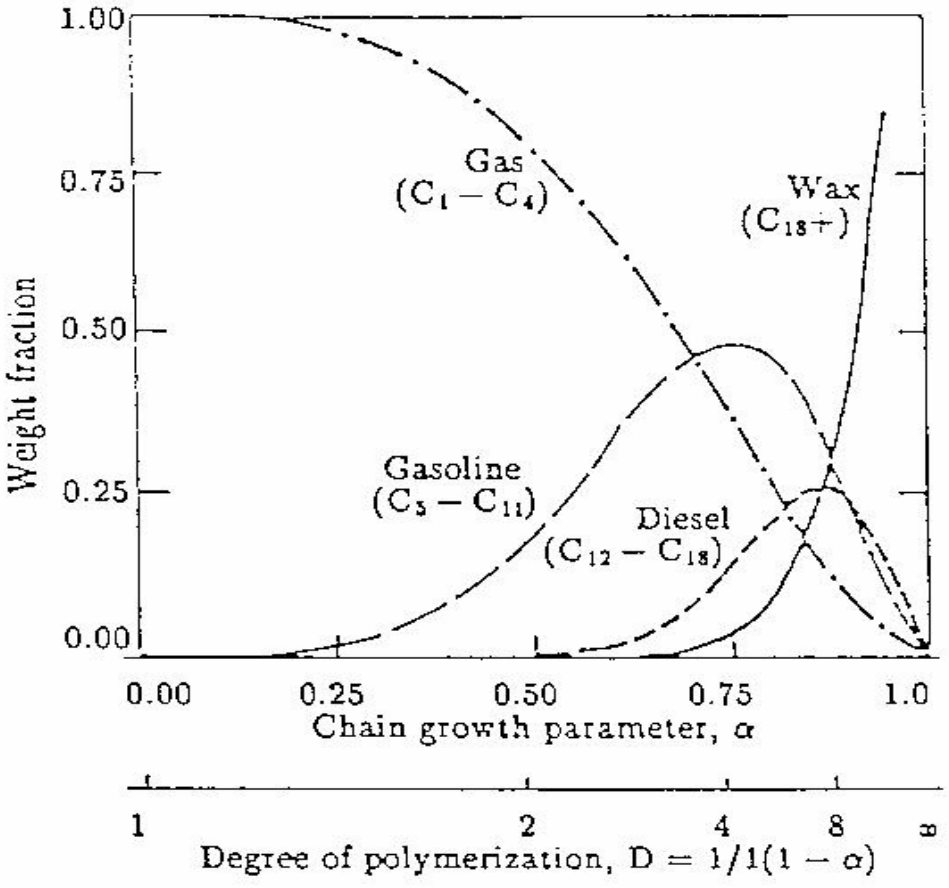

Figure 1.2 *Plot of calculated selectivities vs probability of chain growth* [35]

1.4 FT catalysts

Fe, Ni, Co and Ru are the only metals that have the required FT activity for commercial application [10]. Ni has been reported to produce too much methane under FT conditions [2, 10, 36-38]. On the other hand Ru has been found to be less selective to methane and more selective to the C_{5+} hydrocarbon fraction than other metals [37]. Ru is the most expensive of these four metals and the available amount in the world is insufficient for large scale application. For these reasons Fe and Co are viable catalysts for industrial applications. Fe catalysts are used in the major FTS operation at Sasol and Mossgas projects in South Africa [39, 40]. Extensive reviews of the use of Fe for FTS are reported in the literature [7, 41 – 44]. Low temperature FT process Fe-based catalysts used for wax production are currently prepared by precipitation methods and are promoted with Cu and K_2O and bound with SiO_2 (5g K_2O, 5 g Cu and 25 g SiO_2 per 100g Fe) while the high-temperature FT Fe-based catalyst is prepared by fusing magnetite together with the required chemical (usually K_2O) and structural promoters such as Al_2O_3 or MgO [16]. Cobalt based catalysts are only used in the LTFT process where they possess high activity and selectivity for heavy waxy product and a lower water-gas-shift reaction activity compared to Fe catalysts [10, 45]. A high operating temperature results in production of excess methane. The catalytic behaviour of cobalt for FTS is influenced by many factors such as type of support, Co dispersion and particle size, catalyst preparation method, type of promoters, pre-treatment conditions, etc.

1.5 Effect of support on FT catalysts

The increase in the number of surface metal atoms available for catalysis is achieved by dispersing metals on a variety of supports. The use of a support also stabilizes the resulting dispersed small metal crystallites [46, 47]. The effect of support was assumed to be physical in nature. This assumption would imply that catalytic properties would be independent of the type of support used. However some controversial effects of the support were reported in early studies. For example, Schuit and van Reijen [48] reported that unsupported nickel and silica supported nickel had similar properties when compared per unit area of metal surface. On the other hand Bond [49] reported a subtle influence of the support (silica, silica-alumina, alumina) used for the reaction of ethylene and deuterium on platinum. He then suggested that more sensitive techniques would be needed to approach the problem. Two years later, Eischens and Pliskin [50] first reported the effect of support using a sensitive technique, infrared spectroscopy of adsorbed molecules. They observed differences in the spectra of CO adsorbed on platinum when the support was changed from silica to alumina. More bridged species were present on the alumina supported platinum. O'Neil and Yates [51] have also reported the effect of the support on the infrared spectra of carbon monoxide adsorbed on nickel. They used alumina, silica and titania in their study and found a marked variation in the strength of CO adsorption and the relative numbers of linear and bridged CO species. Alumina and titania were reported to have marked effects on the CO adsorption on nickel while silica seemed to have little or no effect. They speculated that this effect was probably a function of the electrical properties of

the junction formed at the points where the metal is in intimate contact with the substrate. Taylor et al.[52] have studied the effect of the support on the catalytic activity of nickel for ethane hydrogenolysis. They used three different supports: silica, alumina and silica-alumina impregnated with nickel solution to make catalysts containing 10 wt.% Ni. They found that the specific activity of the nickel varied over 50-fold for the various supports. The highest activity was measured on silica supported nickel while silica-alumina supported nickel exhibited the lowest activity. A specific interaction between nickel and the support was suggested to explain the observed effect. Vannice [47] has observed an enhancement of specific activity for CO-H_2 reaction on supported Pt and Pd than on unsupported Pt and Pd. Alumina, silica and H-Y zeolites were used as supports in their study. The increase in specific activity correlated with the increase in the surface concentration of the more weakly bound CO species. This effect was found to be indirect in the case of Pt where the support produced stable, highly dispersed Pt clusters with higher specific activity than large Pt crystallites. A direct effect of the support was found with Pd where the nature of the support itself produced the increase in activity. They found that a direct metal-support interaction appeared to exist with Pd catalysts independently of metal particle size below or around 10 nm. Based on sorption studies in combination with X-ray diffraction and electron microscopy, Tauster et al [53] were the first to report a unique type of metal-support interaction involving titania as a support. They observed a decrease in hydrogen and carbon monoxide sorption to near zero when the reduction temperature of titania supported noble metals was changed from 200°C to 500°C.

Encapsulation of the metal particles following reduction of noble metals at 500°C was unlikely to explain the unique sorption properties of the titania supported noble metals because BET surface area did not vary with the change in reduction temperature. The effects of reduction at 500°C on sorption properties were entirely reversible after oxidation at 400°C and Pd supported on titania with different BET surface area showed the same H_2 sorption suppression after reduction at 500°C. Poisoning of metals following reduction at 500°C was also ruled out because of the small amount of sulphur present in the samples. This amount of sulphur could be expected to be removed at high reduction temperature and restore the sorption properties of the samples. This was not observed. They thus attributed this effect to chemical interactions between the metal and the support. These interactions were referred to as strong metal-support interactions (SMSI). The nature of these interactions was still not well understood but these authors claimed that it was associated with the formation of bonds between the noble metal and titanium cations or titanium atoms (formation of intermetallic compounds). Another study from the same authors [54] involving iridium supported on number of supports consisting of oxides of magnesium, scandium, yttrium, titanium, zirconium, hafnium, vanadium, niobium, tantalum, chromium, and manganese revealed that titania was not the only oxide to exhibit a SMSI. Their study indicated that when carriers like V_2O_3 or Nb_2O_5 were used, hydrogen adsorption after reduction at 500˚C decreased to near-zero. They discussed the SMSI in terms of metal oxide support reducibility.

In the light of a theoretical study on solid state transformations that occur in the Pt/TiO_2 system conducted by Horsley [55] and Tauster et al.[56] suggested that SMSI involves the transfer (whole or partial) of an electron from a subjacent cation to a supported metal atom, resulting in a strong ionic bond between a negatively charged *pillbox* of supported metal atoms and associated surface cations. It was shown that the more reducible oxide supports exhibited more extensive metal support interactions [54, 55]. Strong metal-support interaction is therefore understood to involve an electron exchange between a partially reduced support and the metal and leads to the suppression of hydrogen chemisorption [56-60]. The modification of the H_2 and CO adsorption properties reported by Tauster et al.[53] for TiO_2 supported metals and correlations between the heats of adsorption of CO and H_2 on metals and their specific activities for methanation uncovered by Vannice [37, 38, 47], prompted Vannice to investigate the Ni/TiO_2 system in $CO-H_2$ reaction. Titania supported nickel catalysts were found to exhibit significantly greater activity and selectivity to higher molecular paraffinic hydrocarbons than Ni powder or Ni supported on SiO_2, Al_2O_3 or graphite [61]. This effect induced by the titania support was attributed to the unique metal-support interaction in the Ni/TiO_2 but the nature of the interaction was still obscure. Several other studies have provided evidence that CO and H_2 adsorption properties and the catalytic behaviour of Ni [62, 63] and Ru [64] are significantly affected by the support. Comparisons of CO and H_2 adsorption properties and catalytic behaviour in these previous studies were made using catalysts with different metal loading, metal dispersion, extent of reduction and different preparation method. An unambiguous separation of these effects from the support effect was not possible. To

address this problem, Bartholomew et al.[65] conducted an investigation on adsorption properties and CO hydrogenation catalytic behaviour of well-defined Ni catalysts supported on SiO_2, Al_2O_3 and TiO_2. A wide range of Ni dispersions and concentrations was investigated. They established that at low nickel concentrations and high dispersions, a large fraction of the nickel interacted strongly with the support. The extent of interaction increased in the order $Ni/SiO_2 < Ni/Al_2O_3 < Ni/TiO_2$ for catalysts of the same loading. The activity for CO hydrogenation was found to decrease in the following order $Ni/TiO_2 > Ni/Al_2O_3 > Ni/SiO_2$ for catalysts prepared by either impregnation or precipitation methods. Reuel et al.[66] also reported the effects of alumina, silica, titania, magnesia, and carbon supports on the specific activity and selectivity properties of cobalt in CO hydrogenation. Catalysts of low cobalt loading (3%) provided the best comparison of support effects since they had nearly the same dispersion and also they presumably presented a more intimate interaction of cobalt with the support. For catalysts containing 3 wt.% cobalt (1 atm and 225°C), the hydrogenation activity was reported to decrease in the following order: Co/TiO_2, Co/SiO_2, Co/Al_2O_3, Co/C and Co/MgO. The higher activity of Co/TiO_2 was considered to be a result of strong metal-support interactions as found for the Ni/TiO_2 [61, 65]. Further studies from other research groups have also reported Co/TiO_2 system to have a strong metal-support interaction [67-71] and to show high activities for CO hydrogenation. Also numerous other studies have reported the formation of cobalt-support compounds during catalyst pre-treatment in Co/TiO_2 [72, 73], Co/Al_2O_3 [74 - 77] and Co/SiO_2 [78] systems. For catalyst design, all the parameters

associated with the support effect must be considered in order to get a catalyst which responds to the desired properties.

1.6 Effect of metal dispersion/particle size

The introduction of metal surface area and dispersion measurements has allowed calculation of specific activities which in turn, provide a possibility to make meaningful comparison of different catalysts [37, 79, 80]. Vannice [47, 62] had reported the effect of metal particle size/dispersion on catalytic behaviour of supported Pt, Pd [47] and Ni [62] catalyst during CO hydrogenation. The specific activity was found to increase with the decrease of metal particle size in supported Pt catalyst but no significant dependence of the specific activity with metal particle size was observed with Pd. The product selectivity for both Pt and Pd were not significantly affected by the metal particle size. Dispersing nickel on a support was reported to enhance the formation of higher molecular weight hydrocarbons compared to an unsupported nickel catalyst. The specific activity for total CO conversion was found to increase with the increase of dispersion (decrease of metal particle size) as was reported with Pt, but to a lesser extent in this case. These effects were attributed to changes in the adsorbed state of CO on metal surfaces [47, 62].

King [64] has reported an increase in CO and CH_4 specific activity for supported Ru catalysts during FT reaction with increasing Ru particle size. No consistent

correlation between the product distribution and Ru dispersion was noted. Bartholomew et al.[65], also reported an increase in C_{2+} hydrocarbon selectivity and the CO/H adsorption ratio with increasing metal dispersion in silica and alumina supported nickel catalysts used for CO hydrogenation. This effect was attributed to intimate electronic interactions between the support and the metal crystallite. Based on speculations, these authors proposed that electrons are withdrawn from the nickel crystallites by the support leading to a metallic behaviour more characteristic of cobalt, which is known to have a high specific activity and high selectivity to high-molecular weight hydrocarbons during the CO hydrogenation reaction [38].

Nijs et al.[81] presented an extended Schulz-Flory Model for Fischer-Tröpsch product distribution which also accounted for the metal average particle size in the catalyst. The physical basis for this model implied that any particle of a given size imposed a strict maximum upon the chain length of the hydrocarbons which can be formed on the particle. Hence this model predicts an increase in hydrocarbon chain length with an increase in metal particle size.

Kellner et al.[82] reported the effect of Ru/Al_2O_3 dispersion on CO hydrogenation. For low Ru dispersions i.e. < 0.7, the specific activity for synthesis of products was reported to decrease with increasing dispersion without affecting either the chain growth probability or the olefin-to-paraffin ratio. For dispersions above 0.7, the specific activity decreased dramatically and was accompanied by a slight decrease in the chain growth probability and a rapid decrease in the olefin-to-paraffin ratio. The change in specific activity with dispersion below 0.7 was attributed to a decrease in

the fraction of sites present on planar surfaces of the Ru micro crystallites while for higher dispersion the change in specific activity was attributed to either changes in the electronic properties of the small crystallites or to interactions of the crystallites with the support. The effect of cobalt particle size on CO hydrogenation was only reported in the literature in 1984 [66].

Reuel et al.[66] have reported that the specific activity of supported cobalt catalysts decreased significantly with increasing dispersion and that the molecular weight of hydrocarbon products was lower for catalysts having higher dispersions and a lower extent of reduction. This effect was attributed to the presence of stable oxides in the well dispersed and poorly reduced catalysts, which catalyse the water-gas-shift reaction leading to an increase of the H_2/CO ratio at the surface. This study was extended by Fu et al.[83] using Co/Al_2O_3 catalysts and the changes in specific activity with dispersion were explained by variations in the distribution of low and high coordination sites and by changes in the nature of the adsorbed CO species available for reaction. High specific activity was believed to be favoured on sites to which CO is strongly coordinated. Other studies did not observe a significant effect of cobalt particle size on specific activity [84-93]. Methane selectivity has been reported to increase and selectivity to higher hydrocarbons to decrease with decrease of cobalt particle size [66, 83, 89, 90, 92, 94]. This effect was explained by the presence of cobalt oxides in the catalysts [66, 83] or by olefin readsorption [89]. Some controversial effects of cobalt particle size on CO hydrogenation product selectivity have also been reported [95, 96]. Kikuchi et al.[95] have reported a decrease in methane selectivity and

increase in C_{5+} selectivity with a decrease in particle size. Song and Li [96] have recently reported that higher alpha values could be obtained on smaller cobalt particles. The experiments were done using a slurry reactor and this effect was based on an assumption that hydrogen atoms dissolved in octahedral interstitial positions of the metallic cobalt particle lattice are responsible for hydrogenation of FT hydrocarbon intermediates into the hydrocarbons. The apparent controversy on the effect of cobalt particle size on catalyst behaviour for CO hydrogenation suggests that the reported observations are affected by variables like support, dispersion range etc. Ho et al.[85] have studied the effect of cobalt particle size by using silica as support to minimize the metal-support interaction and selected catalyst range of calcination conditions to allow complete reduction of the cobalt phase. The specific CO hydrogenation activity was found to be invariant with cobalt dispersion in the range of 6 – 20 % dispersion. Barbier et al.[97] have reported that intrinsic activity and chain growth probability on a series of silica supported cobalt catalysts first increased on increasing the particle size and stabilized from a critical diameter of 6 nm. A similar observation was reported in a recent study where Bezemer et al.[98] have studied the intrinsic cobalt particle size effects on an inert support material, graphitic carbon nanofibers (CNF). The critical cobalt particle size over which the specific activity and product selectivity became invariant was 6 and 8 nm for reaction pressures between 1 and 35 bar. These effects were attributed to non classical structure sensitivity in combination with CO-induced surface reconstruction.

1.7 Effect of cobalt precursors

Conventional cobalt FT catalysts are usually prepared using cobalt nitrate as precursor. However the need to control parameters affecting the behaviour of catalyst, e.g. cobalt dispersion, has prompted researchers to study the effect of various cobalt salts used as precursors. Some early studies showed that the use of cobalt carbonyl as a precursor leads to catalysts with higher activity for CO hydrogenation than the conventional, nitrate derived catalysts [86, 87, 99-103]. Some of these studies [100, 102] reported that catalysts prepared using cobalt carbonyl were more selective toward alcohols and also contended that the high activity measured for these catalysts is related to the high dispersion.

Niemela et al.[104] conducted a study where they distinguished between two types of carbonyl complexes, $Co_2(CO)_8$ and $Co_4(CO)_{12}$ and compared the effect on reduction extent, dispersion and reactivity on a silica support. These effects were compared to the conventional silica supported cobalt catalyst. The near surface reduction was found lower for $Co_2(CO)_8$ derived catalysts than for the $Co_4(CO)_{12}$ based ones. The cobalt dispersion was found to decrease in the precursor order $Co_2(CO)_8 > Co_4(CO)_{12} > Co(NO_3)_2$. Also the carbonyl derived catalysts exhibited greater initial activity in CO hydrogenation than catalysts prepared from cobalt nitrate. The effect of organic cobalt precursors have been studied mostly on a silica support [92, 105 - 110].

Matsuzaki et al.[102] used cobalt acetate to prepare highly dispersed cobalt metal catalysts supported on silica. The resulting catalyst was hardly reduced in a hydrogen stream at 723 K compared to catalysts prepared using cobalt nitrate and cobalt chloride. The authors proposed that divalent cobalt is strongly connected to the Si of the SiO_2 support through the oxygen for the cobalt acetate derived catalyst even, after thermal treatment at 723 K in a hydrogen stream. Based on EXAFS results, the authors contended that the structure of cobalt oxide was similar to that of cobalt (II) acetate. They proposed a mechanism for oxide formation and suggested that coordinated ligands such as acetate are more strongly connected to a cobalt cation compared to counter anions such as nitrate or chloride and that the structure of the Co-O bonds is kept under reduction conditions. In the case of nitrate and chloride ions, the uncoordinated counter anions are more easily removed from the cobalt cation and thus the cation is easily reduced to metallic cobalt below 673K. The cobalt acetate derived catalyst was not active for CO hydrogenation.

Sun et al.[107] prepared catalysts by mixed impregnation of cobalt (II) nitrate and cobalt (II) acetate and measured higher activity for the Fischer-Tröpsch reaction than on catalysts prepared from either mono-precursor. A nitrate/acetate ratio of 1 was shown to be the optimum ratio. This effect was explained assuming that readily reduced cobalt metal from cobalt nitrate promoted the reduction of highly dispersed Co^{2+} from cobalt acetate to metallic cobalt by a hydrogen spillover mechanism during reduction. Highly dispersed Co metal provided the main active sites. Some other studies [92, 108-110] have shown that the use of organic precursors such as cobalt acetate and/or cobalt acetylacetonate on silica results in formation of a catalyst with high

dispersion and low reducibility and hence low activity for the CO hydrogenation. The high dispersion in the catalyst leads to formation of poorly-reducible cobalt silicates [108 -110].

Van Steen et al.[111] reported on the dependence of cobalt silicate formation on the pH of the impregnating solution. At pH above 5, for example, when cobalt acetate is used as cobalt precursor, more cobalt silicates are formed. The surface cobalt silicate precursor is destroyed by drying or low-temperature calcination.

Ming et al.[112] have also reported that the pH of the impregnating solution influences cobalt dispersion on a support. They explained that below the point of zero charge for silica (between 2 and 3.5), the surface is positively charged and the adsorption of positively charged Co ions is slowed down leading to a low dispersion. At a pH > point of zero charge, deposition of Co is favoured and improves the cobalt dispersion.

Girardon et al.[110] have reported that Co silicate formation arises from thermal treatment and not from the pH of the impregnating solution as suggested by Ming et al.[112]. They explained that cobalt silicate formation depends on the exothermicity of the cobalt salt decomposition in air and the temperature of the oxidative pre-treatment. The high exothermicity of cobalt acetate decomposition leads primarily to amorphous and low-reducible cobalt silicates. They suggested that a more efficient heat flow control at the stage of cobalt acetate decomposition significantly increases

the concentration of cobalt oxide species which is more easily reducible in the oxidised catalyst.

The effect of organic precursor on alumina and titania supported cobalt catalysts has also been reported in the literature. Van der Loosdrecht et al.[113] have reported that the use of cobalt EDTA and ammonium cobalt citrate in the preparation of low-loaded alumina-supported Co catalysts (2.5 wt %) gave very small oxide particles which reacted with the support during thermal treatment in a reducing gas to form Co aluminates which were not active for the FT reaction. However catalysts prepared from cobalt nitrate had larger particle sizes and were easily reduced to Co metal and were therefore active under FT conditions. Kraun et al.[114] have shown that the use of cobalt oxalate, cobalt acetate or cobalt acetylacetonate as cobalt precursors for the preparation of titania-supported Co catalysts gives higher cobalt dispersions and higher activity for the FT reaction than catalysts prepared using cobalt nitrate. They suggested that various Co precursors seemed to influence the interaction of the active cobalt sites with the support that may be ascribed to the decomposition of the organo-cobalt compounds. They were unable to elucidate the mechanism of the decomposition process.

1.8 Effect of Co catalyst promotion with noble metals

Small amounts of noble metals are often used to enhance the reduction of cobalt interacting with the support and to increase active site density for synthesis. The addition of Ru, Pt, Pd and Re to cobalt catalysts have been the subject of study by many different research groups.

Guczi and co-workers [115-117] have studied the effect of Pt in the Co-Pt system with a metal loading of 10 wt.% and high Pt:Co ratios. They found an enhancement of reduction of Al_2O_3-supported Co catalysts and a stabilisation of Co ions on the Al_2O_3 surface. The presence of Co-Pt bimetallic particles was inferred from a lower catalytic activity (compared with the monometallic Co catalyst) in the synthesis of hydrocarbons from CO and H_2 [116]. The Pt-Co system was reported to have high activity in methanol formation at defined compositions [115-117]. Zyade et al.[118] characterized similar catalysts and observed (by EXAFS) formation of bimetallic particles with a Pt-Co interatomic distance of 0.271 nm. Dees and Ponec [119] studied Co-Pt catalysts supported on silica and alumina, with 5 wt.% total loading and varying Pt:Co ratios. They used X-ray diffraction (XRD) to identify alloy formation on the silica. Schanke et al.[120] attempted to explain the role of Pt as promoter for hydrocarbon synthesis on alumina-supported and silica supported cobalt catalysts. Catalysts were prepared by impregnation and contained 9 wt% Co and 0 or 0.4 wt% Pt. From TPR studies, the presence of Pt shifts TPR peaks to lower temperatures for all catalysts. H_2 chemisorption shows that the dispersion of metallic cobalt on Pt promoted catalysts increased, when compared to that on the unpromoted catalyst. The

largest effect was found with alumina-supported catalysts due to the reduction of highly dispersed surface cobalt oxide. The CO hydrogenation rates (based on weight of cobalt) for Pt-promoted catalysts were 3-5 times higher than those on unsupported catalysts. By using the steady-state isotopic transient kinetic analysis (SSITKA) the authors found that the true Turn Over Numbers (TON) were constant for all catalysts and that Pt-promoted catalysts presented a high coverage of reactive intermediates resulting in an increase in apparent turnover numbers. The selectivity was not influenced by the presence of Pt. The effect of Pt was explained by considering a possible hydrogen spillover effect from Pt to Co or a more direct interaction between Pt and Co in the form of a Co-Pt interface or bimetallic Co-Pt particles.

Kogelbauer et al.[121] conducted a study to determine the manner in which Ru promotion of Co/Al_2O_3 catalysts occurs. The catalysts contained 0.5wt.% Ru and 20 wt.% Co. TPR analysis, after complete decomposition of Co nitrate, showed that both promoted and unpromoted Co/Al_2O_3 catalysts reduced in two steps. A shift of 100°C to lower temperature was observed for the low temperature reduction peaks for the Ru-promoted catalysts. A broad high temperature reduction feature around 600°C in unpromoted catalyst, associated with Co species, which were extremely difficult to reduce was shifted to ca. 450°C in the Ru promoted catalyst. The extent of reduction after standard reduction treatment in 1 atm of flowing H_2 (50 cc/min) at 350 °C for 10 hours was ca. 60% for unpromoted catalysts compared to 85%-100% for Ru – promoted catalysts. H_2 chemisorption measurement showed that addition of ruthenium not only increased the extent of reduction but also resulted in ca. 3 times

the number of exposed cobalt atoms at the surface of all Ru-promoted catalysts compared to unpromoted catalysts. Also, the average Co metal particle size for Ru-promoted catalysts decreased and was ca. half that of particles formed for the unpromoted Co/Al_2O_3 catalysts. This was probably due to the presence of additional small particles due to reduction enhancement by Ru. The rate of FTS at 220 °C increased by a factor of 3 in the $CoRu/Al_2O_3$ catalyst. Both promoted and unpromoted catalysts had similar chain growth probability and methane selectivity. The authors proposed that noble metals activate hydrogen spillover to Co_3O_4, thus promoting its reduction at lower temperature. They also speculated that Ru could prevent the formation of highly irreducible Co compounds or promote their reduction. They concluded that Ru acts only as reduction promoter for Co by increasing the reducibility and dispersion of Co.

Similar results were observed on other Ru-Co systems supported on titania [71] and alumina [122, 123]. Hosseini et al.[123] varied the amount of Ru (0.5, 1.0, 1.5, 2.0 wt.%) added to alumina supported cobalt catalysts (20 wt.%). The effect of Ru on the catalytic behaviour of $Co/\gamma\text{-}Al_2O_3$ for CO hydrogenation was investigated in a continuous stirred tank reactor (CSTR). Characterization studies (XRD, TGA, TPR, H_2 chemisorption and BET) showed that catalysts promoted with 0.5% and 1.0 % Ru presented a higher extent of reduction, better dispersion of Co on the support, reduction of particle size of the metal, and a reduction of catalyst pore volume. High CO conversions were also measured for these catalysts. By further increasing the Ru content (1.5, 2 wt.%) the results were reversed. C_{5+} selectivity of the products was not

affected. With increasing Ru content, it was observed that complete reduction of the catalyst was shifted to lower temperatures than found for the unpromoted catalyst. The proposed explanation was based on possible interactions of cobalt and ruthenium induced by the higher mobility of Ru as well as the formation of a Co-Ru oxide. The proposed explanation was supported by the assumption that Co_2RuO_4 formed a spinel isostructural to Co_3O_4 [124] and that this spinel could be reduced at lower temperatures than cobalt aluminates. It was also assumed that in the presence of Ru the reduction of Co is accelerated by a spillover process.

Nagaoka et al.[125] studied the influence of the addition of trace amounts of Pt (Pt/Co = 0.005 – 0.05 in atomic ratio) or Ru (Ru/Co = 0.01 – 0.05) to Co/TiO_2 used for dry reforming of CH_4. They indicated that the number of Co oxide particles interacting strongly with TiO_2 was decreased by the addition of noble metals. Also, the addition of both noble metals resulted in a decrease of the reduction temperature of Co oxides and titania, presumably due to hydrogen spillover from the noble metal surface. It was noted that the peak for Co oxides interacting strongly with TiO_2 was shifted only by the addition of Pt and concluded that Pt promoted the reduction of Co oxides more effectively than Ru.

Sarkany et al.[126] investigated the effect of Pd on Co-Pd/alumina catalysts used for the hydrogenation of 1,3-butadien. Catalysts contained 5 wt.% Co and varying amounts of Pd (0.1 to 1.0 wt.%). Based on XRD, XPS, TPR and CO and H_2 chemisorption studies, it was concluded that the presence of Pd increased both the

reducibility of the Co and the number of metallic centres. Pd was believed to act as a hydrogen source and did not significantly affect the reduction behaviour of Co_3O_4 in catalysts with poor contact between PdO and Co_3O_4, i.e. when mechanical mixtures of PdO and Co_3O_4 (11,3 atomic % Pd-Co) were used.

Guczi et al.[127] studied the effect of Pd on silica supported Pd/Co catalysts prepared by the sol/gel method. Using TPR and XPS characterisation they established that Pd facilitated reduction of cobalt which segregated to the catalyst surface to some extent. A CO hydrogenation reaction study (1 bar and between 200 and 300°C, $H_2/CO = 2$), in a plug flow reactor using differential conditions showed a synergistic effect for bimetallic Co/Pd catalysts (ratio = 2) when compared to the use of monometallic Co or Pd catalysts. Also the presence of Pd enhanced the amount of alkanes and the chain length of the products increased up to C_8-C_9. They established that palladium acted in the bimetallic system not only as a component which helped cobalt reduction, but also as sites activating hydrogen participating in the reaction. Similar results were obtained from the same research group using XPS, XRD, XANES, CO hydrogenation and low temperature methane activation under non-oxidative conditions [128].

Tsubaki et al.[129] also investigated the role of noble metals when added to catalysts for FTS. Silica supported catalysts were prepared by incipient wetness impregnation of the support with mixed cobalt salts, $Co(NO_3)_2.6H_2O$ and $Co(CH_3COOH)_2.4H_2O$ as well as $Pd(NH_3)_2(NO_2)_2$, $Pt(NH_3)_2(NO_2)_2$, and $Ru(NO_3)_3$ to obtain catalysts containing 10 wt.% Co (5 wt.% from cobalt nitrate and 5 wt.% from cobalt acetate)

and 0.2 wt.% of Ru, Pt or Pd. The addition of small amount of Ru to Co/SiO_2 catalyst increased both the catalytic activity and the reduction degree remarkably. The TOF increased but the CH_4 selectivity was unchanged. The CO hydrogenation rate followed the order RuCo > PdCo > PtCo > Co. The Pt or Pd catalyst exhibited higher CH_4 selectivity. Pt and Pd hardly exerted any effect on the degree of cobalt reduction; the metals promoted cobalt dispersion and decreased the TOF. Characterisation studies (TPR, XRD, EDS, FT/IR, XPS) suggested that different contacts between Co and Ru, Pt or Pd existed. Ru was enriched on cobalt while Pt or Pd dispersed well to form of Pt-Co or Pd-Co alloys.

The promotional effect of Pd on both methane activation and CO hydrogenation prompted Carlsson et al.[130] to investigate the fundamental properties of Co-Pd bimetallic catalyst supported on a thin alumina film using STM, CO-TPD and XPS characterization techniques. They found that the binding energy of CO to both Pd and Co sites is lowered by the presence of the other metal. CO binds preferentially to Co-atop sites and Pd-3-fold hollow sites. They also suggested a net polarization of charge or redistribution of d-band states in the bimetallic particles as they observed a shift in the Pd 3d level to higher binding energy concurrent with a shift in the Co 2p level to lower binding energy.

Das et al.[131] investigated the effect of rhenium on alumina supported cobalt catalysts (15% Co/Al_2O_3) prepared by a three step incipient wetness impregnation (IWI) of cobalt nitrate followed by IWI of an aqueous solution of rhenium oxide. A Re loading of 0.2; 0.5 and 1.0 wt.% was used in their study. Catalyst characterization (XRD,

TPR, XAS, BET, H_2 chemisorption) showed that addition of small amounts of rhenium decreased the reduction temperature of Co oxides compared to the unpromoted catalyst but the percent dispersion and cluster size did not change significantly. They established from TPR studies that rhenium had no effect on the low temperature reduction peak responsible for the reduction of cobalt oxide. They also showed that Co_3O_4 crystallites are essentially reduced (500-650K) during rhenium oxidation (623K) so that no spillover effect can operate to aid in reducing those species. However, H_2 spillover from the reduced rhenium metal could occur to facilitate reduction of cobalt species interacting with the support, as this phenomenon occurs after reduction of rhenium oxide to rhenium metal is achieved. Catalytic activity tests for the FT reaction using a CSTR showed that addition of Re increased the synthesis gas conversion, based on catalyst weight, but TOF results were similar to that obtained in the absence of Re.

Most of the reports in the literature have unambiguously shown that a small amount of noble metal can enhance the reduction of cobalt in the catalyst but some controversial conclusions on the nature of this promotion are reported.

EXAFS data for Pt and Re [132] promoters have shown that alloy formation (or direct contact between promoter and cobalt) is necessary for noble metals to affect Co catalytic behaviour. Ronning et al.[133] have also suggested that bimetallic formation occurs for low loaded (ca. 5% Co) cobalt/alumina catalysts promoted with 2 wt.% Re.

Jacobs et al.[134] have studied the reduction of a series of Re-promoted and unpromoted Co/Al_2O_3 catalysts using a combination of TPR, H_2 chemisorption, in situ XPS and EXAFS/XANES. The in-situ extended X-ray adsorption fine structure (EXAFS) study at the L_{III} edge of Re showed that there was a direct contact of Re with cobalt atoms, while evidence of Re-Re bonds was not observed. Even though direct atom-to-atom contact was found, their TPR data suggested that hydrogen spillover from the promoter to cobalt oxide clusters is important for cobalt oxide reduction. Reduction of the promoter is required before the cobalt oxide reduction by hydrogen spillover can occur. They established that this is presumably the reason why Pt and Ru promoters shift the profiles for the reduction of cobalt oxide species to lower temperature for both peaks, while Re affects only the second broad peak. Re reduction occurs at the same temperature as the first stage of cobalt oxide reduction. Similar results were reported by Storsaeter et al.[135] who reported that promotion with rhenium shifts the broad peak at high temperature to a narrower peak at lower temperature. Because Re is reduced at 690K, only the reduction of the high-temperature peak was affected by Re, probably by spillover of hydrogen from Re, making the reduction of Co in interaction with the support easier. They found that Re increased the degree of reduction of Co supported on Al_2O_3 but no effect of Re on the degree of reduction for SiO_2 and TiO_2 supported catalysts was observed.

Few studies of cobalt catalysts promoted using Au have been reported in the literature to date. Most of the studies involving Au/Co system used cobalt oxide as a support or promoter for highly dispersed Au and the system was used for low temperature CO

oxidation [136-141], oxidative destruction of dichloromethane [142], selective catalytic oxidation (SCO) of NO in flue gases at a low temperature of 120°C [143], automotive pollution abatement [144], etc.

A promoting effect of gold on the structure and activity of a Co/kaolin catalyst was reported by Leite et al.[145]. Catalysts were prepared by precipitation of $Co(NO_3)_2.6H_2O$ or co-precipitation of $HAuCl_4 .3H_2O$ / $Co(NO_3)_2.6H_2O$ to give Au-Co containing catalysts. Sodium carbonate was used as precipitant. These catalysts were characterized using XRD, DTA, TGA and TPR and were tested for 2,3-dihydrofuran synthesis. The authors concluded that modification by gold leads to the formation of new cobalt species, reducible at significantly lower temperatures in comparison to those of the non-promoted catalysts.

1.9 Effect of water on Co FT catalyst

The effect of water during the FT reaction has been intensively studied in the past decade and continues to be a subject of investigation for many research groups. Controversial results have been reported in the literature. The study of the effect of water has been conducted by adding external water to the reactor feed or by conducting reactions at higher conversions which lead to an increase in the H_2O/H_2 ratio in the reactor.

Reports in literature have shown that water has a positive [89, 146-152], negative [71, 153-161] or no effect [162- 164] on the activity of cobalt catalysts in the FT reaction. Various explanations have been presented to account for the positive effect of water on cobalt catalysts. It has been suggested that water possibly destroys the strong metal-support interaction (SMSI) effect in titania supported catalysts [146, 148]. Berthole et al.[152] explained the increased activity by water on titania supported cobalt catalysts by suggesting that water induced an enhancement of the CO dissociation rate. Most of the studies have explained the negative effect of water on cobalt catalysts by loss of active sites due to Co oxide formation or Co-support compound formation in the presence of water. Huffmann et al.[155] used in situ EXAFS to study unpromoted and K-promoted alumina and silica supported catalysts. They observed some oxidation of the unpromoted Co/SiO_2 during $CO/H_2/H_2O$ exposure. They also found some oxidation with K-promoted Co/Al_2O_3 during reaction while the unpromoted catalyst was not oxidised during reaction. Rothaemel et al.[156] used the Steady-State isotopic transient kinetic analysis (SSITKA) method to study the mechanism of deactivation of Co/Al_2O_3 and $Co/Re/Al_2O_3$ catalysts by water in the FTS. Their results showed that the deactivation was due to loss of active sites, whereas the specific site activity of the remaining active sites was unchanged. They assumed that part of the Co metal surface was oxidised during treatment with water. A subsequent study from the same laboratory [157] investigated the possibility of cobalt oxidation during FT by model studies, where alumina supported catalysts (Co/Al_2O_3 and $Co/Re/Al_2O_3$) were exposed to H_2O/H_2/He mixtures and submitted to several characterization techniques such as TPR, gravimetry, XPS, TPD and pulse adsorption. It was found that

$Co/Re/Al_2O_3$ deactivated when water was added during FTS and the model studies showed that this catalyst oxidized in H_2O/H_2 mixtures with a ratio much lower than expected for oxidation of bulk cobalt. The reoxidation became important with increasing water partial pressure and with increasing water to hydrogen ratio. It was suggested that oxidation of highly dispersed phases or surface oxidation are the cause of the observed deactivation reaction. The $Co/Re/Al_2O_3$ catalyst was reoxidized more easily in the presence of water than the unpromoted catalyst. The higher dispersion presented by the $Co/Re/Al_2O_3$ catalyst as well as a direct influence of Re were proposed to explain this effect. Van Berge et al.[158] also performed model experiments using Mössbauer emission spectroscopy and thermo-gravimetry as well as realistic FTS studies to study the oxidation of alumina supported cobalt catalysts. They indicated that oxidation of reduced Co catalysts occurs under realistic FT conditions. They found that the oxidation depends on the P_{H2}/P_{H2O} ratio, and that oxidation is less than complete under certain conditions. Jacobs et al.[161] concluded from XANES studies that for noble metal-promoted Co/Al_2O_3 catalysts, small clusters that interact with the support undergo oxidation in the presence of water and that significant cobalt cluster growth takes place during the initial period of deactivation.

Recent studies on the effect of water have focused on the influence of the type of support as well as the influence of cobalt cluster size on the reaction. Storsaeter et al.[135] have studied the effect of water on the activity and selectivity of a series of unpromoted and Re-promoted Co on different supports (Al_2O_3, SiO_2 and TiO_2) in a

fixed bed reactor (210°C and 20 bar). They observed an increased in C_{5+} selectivity and a decrease in CH_4 selectivity after water addition for all the catalysts. They found that Co/Al_2O_3 and $Co/Re/Al_2O_3$ catalysts deactivate when water is added during FT. For silica supported catalysts (unpromoted and Re-promoted), they observed an increased rate after water addition and a rapid deactivation for these catalysts was observed at high concentrations of H_2O. Similar behaviour was observed with titania supported catalysts with the difference that at high water concentrations these catalysts do not permanently deactivate. They proposed that for the Al_2O_3-supported catalysts, the deactivation was mainly due to surface oxidation or oxidation of highly dispersed phases interacting with the support and for SiO_2–supported catalysts the deactivation was due to formation of Co silicates in the presence of water. No significant deactivation occurred for TiO_2 supported catalysts. They also concluded that the effect of water could be due to differences in Co cluster size on the various supports. Dalai et al.[165] have recently studied water effects on Co supported on narrow and wide-pore silica using a continuous stirred tank reactor (CSTR). The water addition was achieved by replacement of an equivalent amount of inert gas by water so that all other reaction conditions remained the same, during and after water addition. They indicated that the water effects are influenced by the pore size of the silica support. Water addition up to 20 vol.% did not significantly alter the CO conversion in catalysts with Co average cluster sizes larger than the average pore diameter of the silica support. They concluded that for the silica support, the

beneficial effect on CO conversion mainly occurs when the cobalt cluster is small enough to be located inside the silica pores.

Most studies have reported a decrease of CH_4 selectivity and an increase in C_{5+} selectivity and olefin content upon water addition during FTS [89, 135, 146-150, 152, 157, 159, 162, 164, 166]. It has been proposed that water inhibits the secondary hydrogenation reactions, especially of α-olefins [89, 147, 159, 166]. Schulz et al.[164] also suggested that for the catalysts containing smaller Co particles (< 100 μm) used in FTS processes, there may be selective inhibition of individual reaction routes by water (e.g. inhibition of product desorption and olefin readsorption).

1.10 Scope of this study

Reports in the literature have indicated that the effect of water on Co FT catalyst depends on the type of support used. Water was believed to destroy the SMSI on titania supported cobalt catalysts resulting in an increase of activity [146, 148]. However less is known about the effect of other oxygen containing compounds on the Co/TiO_2 system. In the present study, the effect of ethanol addition to the reactor feed in the FT reaction was investigated. This was achieved by a combination of thermodynamic predictions, TPR and XRD analysis as well as FTS reactor studies. Results are presented in Chapter 3.

Studies on the effects of cobalt precursors reported in the literature have been quite disparate and issues relating to the effect of the *counterion* have not been studied in a systematic manner. In the present work the effect of chain length of cobalt carboxylates as precursor on cobalt FT catalysts have been studied using alumina as a support. TPR, XRD, TGA, H_2 chemisorption and O_2 titration have been used in combination with FT catalyst evaluation studies to evaluate this effect. Results are presented in Chapter 4.

Despite the abundant reports on the effect of noble metals on supported cobalt catalyst systems reported in the literature, to the best of our knowledge no effect of gold on these systems have been reported. Here, the effect of gold doping on cobalt FT catalysts supported on titania (Chap 5), silica (Chap 6) and alumina (Chap 7) have been studied using TPR, XRD, BET, XPS and reactor testing.

References

1 G. Olive-Henrichi and S. Olive, *in The chemistry of the metal-carbon bond – vol 3*, Hertley and Patai (Eds.), John Wiley and Sons, New York, 1985.

2 P. Sabatier and J.B. Senderens, *Hebd. Seances Acad. Sci.* 134 (1902) 514, 680.

3 a BASF, *German Patent,* (1913) 293, 787.; b BASF*, German Patent,* (1914) 295, 202.; c BASF*, German Patent,* (1914) 295, 203.

4 F. Fischer and H. Tröpsch, *Brennstoff. Chem.*, 4 (1923) 276.

5 F. Fischer and H. Tröpsch, *German Patent*, (1925) 484,337.

6 F. Fischer and H. Tröpsch, *Brennstoff. Chem*., 7 (1926) 97.

7 R.B. Anderson, *The Fischer-Tröpsch Synthesis*, *Academic Press. Inc,* 1984.

8 R.B. Anderson, in *Catalysis* Vol. 4*,* P.H. Emmet (Ed.), Von Norstand – Reinhold, New Jersey, 1956.

9 H. Pichler, *Brennstoff. Chem*., 19 (1938) 226.

10 M.E. Dry, *Catal. Today.* 71 (2002) 227.

11 M.E. Dry, in *Applied Industrial Catalysis* – Vol. 2, Samuel, K.M. et al., (Eds.) 1983.

12 a Post, M.F.M. *Shell International Research, Eur Pat*, EP 0,174,696 (1985). b Haggin, *J. Chem. Eng. News*, 27 (1990) 35.

13 P.C. Keith, *Oil Gas J*. 45 (1946) 102.

14 M.E. Dry, *Cat. Lett.* 7 (1990) 241.

15 H. Kolbel, P. Ackermann, F. Engelhart, *Erdol u. Khole* 9 (1956) 153, 225, 303.

16 M.E. Dry, in: J.R. Anderson, M. Boudart, (Eds.), *Catalysis Science and Technology*, Vol. 1, Springer, Berlin, 1981, p 159.

17 R.L. Espinoza, A.P. Steynberg, B. Jager, A.C. Vosloo, *Appl. Catal. A:* General 186 (1999) 13.

18 C.M. Eidt, R.F. Bauman, B. Eisenberg, J.M. Hochman, G.C. Lahn, in : *Proceedings of the 14th World Petroleum Congress, Wiley, New York*, Vol. 1, p. 249, John Wiley and Sons, UK, 1994.

19 C.N. Satterfield, G.A. Huff, and J.P. Longwell, *Ind. Eng. Chem. Process. Dev*., 21,3 (1982) 466.

20 R.J. Madon and W.F. Taylor, *J. Catal.* 69 (1981) 41.

21 N.O. Egiebor, W.C. Cooper and B.W. Wojciechowski, *Can. J. Chem. Eng*. 63 (1985) 826.

22 R.A. Dictor, and A.T. Bell, *Ind. Eng. Chem. Process. Dev.*, 22,4 (1983) 678.

23 V. Ponec, *Coal Science*, 3 (1984) 1.

24 G. Henrichi-Olive, S. Olive, *Angew*. *Chem. Int. Ed. Engl*. 15 (1976) 136.

25 C.N. Satterfield, G.A. Huff, *J. Catal.* 73 (1982) 187.

26 P.B. Pannell, C.L. Kibby, K.S. Chung, *Proceedings of the Advances in Catalytic Chemistry*, vol. II, Salt Lake City, UT, May 18-21, 1982.

27 H. Pichler, H. Schulz, M. Elstner, *Brennst. Chem.* 48 (1967) 78.

28 H.E. Atwood, C.O. Bennett, *Ind. Eng. Chem. Process. Des. Dev.* 18 (1979) 163.

29 R.J. Madon and W.F. Taylor, *J. Catal.* 69 (1981) 32.

30 L. Konig, G. Gaube, *Chem. Ing. Techn.* 55 (1983) 14.

31 G.A. Huff, C.N. Satterfield, *J. Catal.* 85 (1984) 370.

32 E. Iglesia, S.C. Reyes, R.J. Madon, *J. Catal.* 129 (1991) 238.

33 E.W. Kuipers, C. Scheper, J.H. Wilson, I.H. Vinkenburg, H. Oosterbeek, *J. Catal.* 158 (1996) 288.

34 B. Shi and B.H. Davis, *Appl. Catal. A*: General 277 (2004) 61.

35 M.E. Dry, *Ind. Chem. via C_1 process*, 2 (1987) 24.

36 G.Y. Chai and J.L. Falconer, *J. Catal.* 93 (1985) 152.

37 M.A. Vannice, *J. Catal.* 37 (1975) 449.

38 M.A. Vannice, *J. Catal.* 50 (1977) 228.

39 M.E. Dry, *J. Mol. Catal.* 17 (1982) 133.

40 M.E. Dry, *Appl. Catal. A*: General 138 (1996) 319.

41 P.D. Caesar, J.A. Brennan, W.E. Garwood and J. Ciric, *J. Catal.* 56 (1979) 274.

42 M.E. Dry and H.B. Erasmus, *Ann. Rev. Energy*, (1987) 1.

43 M. Jonardanarao, *Ind. Eng. Chem. Res*. 29 (1990) 1735.

44 V.U.S. Rao, G.J. Stiegel, G.J. Cinquegrane and R.D. Strvastava, *Fuel Proc. Tech.*, 30 (1992) 83.

45 H. Schulz, *Appl. Catal. A*: General 186 (1999) 3.

46 G.C. Bond, *Academic Press, Inc*., New York. N.Y., 192, pp. 38 - 42.

47 M.A. Vannice, *J. Catal.* 40 (1975) 129.

48 G.C.A. Schuit and L.L. van Reijen, *Adv. Cat.* 10 (1958) 242.

49 G.C. Bond, *Trans. Faraday Soc*. 2 (1956) 1235.

50 R.P. Eischens and W.A. Pliskin, *Adv. Cat.* 10 (1958) 2.

51 C.E. O'Neill, D.J.C. Yates, *J. Phys. Chem*. 65 (1961) 901.

52 W.F. Taylor, D.J.C Yates, and J.H. Sinfelt, *J. Phys. Chem.* 68 (1964) 2962.

53 S.J. Tauster, S.C. Fung, and R.L. Garten. *J. Am. Chem. Soc.* 100 (1978) 170.

54 S.J. Tauster, S.C. Fung, *J. Catal.* 55 (1978) 29.

55 J.A.Horsley, *J. Am. Chem. Soc*. 101 (1979) 2870.

56 S.J. Tauster, S.C. Fung, R.T.K. Baker, and J.A. Horsley, *Science* 211 (1981) 1121.

57 G.B. Raupp, J.A. Dumestic, *J. Phys. Chem.* 88 (1984) 660.

58 J. Santos, J. Phillips, J.A. Dumestic, *J. Catal.* 81 (1983) 147.

59 M. Del Arco, V. Rives, *Mater, J. Sci.* 21 (1986) 2938.

60 S.W. Ho, J.M. Cruz, M. Houalla, D.M. Hercules, *J. Catal.* 135 (1992) 173.

61 M.A. Vannice and R.L. Garten, *J. Catal.* 56 (1979) 236.

62 M.A. Vannice, *J. Catal.* 44 (1976) 152.

63 C.H. Bartholomew and R.B. Panell, *J. Catal*. 65 (1980) 390.

64 D.L. King, *J. Catal*. 51 (1978) 386.

65 C.H. Bartholomew, R.B. Pannell and J.L. Butler, *J. Catal*. 65 (1980) 335.

66 R.C. Reuel and C.H. Bartholomew, *J. Catal.* 85 (1984) 78.

67 D.J. Duvenhage, N.J. Coville, *Appl. Catal. A*: General 233 (2002) 63.

68 J. Li, N.J. Coville, *Appl. Catal*. *A*: General 181 (1999) 201.

69 J. Li, N.J. Coville, *Appl. Catal*. A: General 208 (2001) 177.

70 J. Li, G. Jacobs, Y. Quig, T. Das, B.H. Davis, *Appl. Catal*. A: General 223(2002) 195.

71 J. Li, Y. Jacobs, T. Das, B.H. Davis, *Appl. Catal*. A: General 223 (2002) 255.

72 K. Sato, Y. Inoue, I. Kojima, E. Miyazaki, I. Yasumori, *J. Chem. Soc., Faraday Trans*. 1 80 (1984) 841.

73 B. Jongsomjit, C. Sakdamnuson, J.G. Good Jr, and P. Praserthdam, *Cat. Lett.* 94 (2004) 209.

74 B. Jongsomjit, J. Panpranot, and J.G. Goodwin Jr., *J. Catal*. 204 (2001) 98.

75 B. Jongsomjit and J.G. Goodwin Jr, *Catal. Today*. 77 (2002) 191.

76 B. Jongsomjit, J. Panpranot and J.G. Goodwin Jr., *J. Catal.* 205 (2003) 66.

77 Y. Zhang, D. Wei, S. Hammache and J.G. Goodwin Jr, *J. Catal.* 188 (1999) 281.

78 A. Kogelbauer, J.C. Weber and J.G. Goodwin Jr, *Cat. Lett.* 34 (1995) 269.

79 R.A. Dalla Betta, A.G. Piken and M. Shelef, *J. Catal*. 35 (1974) 54.

80 C.H. Bartholomew, *J. Catal.* 45 (1976) 41.

81 H.H. Nijs and P.A. Jacobs, *J. Catal.* 65 (1980) 328.

82 C.S. Kellner and A.T. Bell, *J. Catal.* 75 (1982) 251.

83 L. Fu and C.H. Bartholomew, *J. Catal*. 92 (1985) 376.

84 M.I. Fernandez, R.A. Guerrero, G.F.J. Lopez, R.I. Rodriguez, C.C. Moreno, *Appl. Catal.* 14 (1985) 159.

85 S.W. Ho, M. Houalla and D.M. Hercules, *J. Phys. Chem*. 94 (1990) 6396.

86 B.G. Johnson, C.H. Bartholomew, D.W. Goodman, *J. Catal.* 128 (1991) 231.

87 E. Iglesia, S.L. Soled, R.A. Fiato, G.H. Via, *Stud. Surf. Sci. Catal*. 81 (1994) 433.

88 E. Iglesia, S.L. Soled, R.A. Fiato, *J. Catal.* 137 (1992) 212.

89 E. Iglesia, *Appl. Catal.* A 161 (1997) 59.

90 B. Ernst, C. Hilaire, A. Kiennemann, *Catal. Today*. 50 (1999) 413.

91 A.Y. Khodakov, A. Griboval-Constant, R. Bechara, V.L. Zholobenko, *J. Catal*. 206 (2002) 230.

92 A. Martinez, C. Lopez, F. Marquez and I.J. Diaz, *J. Catal.* 220 (2003) 486.

93 W.P. Ma, Y.J. Ding and L.W. Lin, *Ind. Eng. Chem. Res*. 43 (2004) 2391.

94 S. Storsaeter, B. Tϕtdal, J.C. Walmsley, B.S. Tanem, A. Holmen, *J. Catal*. 236 (2005) 139.

95 E. Kikuchi, R. Sorita, H. Takahashi and T. Matsuda, *Appl. Catal. A*: General 186 (1999) 121.

96 D. Song and J. Li, *J. Mol. Catal*. *A*: Chemical 247 (2006) 206.

97 A. Barbier, A. Tuel, I. Arcon, A. Kodre and G.A. Martin, *J. Catal*. 200 (2001) 106.

98 G.L. Bezemer, J.H. Bitter, H.P.C.E. Kuipers, H. Oosterbeek, J.E. Holewijn, X. Xu, F. Kapteijn, A.J. van Dillen and K.P. de Jong, *J. Am. Chem. Soc*. 128 (2006) 3956.

99 K. Takeuchi, T. Matsuzaki, H. Arakawa, T. Hanaoka and Y. Sugi, *Appl. Catal.* 48 (1989) 149.

100 K. Takeuchi, T. Matsuzaki, T. Hanaoka, H. Arakawa and Y. Sugi, *J. Mol. Catal.* 55 (1989) 361.

101 C.H. Bartholomew, *Stud. Surf. Sci. Catal.* 64 (1991) 158.

102 T. Matsuzaki, K. Takeuchi, T. Hanaoka, H. Arakawa and Y. Sugi, *Appl. Catal.* 105 (1993) 159.

103 M.K. Niemela, A.O.I. Krause, T. Vaara, J. Lathinen, *Top. Catal*. 2 (1995) 45.

104 M.K. Niemela, A.O.I. Krause, T. Vaara, J.J. Kiviaho, M.K.O. Reinikainen, *Appl. Catal. A*: General 147 (199) 32.

105 M.P. Rosynek and C.A. Polansky, *Appl. Catal.* 73 (1991) 97.

106 T. Matsuzaki, K. Takeuchi, T. Hanaoka, H. Arakawa, Y. Sugi, *Catal. Today*. 28 (1996) 251.

107 S. Sun, N. Tsubaki, K. Fujimoto, *Appl. Catal. A*: General 202 (2000) 121.

108 Y. Wang, M. Noguchi, Y. Takahashi, Y. Ohtsuka, *Catal. Today*. 68 (2001) 3.

109 J. Panpranot, S. Kaewkun, P. Praserthdam and J.G. Goodwin Jr, *Cat. Lett.* 91 (2003) 95.

110 J.S. Girardon, A.S. Lermontov, L. Gengembre, P.A. Chernavskii, A. Griboval - Constant, A.Y. Khodakov, *J. Catal.* 230 (2005) 339.

111 E. van Steen, G.S. Sewel, R.A. Makhote, C. Micklethwaite, H. Manstein, M. de Lange, C.T. O'Connor, *J. Catal.* 162 (1995) 220.

112 H. Ming, B.G. Baker, *Appl. Catal.* 123 (1995) 23.

113 J. van der Loosdrecht, M. van der Haar, A.M. van der Kraan, A.J. van Dillen, J.W. Geus, *Appl. Catal. A*: General 150 (1997) 365.

114 M. Kraun and M. Baerns, *Appl. Catal.* 186 (1999) 189.

115 L. Guczi, T. Hoffer, Z. Zsoldos, S. Zyade, G. Maire and F. Garin, *J. Phys. Chem*. 95 (1991) 802.

116 Z. Zsoldos, T. Hoffer and L. Guczi, *J. Phys. Chem*. 95 (1991) 795.

117 Z. Zsoldos and L. Guczi, *J. Phys. Chem*. 96 (1992) 9393.

118 S. Zyade, F. Garin and G. Maire, *New J. Chem.* 11 (1987) 429.

119 M.J. Dees and V. Ponec, *J. Catal.* 119 (1989) 376.

120 D. Schanke, S. Vada, E.A. Blekkan, A.M. Hilmen, A. Hoff and A. Holmen*, J. Catal.* 156 (1995) 85.

121 A. Kogelbauer, J.G. Goodwin Jr and R. Oukaci*, J. Catal.* 160 (1996) 125.

122 S.A.Hosseini, A. Taeb, F. Feyzi, *Catal. Comm.* 6 (2005) 233.

123 S.A. Hosseini, A. Taeb, F. Feyzi, F. Yaripour, *Catal. Comm*. 5 (2004) 137.

124 J. Dullac, *Bull. Soc. Fr. Mineral. Crystallogr*. 92 (1969) 487.

125 K. Nagaoka, K. Takanabo and K. Aika, *Appl. Catal.* 268 (2004) 151.

126 A. Sarkany, Z. Zsoldos, G. Stefler, J.W. Hightower, and L. Guczi, *J. Catal*. 157 (1995) 179.

127 L. Guczi, Z. Schay, G. Stefler, F. Mizukami, *J. Mol. Catal*. *A*: Chemical 141 (1999) 177.

128 L. Guczi, L. Borko, Z. Schay, D. Bazin, F. Mizukami, *Catal. Today*. 65 (2001) 51.

129 N. Tsubaki, S. Sun, and K. Fujimoto, *J. Catal.* 199 (2001) 236.

130 A.F. Carlsson, M. Naschitzki, M. Baumer, and H.J. Freund, *J. Phys. Chem. B* 107 (2003) 778.

131 T.K. Das, G. Jacobs, P.M. Patterson, W.A. Conner, J. Li, B.H. Davis, *Fuel* 82 (2003) 805.

132 L. Guczi, D. Bazin, I. Kovacs, L. Borko, Z. Schay, J. Lynch, P. Parent, C. Lafon, G. Stefler, Z. Koppany, I. Sajo, *Top. Catal.* 20 (2002) 129.

133 M. Ronning, D.G. Nicholson, A. Holmen, *Catal. Lett.* 72 (2001) 141.

134 G. Jacobs, J.A. Chaney, P.M. Patterson, T.K. Das, B.H. Davis, *Appl. Catal. A:* General 264 (2004) 203.

135 S. Storsaeter, *ϕ.* Borg, E.A. Blekkan, A. Holmen, *J. Catal.* 231 (2005) 405.

136 M. Haruta, *Catal. Today.* 36 (1997) 153.

137 M.A.P. Dekkers, M.J. Lippits, B.E. Nieuwenhuys, *Catal. Today.* 54 (1999) 381.

138 W.S. Epling, G.B. Hoflund, J.F. Weaver, S. Tsubota, and M. Haruta, *J. Phys. Chem.* 100 (1996) 9929.

139 M. Haruta, N. Yamada, T. Kabayashi, S. Lijima, *J. Catal.* 115 (1989) 301.

140 M. Haruta, S. Tsubota, T. Kabayashi, H. Kageyama, M.J. Genet, B. Delmon, *J. Catal.* 144 (1993) 175.

141 R.J.H. Grisel, B.E. Nieuwenhuys, *Catal. Today.* 64 (2001) 69.

142 B. Chen, C. Bai, R. Cook, J. Wright, C. Wang, Catal. *Today.* 30 (1996) 15.

143 H. Wang, J. Wang, W.D Xiao, W.K. Yuan, *Powd. Techn.* 111 (2000) 175.

144 J.R. Meller, A.N. Palazov, B.S. Grigorova, J.F. Greyling, K. Reddy, M.P. Letsoalo, J.H. Marsh, *Catal. Today.* 72 (2002) 145.

145 L. Leite, V. Stonkus, L. Llieva, L. Plyasova, T. Tabakova, D. Andreeva, E. Lukevics, *Catal. Comm*. 3 (2002) 341.

146 J.C. Kim, *U.S. patent* No 5227407 (1993) to Exxon Res. Eng. Co.

147 E. Iglesia, S.C. Reyes, R.J. Madon, S. Soled, *Adv. Catal.* 39 (1993) 221.

148 J.C. Kim, *Eur. Appl. patent* No 89304092.3 (1994), to Exxon Res. Eng. Co.

149 H. Schulz, E. van Steen, M. Claeys, *Stud. Surf. Sci. Catal.* 81 (1994) 455.

150 S. Krishnamoorthy, M. Tu, M.P. Ojeda, D. Pinna, E. Iglesia, *J. Catal.* 211 (2002) 422.

151 J. Li, G. Jacobs, T. Das, Y. Zhang, B.H. Davis, *Appl. Catal*. *A*: General 236 (2002) 67.

152 C.J. Berthole, C.A. Mims, G. Kiss, *J. Catal.* 210 (2002) 84.

153 F.M. Gottschalk, R.G. Copperthwaite, M. van der Riet, G.J. Hutchings, *Appl. Catal.* 38 (1988) 103.

154 D. Schanke, A.M. Hilmen, E. Bergene, K. Kinnari, E. Rytter, E. Adnanes, and A. Holmen, *Catal. Lett.* 34 (1995) 269.

155 G.P. Huffmann, N. Shah, J. Zhao, F.E. Huggins, T.E. Hoost, S. Halvorsen, J.G. Goodwin Jr, *J. Catal.* 151 (1995) 17.

156 M. Rothaemel, K.F. Hanssen, E.A. Blekkan, D. Schanke, A. Holmen, *Catal. Today.* 38 (1997) 79.

157 A.M. Hillmen, D. Schanke, K.F. Hanssen, A. Holmen, *Appl. Catal. A*: General 186 (1999) 169.

158 P.J. van Berge, J. van de Loosdrecht, S. Barradas, A.M. van der Kraan, *Catal. Today.* 58 (2000) 321.

159 A.M. Hillmen, O.A. Lindvag, E. Bergene, D. Schanke, S. Eri, A. Holmen, *Stud. Surf. Sci. Catal.* 136 (2001) 295.

160 J. Li, X. Zhan, Y. Zhang, G. Jacobs, T. Das, B.H. Davis, *Appl. Catal. A:* General 228 (2002) 203.

161 G. Jacobs, P.M. Patterson, Y. Zhang, T. Das, J. Li, B.H. Davis, *Appl. Catal. A*: General 233 (2002) 215.

162 H. Schulz, M. Claeys, S. Harms, *4th Int. Natural Gas Conversion Symp, Kruger National Park, South Africa,* 19 – 23 November 1995.

163 J.K. Minderhoud, M.F.M. Post, S.T. Sie, *Eur. Appl. patent* No 83201557.2 (1988), to Shell Int Res.

164 H. Schulz, M. Claeys, S. Harms, *Stud. Surf. Sci. Catal.* 107 (1997) 193.

165 A.K. Dalai, T.K. Das, K.V. Chaudhari, G. Jacobs, B.H. Davis, *Appl. Catal*. *A*: General 289 (2005) 135.

166 C. Aaserud, A.M. Hilmen, E. Bergene, S. Eri, D. Schanke, A. Holmen, *Catal. Lett.* 94 (2004) 171.

Chapter 2

Experimental

2.1 Introduction

The performance of the FT reaction at the laboratory scale demands a cautious handling of various parameters which can affect the final outcome of the experiment. The main problems associated with the FT reaction include the product analysis. The system is complex as it involves a large spectrum of products usually distributed in the gas, liquid and solid phases. The process mass balance is usually complicated as the collection of reaction products is not easily done without disturbing the reaction conditions and usually some of the products accumulate in the system. Thus, special attention is needed in order to ensure that the experimental procedure does not contribute systematic errors to the analysis of the results. Based on the studies of accumulated products in FT reactions conducted in a continuously stirred autoclave reactor, Shi and Davis [1] have proposed that the apparent products of the FT reaction is a mixture of freshly produced FT products and the products left in the reactor. Their results predicted that the correct α-value of hydrocarbon greater than C_8 and the paraffin to olefin ratios will be smaller than the values reported and have indicated that it is necessary to find a way to evaluate or eliminate the contribution of the products left in the reactor. Some studies performed in this field in the past have avoided this problem by reporting on results obtained during the first few hours of reaction or by examining the gas phase product only [2].

In this section, we describe the general procedure that was followed to achieve catalyst testing for the FT reaction. As many experiments were performed using different systems in this study, this section only presents a general procedure and description of equipment. The specific details on the experimental data measurement will be described for each system used in the appropriate chapter.

We also describe the principles and methods that were used to characterize the catalysts. Numerous tools have been developed in the past years to characterize the physical and chemical properties of supported catalysts. Hence, the design of supported catalysts and the interpretation of phenomena occurring in the catalyst has become a feasible task.

2.2 Catalyst preparation

The catalysts used in this thesis were prepared by the incipient wetness impregnation method (chapter 3 and 4) and by the deposition precipitation (or co-precipitation) method (chapter 5 – 7).

The catalyst supports used were Degussa Titania (TiO_2) P25, SA = 50 m^2g^{-1} (Chapter 3 and 5), Laporte γ-alumina, SA = 292 m^2g^{-1}(Chapter 4), γ-Alumina, Condea Vista Catalox B, S.A = 150 m^2g^{-1} (Chapter 6) and Matrex silica, SA = 300 m^2g^{-1} (chap 7).

The metal precursors used were Aldrich $Co(NO_3)_2.6H_2O$ (chap 3 and chap 5 – 7), Co carboxylates that were prepared in our laboratory (chap 4) and Aldrich $HAuCl_4.3H_2O$ (chap 5 – 7).

2.3 Catalyst evaluation

2.3.1 Apparatus

The catalysts were evaluated for activity and selectivity for the FT reaction using two reactor systems. A set of experiments was done in a stirred basket reactor system and the second set of experiments was achieved in a plug flow reactor (PFR) system. The two reactor systems are shown in Figures 2.1 and 2.2 respectively.

Stirred basket reactor system

System description. The FT reaction was carried out in the same reactor described by Price [2]. The basic design of this reactor was developed from that of the "Berty" reactor [3]. The reactor mainly consisted of a stirred, cruciform shaped catalyst basket fitted into a cylindrical reactor chamber. Figure 2.3 shows the schematic of the reactor while Figures 2.4 and 2.5 show the construction details of the reactor chamber and the catalyst basket respectively. In order to create a good turbulence in the reactor

a four bladed propeller was mounted on either side of the catalyst with the pitch set in opposite directions. Phosphor-bronze bushes were used to support the propeller shaft, and thus the set-up required no lubrication. The propeller shaft was coupled to a Parr magnedrive screwed into the top flange of the reactor and which was belt driven by an externally mounted universal electric motor.

Stirring speeds greater than 780 rpm were shown to lead to CSTR behaviour in the reactor [2]. Thus, stirring speeds between 840 and 960 rpm were used for the experiments.

The supply of heat to the reactor was achieved by a heating jacket connected to a temperature controller and mounted around the reactor outer casing. A thermocouple was placed near the centre of the reactor to record the temperature in the reactor chamber.

The reactor feed was a pre-mixed synthesis gas (10% N_2, 30% CO, 60% H_2) and was used for all the runs except for runs described in chapter 3 where ethanol was also added to the feed. A by-pass line was used to allow a direct GC analysis of the feed for calibration purposes. The synthesis gas was introduced through the reactor and then allowed to flow through the catalyst bed and then passed through a hot trap maintained at 150˚C for wax collection. This was followed by a cold trap maintained at room temperature for the liquid (oil and aqueous) fraction collection.

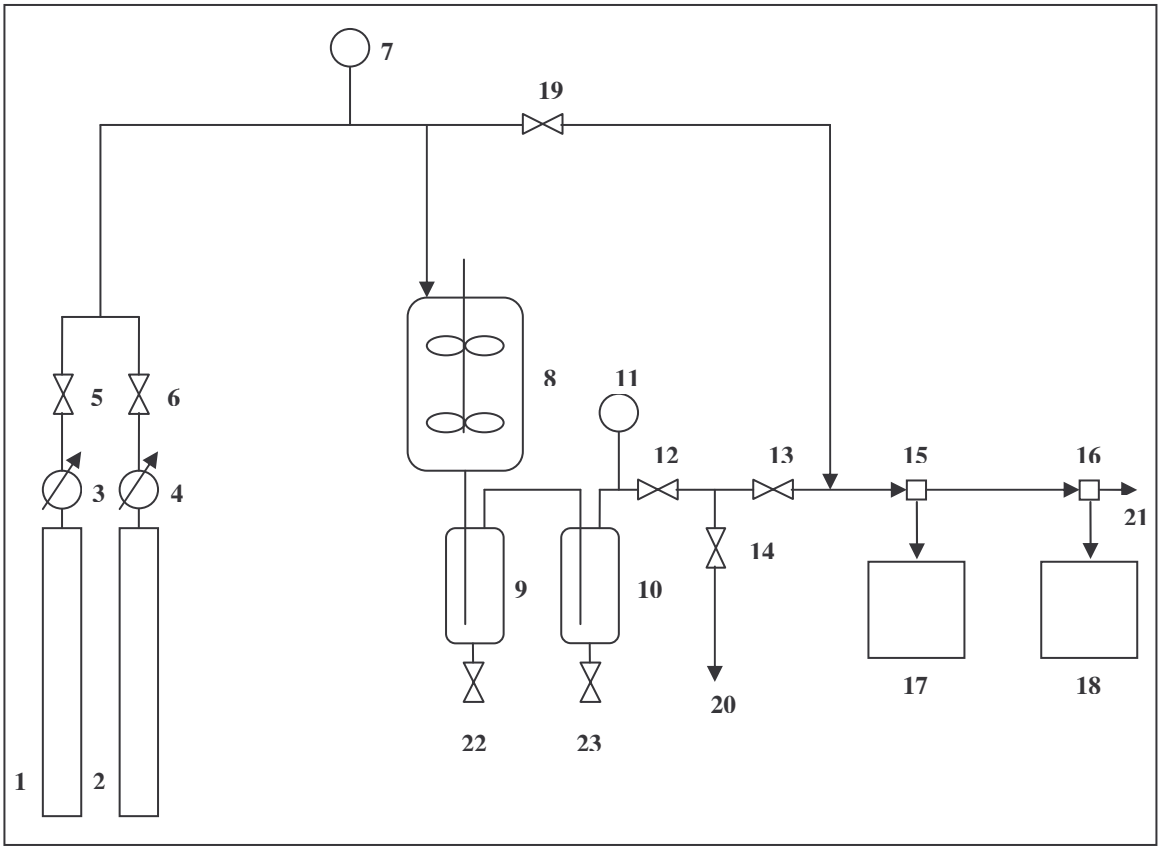

Figure 2.1 *Stirred basket reactor set up*

1: Syngas cylinder;
2: H_2 cylinder;
3 and **4**: Pressure regulators;
5, 6, 19, 22, 23: Shut off valves;
7 and **11**: Pressures gauges;
8: Reactor;
9: Wax trap;
10: Liquid trap;
12: Needle valve;
13 and **14**: Solenoid valves;
15 and **16**: GC sampling valves;
17: GC (FID);
18: GC (TCD);
20, 21: Gas venting

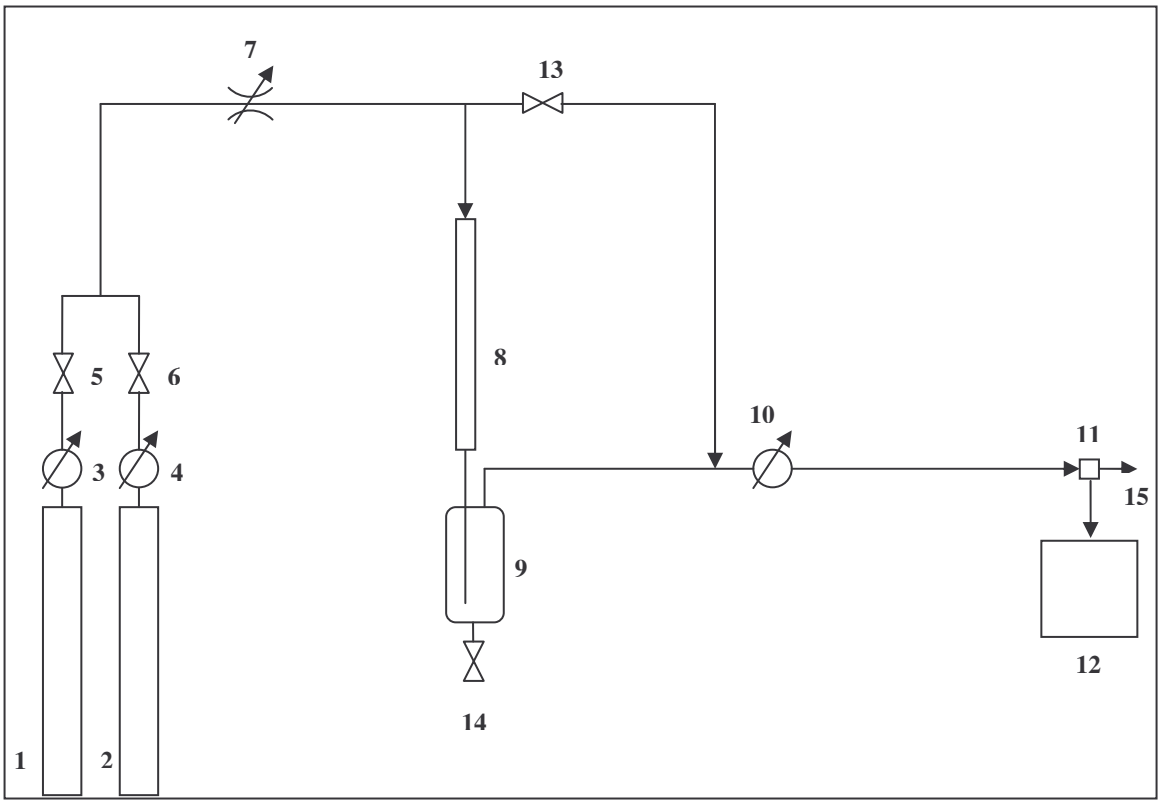

Figure 2.2 *Plug flow reactor set up*

1: Syngas cylinder;
2: H_2 cylinder;
3 and **4**: Pressure regulators;
5, 6, 13, 14: Shut off valves;
7: Mass flow controller;
8: Reactor;
9: Liquid trap;
10: Back pressure regulator;
11: GC sampling valve;
12: GC (TCD and FID);
15: Gas venting.

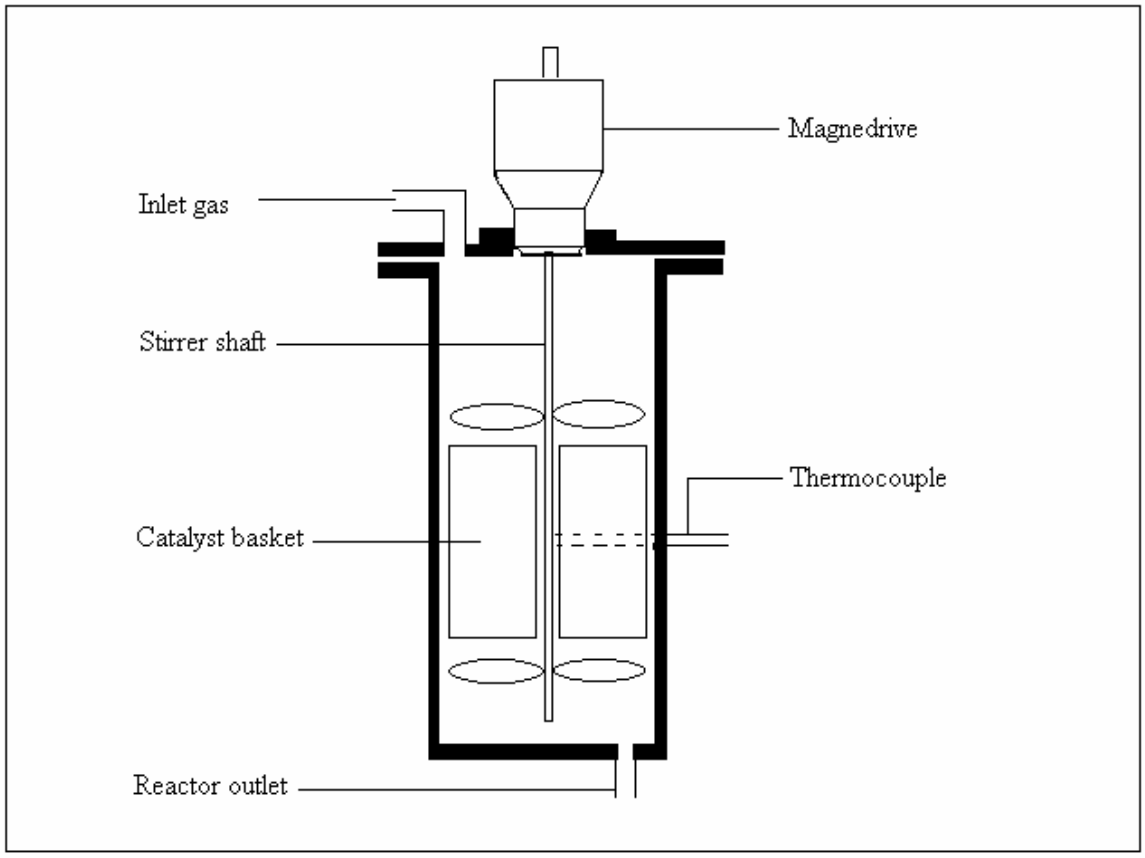

Figure 2.3 *Schematic of the stirred basket reactor*

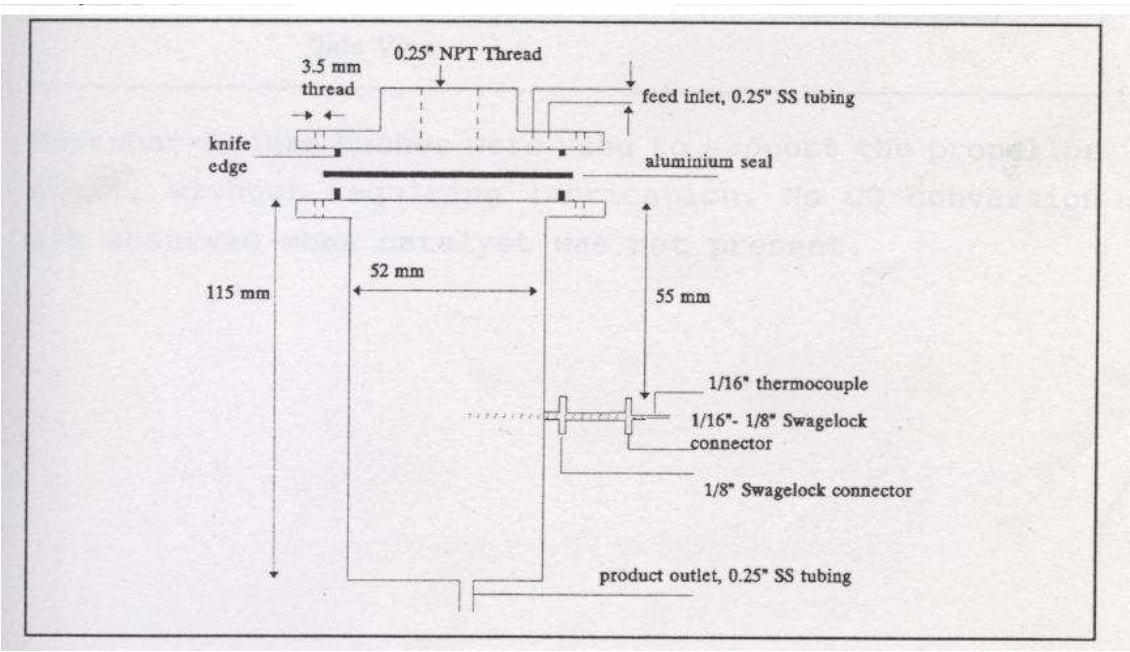

Figure 2.4 *Construction details of the reactor chamber*

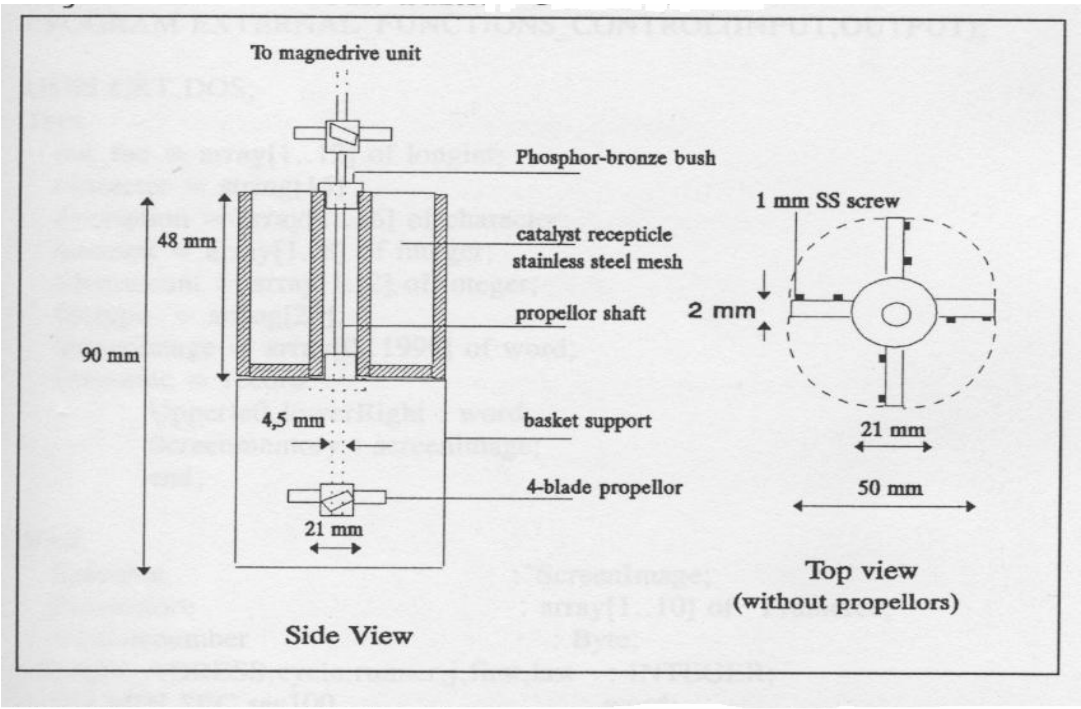

Figure 2.5 *Construction details of the catalyst basket*

The operating pressure in the reactor was maintained at 8 bar for all the runs done on this reactor system, using a pressure regulator on the gas cylinder and a needle valve at the reactor exit. The needle valve was also used to control the gas space velocity in the reactor and to de-pressurize the outlet gas stream before the GCs. Two pressure indicators were used, one at the reactor feed and another at the reactor exit, to check the total pressure in the reactor. Two solenoid valves were mounted after the needle valve and they automatically directed the reactor outlet gas to the atmosphere or the GCs for analysis. The set of solenoid valves directed the gas to the GCs only for a short period of time that was necessary for flushing out the residual gas in the sampling loops of the GC in order to allow for further sampling. For the rest of the time the outlet gas was vented to the atmosphere to keep the sampling line clean. A new sample was analyzed every two hours.

Product analysis. The gas analysis was done online using two GCs, one with a flame ionization detector (FID) and the other with a thermal conductivity detector (TCD).
A Poropak-Q (PPQ) column was used to separate hydrocarbons from C_1 to C_9 while a ZB-1 capillary column which was able to separate from C_4 to C_{15} hydrocarbons was used to analyze C_{9+} hydrocarbons. The C_7 product was detected with a good reproducibility in both columns and therefore the C_7 area (PPQ)/C_7 area (capillary) ratio was used to combine the data from two chromatograms into one set of data. The GC, equipped with the TCD, was used for the analysis of the inorganic gases H_2, He, N_2, CO on a carbosieve S-II packed column. The actual molar composition of the gas

was determined by using calibration data and relative response factors. The calibration gas used contained 2.5% CH_4, 0.2% C_2H_4, 0.5% C_2H_6, 10% CO, 5% CO_2, balance Ar.

The molar percentage of a compound θ in the gas was calculated as:

$$\%\theta_{gas} = \left(\frac{A_{\theta.gas}}{A_{\theta.cal}} \right) \times \%\theta_{cal.} \qquad 2.1$$

where: $\%\ \theta_{gas}$ = molar percentage of compound θ in the analyzed gas;

$A_{\theta\ gas}$ = integrated area of the GC peak corresponding to the compound θ in the analyzed gas;

$A_{\theta\ cal}$ = integrated area of the GC peak corresponding to the compound θ in the calibration mixture;

$\%\theta_{cal.}$ = molar percentage of compound θ in the calibration mixture.

For compounds whose calibration data could not be obtained directly from the calibration mixture, calibration data of a reference compound and relative molar response factors were used. The following expression was used:

$$\%\theta_{gas} = \left(\frac{A_{\theta.gas}}{A_{\alpha.cal}} \right) \times \%\alpha_{cal.} \times RF_{\theta.\alpha} \qquad 2.2$$

where: $\%\alpha_{cal.}$ = molar percentage of the reference compound α in the calibration mixture; $A_{\alpha\ cal}$ = integrated area of the GC peak corresponding to the reference compound α in the calibration mixture and $RF_{\theta\alpha}$ = relative response factor of the compound θ with respect to the reference compound α.

C_2H_4 was used as reference for olefins while C_2H_6 was used as reference for paraffins.

Molar response factors for hydrocarbon products are presented in Table 2.1 [2].

The analysis of the oil and wax fractions was carried out using an off-line GC with a flame ionisation detector on a BP-5 capillary column. For the analysis of these condensed phases a mass composition was directly obtained from the GC peak area percentages as the mass response factors were around one.

***Mass balance calculations*.** The configuration of the experimental set up used in this study (Figure 2.1) allows setting the exit volumetric flow-rate from which the inlet flow rate can be calculated. N_2 was used in the reactor feed to serve as an internal standard. As it is an inert gas during the FT reaction, N_2 is only present in the feed stream and in the reactor outlet gas stream. The N_2 balance across the reactor is therefore expressed as:

Table 2.1 Molar response factors for hydrocarbon products

Carbon number	Olefin	Paraffin
2	1.00	1.00
3	0.70	0.74
4	0.78	0.55
5	0.47	0.47
6	0.40	0.40
7	0.35	0.35
8	0.32	0.32
9	0.28	0.28
10	0.24	0.24
11	0.21	0.21
12	0.19	0.19
13	0.18	0.18
14	0.17	0.17
15	0.15	0.15

$$F_{in} \times X_{N_2 in} = F_{out} \times X_{N_2 out} \qquad 2.3$$

where: F_{in} = total molar flowrate [moles/min] of the reactor feed;

F_{out} = total molar flowrate [moles/min] of the reactor outlet gas stream;

$X_{N2\ in}$ = molar fraction of nitrogen in the reactor feed;

$X_{N2\ out}$ = molar fraction of nitrogen in the reactor outlet gas.

The rate of CO conversion can be calculated as follows:

$$-r_{CO} = \frac{F_{CO,in} - F_{CO,out}}{m_{cat}} \qquad 2.4$$

where: $F_{CO,in}$ = molar flowrate [moles/min] of CO in the reactor feed;

$F_{CO,in}$ = molar flowrate [moles/min] of CO in the reactor outlet gas;

$m_{cat.}$ = mass [gram] of catalyst;

r_{CO} = rate of CO conversion [moles.min^{-1}.g$_{cat}^{-1}$]. This rate is multiplied by -1 in (2.4) to report positive values.

$$F_{CO,in} = F_{in} \times X_{CO,in} \qquad 2.5$$

$$F_{CO,out} = F_{out} \times X_{CO,out} \qquad 2.6$$

where $X_{CO,in}$ *and* $X_{CO,out}$ are the CO molar fraction in the reactor feed and outlet gas respectively.

After introducing expressions (2.5) and (2.6) in expression (2.4) and after expressing F_{in} as a function of F_{out} using equation 2.3, the rate of CO conversion rate was expressed as:

$$-r_{CO} = \frac{F_{out} \times [X_{CO,in} \times (\frac{X_{N_2,out}}{X_{N_2,in}}) - X_{CO,out}]}{m_{cat}} \qquad 2.7$$

In this thesis expression (2.7) was used to calculate the rate of CO conversion directly as $X_{CO,in}$ and $X_{N2,\ in}$ were known from the pre-mixed gas cylinder and $X_{CO,\ out}$ and $X_{N2,\ out}$ were obtained from the reactor outlet gas analysis. F_{out} was also calculated from the total gas volumetric flowrate at the reactor exit assuming the ideal gas law. In some cases the the rate of CO conversion was further converted to some other units, e.g. $\mu mol.min^{-1}.g_{active\ metal}^{-1}$, etc.

The CO conversion was calculated as follows:

$$\%CO_{conv} = \frac{[X_{CO,in} - X_{CO,out} \times (\frac{X_{N_2,in}}{X_{N_2,out}})] \times 100}{X_{CO,in}} \quad 2.8$$

The rate of formation of a gas product θ_i was calculated as follows:

$$r_{\theta_i} = \frac{F_{out} \times X_{\theta_i,in}}{m_{cat}} \quad 2.9$$

where $r_{\theta i}$ is the rate in mole.min^{-1}.g$_{cat}^{-1}$ and $X_{\theta i}$ the molar fraction of product θ_i in the reactor outlet gas.

The carbon balance was checked as follows:

$$[nC]_{gas.product} + [nC]_{liquid.product} + [nC]_{wax.product} = -r_{CO} \times t \times m_{cat} \quad 2.10$$

where nC represents the total number of moles of carbon contained in a product fraction (gas, liquid or wax) at the end of the mass balance period, *t*.

The error on the carbon balance was calculated as:

$$\%error = \frac{\{-r_{CO} \times t \times m_{cat} - [nC]_{gas.product} - [nC]_{liquid.product} - [nC]_{wax.product}\} \times 100}{-r_{CO} \times t \times m_{cat}} \qquad 2.11$$

The carbon balance was considered satisfactory when the % error was $\leq 5\%$.

The product selectivity was calculated on moles of carbon basis as follows:

$$Sel(\theta) = \frac{[nC]_{\theta}}{-r_{CO} \times t \times m_{cat}} \qquad 2.12$$

where $Sel(\theta)$ represents the selectivity of product θ and $[nC]_{\theta}$ represents the moles of carbon contained in the product θ.

The Turnover frequency (TOF) was expressed as the number of molecules of CO converted per surface active site per second and was calculated from the rate of CO conversion and the number of accessible metal sites determined by H_2 chemisorption and O_2 titration.

Plug flow reactor system

The FT reaction was carried out in a stainless-steel fixed bed micro-reactor (internal diameter 5 mm) connected to an on-line VARIAN CP-3800 gas chromatograph equipped with two columns mounted in series (a Poropak Q 80 – 100 MESH followed by a 13X molecular sieve; 60 – 80 MESH) and two detectors. The two detectors were a thermal conductivity detector (TCD) for the analysis of the inorganic gases H_2, He, N_2, CO and CO_2 followed by a flame ionisation detector (FID) for the analysis of organic compounds.

The operating pressure was maintained at 20 bar for all the runs done in this reactor system by using a Brooks Model 5850 mass flow controller at the reactor feed and a back pressure regulator at the reactor exit. Only a cold trap maintained at room temperature was used at the exit of the reactor. No hot trap for wax collection was mounted as the testing was done on a small amount of catalyst (0.1 g) and under these conditions no significant amount of wax was collected at the bottom of the reactor. This was because most of the wax that was produced was found in the catalyst bed and on the reactor wall after reaction. The thermocouple was always immersed in the catalyst bed to ensure an effective temperature control. A by-pass of the feed to the GC was also made possible for calibration purposes.

Mass balance calculations were done as described for the stirred basket reactor.

2.4 Catalyst characterization

2.4.1 Catalyst composition

Atomic Absorption (AA) Spectroscopy. Atomic adsorption (AA) spectroscopy was done using a VARIAN 55B Atomic Adsorption spectrometer to verify the Co and Au loadings in the catalysts. The analysis was done using dried catalysts dissolved in aqua regia [3 HCl : 1 HNO_3].

2.4.2 X-ray Analysis

X-ray diffraction (XRD) analysis was done on an ENRAF NONIUS FR590 powder diffractometer to investigate the solid structure of catalysts. A Cu-Kα radiation (30 mA, 40 kV) source was used. The scan was taken from 2θ = 10° to 2θ = 70° with a step width of 2θ = 0.02969°. X-ray photoelectron spectroscopy (XPS) analysis was performed on a KRATOS AXIS ULTRA photoelectron spectrometer to obtain information on the catalyst surface composition, which gave information on the distribution of metallic species on the catalyst support. The binding energies were corrected by setting the oxidic O1s binding energy to 530 eV [4 – 7].

2.4.3 Thermo-gravimetric Analysis (TGA)

The TGA analysis was done on Du Pont 910 Thermogravimetric analyzer to determine the purity of cobalt carboxylates of different chain length used as precursor in the preparation of cobalt catalysts (see chapter 4). The analysis was done in flowing N_2 (40 ml), heating rate 5°C/min and the mass of the sample for analysis was around 50 mg in all experiments. The weight loss was used to calculate the purity of the samples.

2.4.4 Temperature Programmed Reduction (TPR)

The TPR analysis is a powerful tool which is extensively used in heterogeneous catalysis to analyze the reduction behaviour of oxidic catalyst precursors [8]. The principle of this technique consists of submitting a catalyst sample to a linear temperature ramp in a flow of hydrogen while continuously monitoring the hydrogen consumption. The hydrogen is always diluted in an inert gas, usually Ar (5 - 10 % H_2 in Ar) to make the determination of the hydrogen uptake possible by a TCD placed at the reactor exit. Under selected conditions fingerprint profiles are obtained and can be used to study the effect of various parameters like support, promoters, etc. on the catalyst reducibility.

This technique can also be used quantitatively to determine the amount of reducible species in the catalyst and their reduction extent from the integrated hydrogen

consumption. It is to be noted that the quantitative analysis can only be made possible if a calibration of the apparatus has been done with a calibrant whose stochiometry of reaction with hydrogen is known. The shape and position of reduction peaks can give information about the degree of interaction of the oxidic precursor with the support. In some cases the TPR analysis can also be used to determine the oxidation state of some species in the catalyst. To obtain a good reduction profile an optimal combination of operating parameters is needed. The parameters that determine the position and the shape of the peaks are the heating rate β (K/s), the initial amount of metal oxides species in the catalyst n_0 (μmoles), the volumetric flowrate, F, (cm^3 (NTP)/s) of the reducing mixture and the concentration c_0 (μmoles/cm^3) of reactant gas in the gas stream. Monti and Baiker have defined a number K combining these parameters as follows [9]:

$$K = \frac{n_0}{F \times c_0} \qquad 2.13$$

They have suggested that the analysis parameters should be combined in a way to get the number K fall between 55 and 140 s for heating rates of $0.1 \leq \beta \leq 0.3$ K/s.

The TPR analysis has been extensively used in this thesis to study the effect of various factors on the reduction properties of various supported cobalt catalyst. It has also been used to determine the type of Co oxides present in the catalyst after submission to some treatment conditions (see chapter 3).

The equipment used in this study was constructed in our laboratory (figure 2.6). The system mainly comprised of gas selection valves allowing the selection of the gas to be fed to a quartz glass reactor containing some quartz wool to support the catalyst sample and a TCD detector placed at the reactor exit. All piping consisted of 1/8'' stainless steel. A temperature programming unit fine controlled the temperature ramping and the thermocouple was placed on the wall of the reactor at the sample location. The whole unit was computer controlled. The analysis procedure is described in each appropriate chapter.

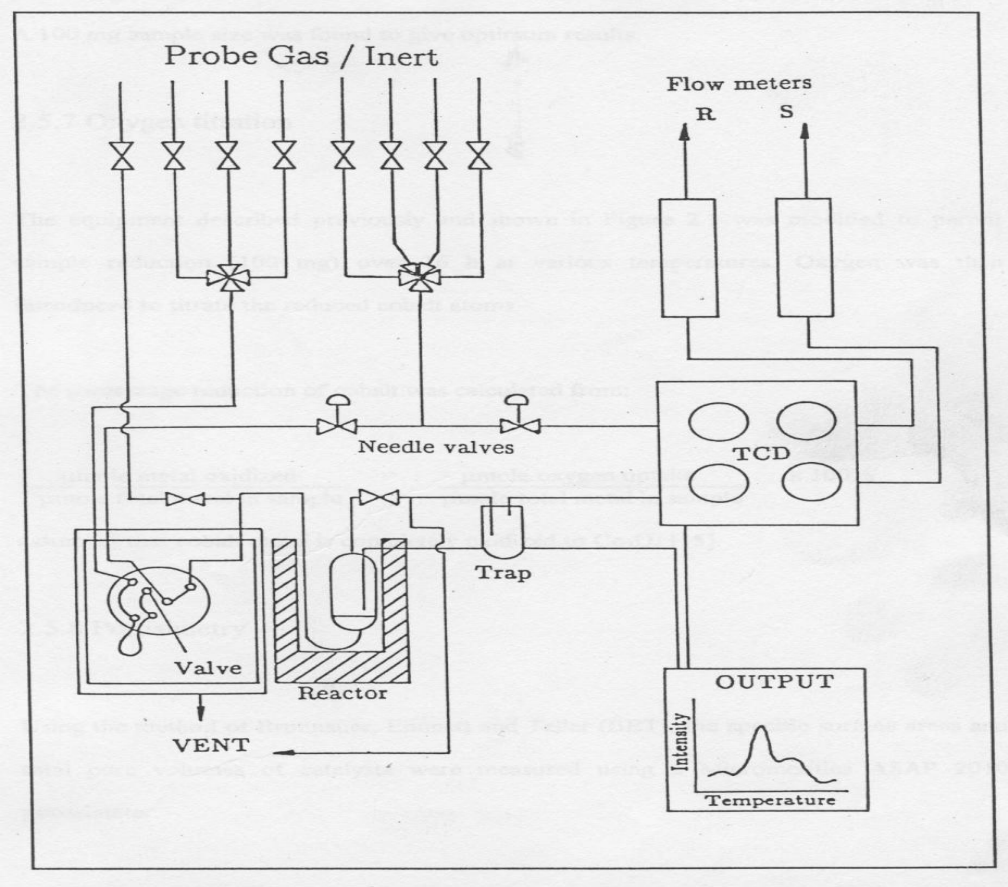

Figure 2.6 *Temperature Programmed Reduction set-up*

2.4.5 H_2 chemisorption and oxygen titration

H_2 chemisorption is extensively used in heterogeneous catalysis to determine the number of accessible active sites and the metal dispersion from which the average metal particle size can be estimated. The analysis involves a combination of H_2 chemisorption and physisorption on an active metal surface. The initial analysis consists of H_2 adsorption on the freshly reduced active metal surface. The amount of H_2 adsorbed is a combination of physisorbed and chemisorbed H_2 molecules (reversible and irreversible, respectively). The amount of H_2 adsorbed on the metal surface is determined at constant temperature as a function of the relative pressure. The obtained plot of adsorbed gas volume as a function of the relative pressure is termed an isotherm. To differentiate the chemisorption from the physisorption contribution, the sample is evacuated after completion of the initial analysis to remove only the reversibly adsorbed H_2. The analysis is repeated under conditions identical to the initial analysis and the amount of H_2 adsorbed in this second analysis represents the physisorption contribution (Physisorption isotherm) as the active area of the sample is already saturated with chemisorbed H_2 molecules. The subtraction of the physisorption isotherm (generated in the second analysis) from the isotherm generated in the initial analysis (physisorprtion versus chemisorption) represents the quantity of H_2 irreversibly adsorbed on the sample known as the monolayer volume (Vm). The monolayer volume can also be determined by extending a line tangential to the plateau of the adsorption isotherm obtained in the initial analysis (combination of physisorption and chemisorption) to the Y-axis (zero pressure).

In this thesis the H_2 chemisorption was performed on a Micromeritics ASAP 2010 Instrument, which was designed for the use of the static volumetric method [10].

A sample of 0.5 g of cobalt catalyst was placed in a U shaped sample holder which was evacuated under vacuum and the catalyst was degassed using pure He at 100°C for 1.5 h. Degassing was continued at 350°C with He and then catalyst reduction was done using pure hydrogen at 350°C for 14 hours. After reduction the sample was evacuated with He at 325°C for 1 hour and then at 100°C for 30 min. H_2 chemisorption was done at 100°C.

After H_2 chemisorption the same sample was flushed and then evacuated using He at 100°C for 30 min. Evacuation was continued at 400°C for 30 min after which oxygen titration was done using a stream of pure oxygen at 400°C. The oxygen uptake was used to calculate the reduction extent assuming complete oxidation of all Co^o to Co_3O_4.

The number of accessible active sites was calculated as [10]:

$$N_s = \frac{V_m \times N_A \times F_s}{V_{mol}} \qquad 2.14$$

where N_A is Avogadro's number and V_{mol} is the molar volume of the adsorptive gas. F_s is the stochiometry factor and was considered equal to 2 on cobalt. The number of accessible active sites combined with the rate of CO conversion during the FT

reaction allowed the evaluation of the reaction Turnover frequency (TOF) expressed as the CO conversion rate per active site per second.

The metal dispersion percentage (D%) was calculated as follows [11]:

$$D\% = \frac{1.179X}{Wf} \qquad 2.15$$

where $\boldsymbol{X}$ is the total H_2 uptake in micromoles per gram of catalyst; $\boldsymbol{W}$: weight percentage of cobalt; $\boldsymbol{f}$: cobalt reduction extent determined by oxygen titration.

The average crystallite diameters ($\boldsymbol{d_p}$) in nanometers were calculated from $D\%$ assuming spherical metal crystallites of uniform diameter with a site density of 14.6 atoms / nm^2 [11]:

$$d_p = \frac{96}{D\%} \qquad 2.16$$

References

1 B. Shi, and B.H. Davis, *Appl. Catal. A*: General 277 (2004) 61.

2 J.G. Price, *PhD Thesis, University of the Witwatersrand, Johannesburg, South Africa*, 1994.

3 J.M. Berty, *Chem. Eng. Prog.* 70 (5) (1974) 78.

4 M. Oku, K. Hirokawa and S. Ikeda, *J. Electron. Spectrosc. & Related Phenomena.* 7 (1975) 465.

5 C.R. Brundle, T.J. Chuang and K. Wandelt, *Surf. Sci.* 68 (1977) 459.

6 U. Lindner and H. Papp, *Appl. Surf. Sci.* 32 (1988) 75.

7 J. Garcia-Serrano, A.G. Galindo, U. Pal, *Solar En. Mat & Solar Cells* 82 (2004) 291.

8 N.W. Hurst, S.J. Gentry, A. Jones and B.D. McNicol, *Catal. Rev.-Sci. Eng*. 24 (1982) 233.

9 G. Ertl, H. Knozinger and J. Weitkamp, *Handbook of Heterogeneous Catalysis*, Vol. 2, 1997.

10 P.A. Webb and C. Orr, "*Analytical Methods in Fine Particle Technology*", p 229, Micromeritics, 1997.

11 C.H. Bartholomew, B.P. Richard, and J.L Butler, *J. Catal.* 65 (1980) 335.

Chapter 3

Fischer-Tröpsch synthesis over Co/TiO_2: Effect of ethanol addition

3. 1 Introduction

Numerous studies have shown how the presence of additives in the reactor feed affects the efficiency of the FT (Fischer-Tröpsch) reaction. For example, the effect of water on Co [1-19], Fe [19-25] and Ru [26], has been extensively studied in recent years. Water was reported to have a positive [1-3, 12, 15-19], a negative [5, 7-11, 13-15, 17, 19] or no effect [4, 11] on the activity of cobalt based catalysts; the results obtained were dependent on the type of the support used. The negative effect of water on Co catalysts is ascribed to the formation of inactive metal oxides by the water or to the formation of alternative catalytic forms of cobalt on the catalyst. On the other hand Kim et al.[1, 2] have reported increased activity for a Co/TiO_2 catalyst (unpromoted and promoted by Re) that was due to a possible destruction of a strong metal-support interaction by water.

The effect of the addition of alcohols to FT syngas streams over both Fe and Co catalysts has been reported in the literature. Kummer and Emmet [27] reported that primary alcohols adsorbed on iron catalysts can act as starting nuclei in building up higher hydrocarbons. Tau et al.[28] have also reported that 1- and 2-propanol incorporate into the products of the Fischer-Tröpsch synthesis. 1-and 2-Propanol produce surface species that remain distinct and initiate different synthesis reaction

pathways. Hanlon et al.[29] have reported that the addition of ethanol (or ethene) to iron catalysts increased the olefin to paraffin ratio of the products. Neither reagent affected the Anderson–Schulz–Flory alpha parameter.

Since ethanol can readily be dehydrated to ethene, studies on the addition of ethene to syngas are also relevant to this study. Schulz and Claeys [30], Portzlaff et al.[31] as well as Kibby et al.[32] have reported that when ethene is co-fed over a cobalt catalyst during FT synthesis an increased fraction of hydrocarbons in the range of low carbon numbers is observed.

The present study aims to evaluate the effect of ethanol on the product selectivity and activity of a Co catalyst during FT synthesis. According to the literature, the critical factor in terms of the addition of water is the ability of the support to stabilise the Co metal and prevent or inhibit oxide formation. Titania has been found to improve both product selectivity and catalytic activity after addition of an oxygen containing additive (water) [1, 2]. For the above reason, it was decided to use titania as the support in the ethanol addition study.

3. 2 Experimental

3.2.1 Catalyst synthesis

Support preparation

TiO_2 (Degussa P25, SA = 50 m^2g^{-1}) was mixed with deionised water in a mass ratio of 1:1 and dried in air at 120°C for 1 hour. The support was then calcined in air at 400°C for 16 hours [33]. After calcination the support was crushed and sieved and the particles with diameters between 0.5 – 1 mm were used in the FT study.

Catalyst preparation

The catalyst was prepared by a single step incipient wetness impregnation of the support with a cobalt nitrate $Co(NO_3)_2.6H_2O$ solution. After the one step impregnation the support was dried in air at 120°C for 16 hours and then calcined in air at 400°C for 6 hours to decompose and transform the cobalt nitrate to cobalt oxide. The impregnating solution was added to the TiO_2 to give a cobalt metal loading of 10% by mass.

3.2.2 Catalyst characterization

TPR analysis was achieved in the apparatus described in chapter 2 where 0.1 g of catalyst sample was placed in a U shaped quartz tube reactor and exposed to a flow of pure nitrogen at 150°C for 30 min prior to the catalyst reduction. The reduction was done using a 5% H_2 in Ar gas mixture at a flowrate of 20 ml/min. The temperature was increased at 10°C/min for 45 min and then maintained at 450°C for 60 minutes. The hydrogen uptake was measured using a TCD at the exit of the reactor. The extent of reduction was calculated using an AgO calibrant.

XRD analysis was described in chapter 2.

3.2.3 Fischer-Tröpsch (FT) synthesis

The FT reaction was studied using the stirred basket reactor system described in chapter 2. However, to allow the addition of ethanol to the feed, the system was slightly modified by adding an ethanol temperature controlled saturator (Figure 3.1). The synthesis gas was not allowed to pass through the saturator until steady state was reached. A set of valves directed the inlet stream either through the saturator for ethanol addition studies or through the saturator by-pass for the ethanol free feed studies.

In the present study the investigation of the effect of the ethanol addition during FT reaction is based on mass balance calculations. The effect of the ethanol addition on the catalyst activity and selectivity was investigated by adding/removing ethanol to/from the feed. The results obtained were then compared to a base case study in which an ethanol free gas stream was used to study the FT reaction.

Before the FT reaction was commenced the catalyst was pre-treated in pure hydrogen (T = 250°C, 18 hours, atmospheric pressure, flow rate 30 ml/min STP; exit conditions), during which time the cobalt oxide particles were reduced to cobalt metal, the active catalyst form for the FT reaction. To allow for comparison, in this study the reduction conditions used were the same for each run. After reduction the reactor was cooled and maintained at 220°C. The pure hydrogen was then replaced with synthesis gas (H_2: CO ratio of 2; 10% N_2 as internal standard for mass balance calculations) and the total pressure in the reactor was increased and maintained at 8 bar for the FT reaction. After the catalyst has stabilised the liquid and wax traps were emptied and the mass balance evaluation commenced.

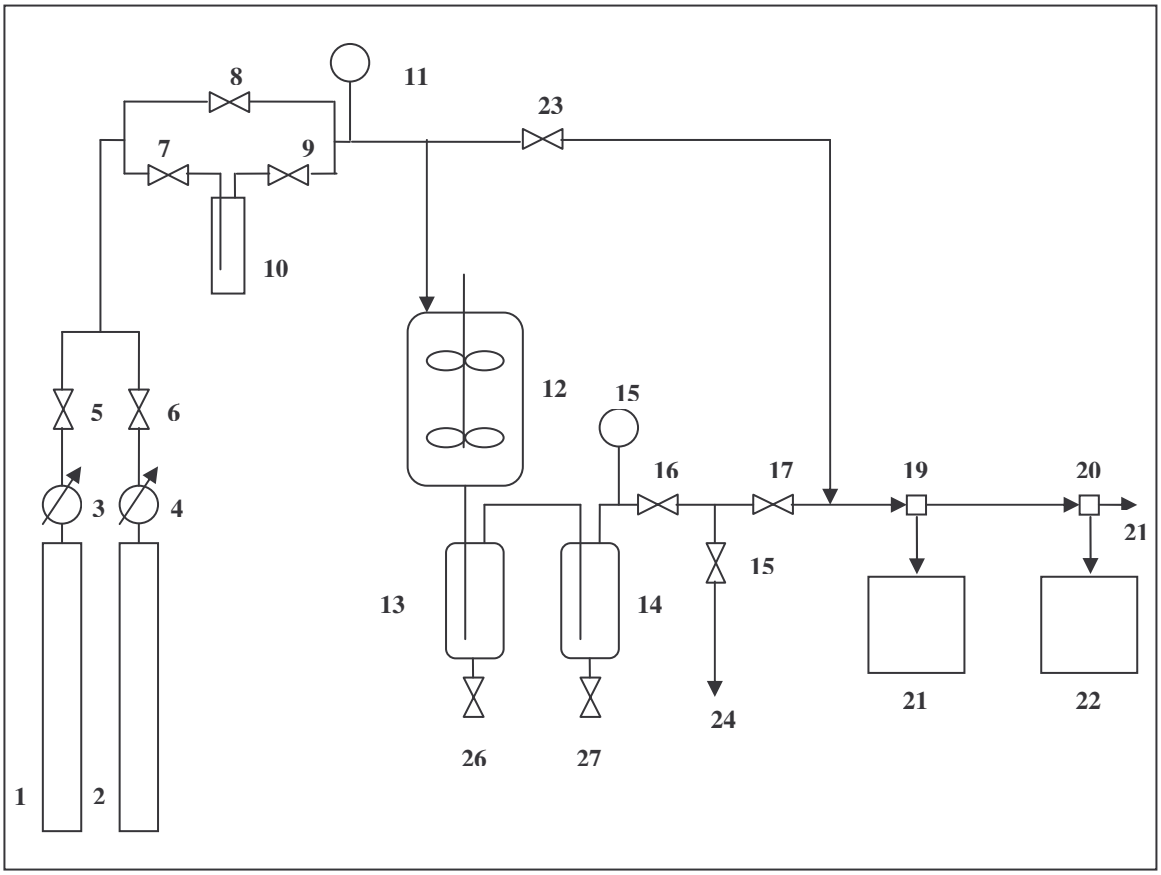

Figure 3.1 *Modified stirred basket reactor set up*

1: Syngas cylinder;
2: H_2 cylinder;
3 and **4**: Pressure regulators;
5, 6, 7, 8, 9, 23, 26, 27: Shut off valves;
10: Temperature controlled ethanol saturator;
11 and **15**: Pressures gauges;
12: Reactor;
13: Wax trap;
14: Liquid trap;
16: Needle valve;
17 and **18**: Solenoid valves;
19 and **20**: GC sampling valves;
21: GC (FID);
22: GC (TCD);
24, 25: Gas venting

3.3 Results and discussion

3.3.1 Effect of ethanol addition on the catalyst activity

Results from FT reactions

The effect of ethanol addition on the catalyst activity has been investigated under two sets of FT reaction conditions referred to as high (ca. 40%) and low (ca. 15%) CO conversions. The space velocities used in this study to achieve these conversions were 0.44 NL/g of catalyst/h and 1.61 NL/g of catalyst/h (or 4.4 NL/gCo/h and 16.1NL/gCo/h) respectively. It is to be noted that the ethanol added to the feed is also a carbon containing compound. Calculations showed, however, that the rate of carbon transformation from ethanol (measured ethanol conversion about 10 - 28% during FT runs) can be neglected (less than 10%) when compared to the rate of CO consumption. Hence the CO conversion rate is a good approximation of the total carbon conversion rate.

Figure 3.2 shows the effect of ethanol addition on the catalyst activity under a range of experimental conditions. The CO conversion rate markedly decreased with an increase of ethanol partial pressure in the feed. This effect was even more significant for the high space velocity experiments where a 6% ethanol addition to the feed resulted in an approximately 75% decrease of the initial catalyst activity. It can be seen in Figure 3.2 that for the low synthesis conversion this effect is near reversible when the ethanol is removed from the feed.

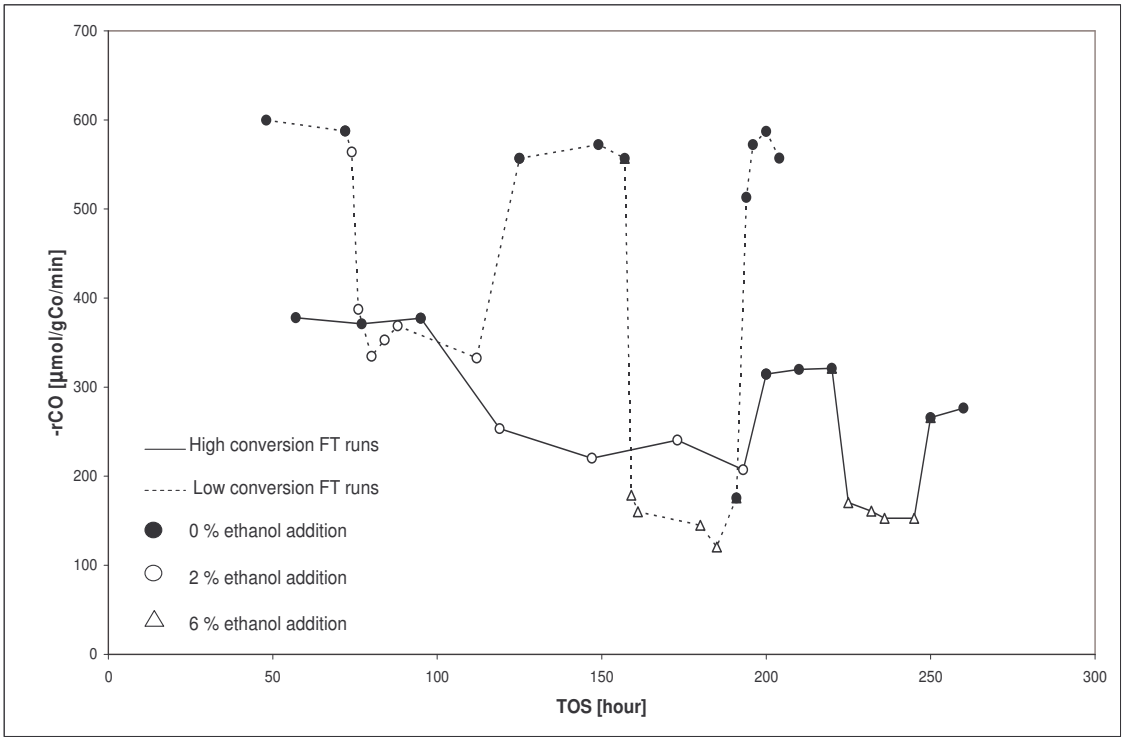

Figure 3.2 *Effect of the ethanol addition on the catalyst activity during FT runs as a function of time-on-stream (TOS)*

For the higher conversion data, an irreversible drop in activity (15 % of the initial activity) is to be noted after 6% ethanol was added to the feed.

A similar effect was observed by Li et al.[11] when water (around 25 mol %) was added to the feed during Fischer-Tröpsch synthesis over a titania supported cobalt catalyst in a continuous stirred tank reactor (CSTR). It was shown that this effect was reversible for low CO conversion while at high CO conversion, the addition of water resulted in permanent catalyst deactivation. The latter study and other studies

involving water addition suggest that the catalyst deactivation is due to the loss of active sites via the oxidation of highly dispersed metal phases [7-11].

While thermodynamic calculations do not predict the oxidation of bulk phase cobalt by water under FT conditions (see appendix, Figure 1), it can be shown that the oxidation of cobalt by ethanol is thermodynamically possible under typical reaction conditions.

Thermodynamic calculations for the oxidation of cobalt by ethanol were carried out, assuming formation of ethane as the product:

$$C_2H_6O + Co = C_2H_6 + CoO \qquad 3.1$$

$$3\ CoO + C_2H_6O = Co_3O_4 + C_2H_6 \qquad 3.2$$

For each of the above reactions the equilibrium constant can be written as ratio of the partial pressure of ethane to ethanol:

$$K = \frac{P_{C_2H_6}}{P_{C_2H_6O}} \qquad 3.3$$

and

$$\ln K_o = \frac{-\Delta G^o_{rxn}}{RT_o} \qquad 3.4$$

where K_o is the equilibrium constant at the temperature, T_o, for which ΔG^o_{rxn} is known, usually 298 K. However since ΔG_{rxn} is a strong function of temperature, the

relationship between the equilibrium constant and the temperature i.e. when the above two reactions are at their respective equilibria, is given by:

$$\ln \frac{P_{c_2H_6}}{P_{c_2H_6O}} = \ln K_o - \frac{\Delta H_{rxn}}{R}\left(\frac{1}{T} - \frac{1}{T_o}\right) \qquad 3.5$$

where T is the temperature [K] of reaction and R is the ideal gas constant.

When $\ln(P_{C_2H_6} / P_{C_2H_6O})$ in equation 3.5 is plotted against temperature for reactions 3.1 and 3.2 an equilibrium diagram for Co in the presence of ethanol is obtained (see appendix; Figure 2). Use of typical FT operating conditions reported in this study gave values for the ethane to ethanol ratio as shown in Table 3.1. At 220ºC the ethane to ethanol ratio required for the possible oxidation of bulk Co to CoO by ethanol is calculated to be ca. exp 17.7 (ln (C_2H_6/C_2H_6O) ca.17.7). If this ratio decreases to exp -143 a second oxidation leading to Co_3O_4 becomes thermodynamically possible. Under the operating conditions used in this study the Co oxidation to Co_3O_4 is hence not predicted because the ethane to ethanol ratio is far above the required value for this second oxidation reaction to occur.

Based on thermodynamic calculations, catalyst deactivation can be predicted to be due to the oxidation of the Co metal to CoO on the addition of ethanol. Thermodynamic predictions alone are not sufficient to confirm the Co oxidation by ethanol during FT reaction because the process only considers cobalt being exposed to ethanol and not the presence of synthesis gas which would rather push the reaction

in the direction of CoO reduction to Co^0. Moreover thermodynamic predictions do not give any information on the kinetics of Co oxidation by ethanol.

To confirm the above prediction of catalyst deactivation due to ethanol addition in the feed, TPR and XRD analyses were undertaken.

Table 3.1 Ethane to ethanol ratios in the reactor for different FT runs in ethanol

Run	$\frac{P_{C_2H_6}}{P_{C_2H_6O}}$	$\ln(\frac{P_{C_2H_6}}{P_{C_2H_6O}})$
1. Low conversion FT and 2% C_2H_6O added	0.064	- 2.751
2. Low conversion FT and 6% C_2H_6O added	0.010	- 4.605
3. High conversion FT and 2% C_2H_6O added	0.151	- 1.890
4. High conversion FT and 6% C_2H_6O added	0.034	- 3.389

Results from TPR analysis

TPR analysis was performed under typical FT reaction temperature conditions but at 1 bar P. Figure 3.3 shows TPR profiles of the cobalt FT catalyst after different treatments.

An unreduced and calcined cobalt FT catalyst sample was reduced under the conditions described in the experimental section (Figure 3.3a). The two peaks observed at 360°C and 450°C were attributed to the reduction of Co_3O_4 to CoO and CoO to Co^o respectively [34, 35]. The calculated extent of reduction under these conditions revealed that almost all the cobalt oxide on the catalyst was reduced to metallic cobalt. This was confirmed by submitting the sample to a second TPR analysis (Figure 3.3b). No H_2 uptake was detected. Further TPR analyses were then performed on samples after reduction of a calcined catalyst sample followed by passage of 6% C_2H_6O in N_2 (or in syngas) at 220°C over the catalyst sample (Figure 3.3). A stream of pure nitrogen was bubbled through the ethanol in the bubbler for 30 min before being directed to the reduced catalyst to eliminate any residual air that was present in the bubbler.

TPR profiles **c** and **d** clearly show reduction peaks at lower temperatures compared to the TPR profiles of the unreduced and calcined catalyst (profile **a**). These low temperature peaks at 319°C and 311°C for the TPR profiles **c** and **d** respectively could not be attributed to the reduction of Co_3O_4 species since their respective areas are about 2.2 times bigger than the area corresponding to the reduction of Co_3O_4 species on the calcined catalyst.

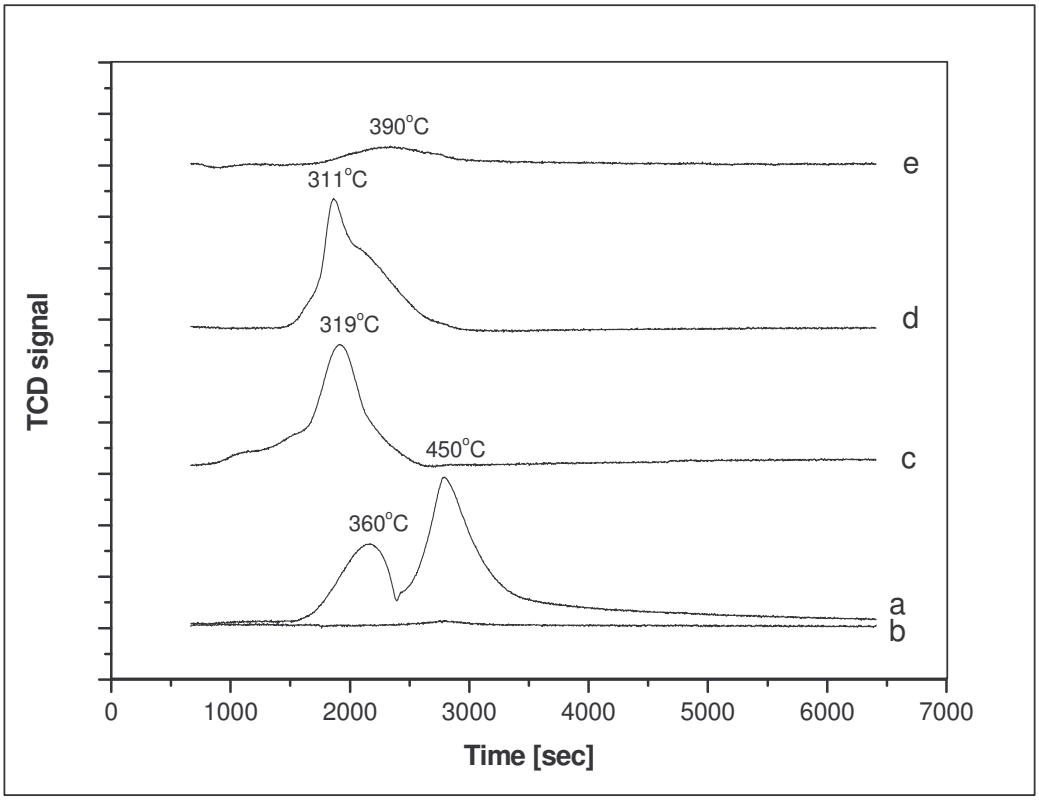

Figure 3.3 *TPR profiles for 10%Co/TiO_2 after various treatments: (a) TPR profile for the calcined and unreduced catalyst; (b) TPR profile for the reduced catalyst; (c) TPR profile for the reduced catalyst after exposure to 6% C_2H_6O in N_2 at 220°C for 0.5 hour;(d) TPR profile for the reduced catalyst after exposure to 6% C_2H_6O in N_2 at 220°C for 12 hours; (e) TPR profile for the reduced catalyst after exposure to 6% C_2H_6O in syngas at 220°C for 0.5 hour*

Results from XRD analysis

The XRD analysis was done in order to establish the form of the cobalt oxide species that had formed on the catalyst as a result of Co oxidation by ethanol.

Figure 3.4 shows the XRD patterns of the calcined catalyst (pattern **a**) and the reduced catalyst which was exposed to the ethanol-nitrogen stream for 30 minutes (pattern **b**). It can be seen that no Co_3O_4 peak was detected in the XRD pattern **b**. This confirms that the oxidation of Co by ethanol only leads to the formation of CoO species.

TPR and XRD results, and thermodynamic predictions have revealed that metallic cobalt species can be oxidised to CoO by ethanol under typical FT reaction temperatures (i.e. 220°C). The CoO species formed from the oxidation of metallic cobalt by ethanol are relatively easy to reduce. This can be deduced from their lower reduction temperatures, namely 311 and 319ºC rather than 450ºC (see Figure 3.3). The catalyst reduction properties after a preceding oxidation with ethanol at 220°C in this study are in agreement with previous studies [36, 37] which showed that low-temperature oxidation of cobalt catalyst leads to the formation of cobalt oxide species which exhibit low reduction temperature peaks as compared to the calcined catalyst. This is an indication that cobalt catalyst re-oxidation decreases the metal-support interaction as was also observed by others [38]. The results shown in Figure 3.3 revealed that the extent of oxidation after 30 min (profile **c**) and 12 hours (profile **d**) are, within experimental error, the same. This suggests that the oxidation reaction is

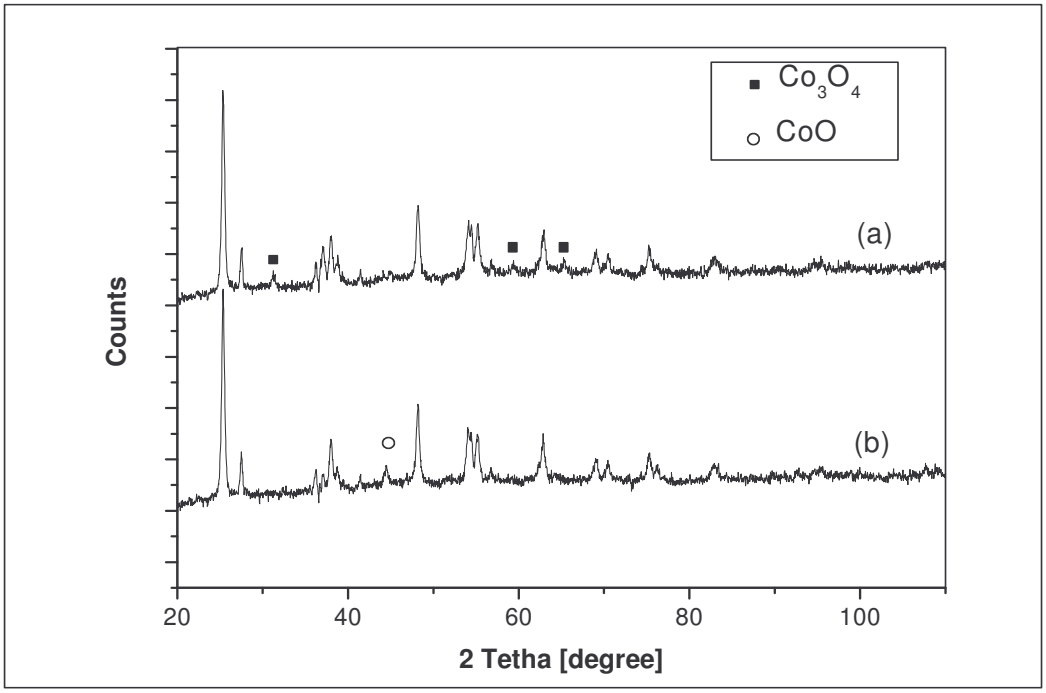

Figure 3.4 *XRD patterns for 10%Co/TiO_2: (a) XRD pattern for the calcined and unreduced catalyst; (b) XRD pattern for the reduced catalyst and exposed to ethanol/nitrogen for 30 min*

fast and proceeds to equilibrium in less than half an hour. All of this points to surface oxidation of the metallic Co by the ethanol. The extent of oxidation of metallic cobalt by ethanol is reduced (42 %) in the presence of syngas as shown in Figure 3.3 (TPR profile **e**) where the peak at 390°C was also ascribed to the reduction of CoO to Co^{o}. This is expected as the metallic cobalt is simultaneously exposed to an oxidising agent (ethanol) and to a reducing gas mixture (syngas).

The catalyst deactivation due to ethanol addition during FT synthesis is therefore attributed to the change in the catalyst surface as a result of the oxidation of surface Co by ethanol. The TPR data for the oxides reveals that the complexes are easy to reduce after the ethanol was removed from the feed.

When normalised per gram of cobalt on the catalyst, the rate of CO consumption was significantly higher for the lower conversion data. Therefore any loss of active sites due to cobalt oxidation results in a more significant decrease in catalytic activity for low conversion runs compared to high conversion runs (Figure 3.2).

Previous studies have shown that cobalt catalysts used for FT deactivate with time on stream and a higher rate of catalyst deactivation was observed for high conversion runs [39, 40].

Other possibilities also exist to explain the data:

(i) Accelerated sintering through an oxidation-reduction cycle could also explain the eventual catalyst deactivation after ethanol addition. The accelerated sintering would lead to permanent catalyst deactivation. However, the good recovery of catalytic

activity (at low conversion) after ethanol is removed from the feed, suggests limited sintering at low conversions.

(ii) The decrease in CO conversion rate after ethanol addition could also be due to a competitive adsorption of ethanol on the catalyst surface; this would reduce the availability of active sites to CO. The higher the ethanol partial pressure in the reactor, the more ethanol would be competitively adsorbed on the catalyst surface.

3.3.2 Effect of the ethanol addition on the product selectivity

To investigate the effect of ethanol addition on FT product selectivity, FT runs were compared to other runs where only ethanol in nitrogen (i.e. in the absence of syngas) was passed over a Co FT catalyst.

Ethanol transformation on cobalt FT catalyst in the absence of syngas

For these runs the catalyst was pre-treated and exposed to the same operating conditions as for the high conversion FT runs used in this study (space velocity of 0.44 NL/g of catalyst/h). The results for these runs are summarized in Table 3.2.

Table 3.2 Rates of product formation after ethanol reaction to cobalt FT catalyst in the absence of syngas

Run	Rates [µmol/gCo/min]						
	CH_4	olefins			paraffins		
		C_2	C_3	C_4	C_2	C_3	C_4
1. With 2% ethanol in N_2	3.5	0.2	1.4	0.7	0.5	0.0	0.4
2. With 2% ethanol in N_2	3.8	0.3	2.4	1.2	0.8	0.0	0.6

The formation of methane and light hydrocarbons was observed. The mechanism leading to methane formation from ethanol on cobalt was not investigated.

The presence of C3 and C4 hydrocarbons clearly indicates that ethanol oligomerises on the cobalt FT catalyst. The ethylene formation arises from the catalytic ethanol dehydration reaction.

Effect of ethanol on product selectivity during FT runs

The addition of ethanol during FT synthesis was found to decrease the rate of product formation and CO consumption. Table 3.3 shows that the rate of methane formation decreases as the ethanol partial pressure in the feed increases. However, the rate

actually increases when normalised per CO consumption rate (-rCO) as shown in Figures 3.5 a and b. This indicates that ethanol induces both catalyst deactivation and also increases the methane selectivity.

This effect is seen to be almost completely reversible on removal of ethanol in the feed for the low conversion run but an increase in methane selectivity is noted for the high conversion run after 200 h on stream.

The effect of ethanol addition on the selectivity of light olefins (C_2 to C_4) is shown in Figures 3.6a and 3.6b. It was observed that their respective selectivities increased with increase in the ethanol partial pressure in the feed. Due to the reproducibility of light olefins analysis results, it was also found possible to use the olefin to paraffin ratio to comment on the C_2 to C_4 products. As seen in Figures 3.7a and 3.7b the olefin fraction increased with the ethanol partial pressure in the feed.

Previous studies have revealed that high methane selectivity over cobalt catalysts is generally attributed to the presence of unreduced cobalt oxides. Reuel and Bartholomew [41] reported that cobalt oxides catalyse the WGS reaction which increases the local H_2/CO ratio near the Co metal sites, hence favouring the hydrogenation of the adsorbed species leading to higher methane selectivity.

Table 3.3 Product formation rates and selectivity during FT runs

FT run	Rates [µmol/gCo/min]							*Selectivity
	CH_4	olefins			paraffins			(%)
		C_2	C_3	C_4	C_2	C_3	C_4	C_1-C_5
High conversion								
1. 0% ethanol added	34.64	0.18	1.45	1.13	2.29	2.52	2.56	21.79
2. 2% ethanol added	30.20	0.19	1.40	1.09	2.33	2.25	2.15	31.44
3. Ethanol switched off	33.72	0.18	1.42	1.11	2.23	2.47	2.49	22.56
4. 6% ethanol added	30.89	0.22	1.35	1.12	2.74	2.14	2.04	45.66
5. Ethanol switched off	32.11	0.17	1.39	1.05	2.12	2.34	2.42	24.71
Low conversion								
1. 0% ethanol added	69.05	0.50	2.81	1.88	5.59	4.05	3.59	24.97
2. 2% ethanol added	59.22	0.66	2.80	2.82	5.16	3.11	2.83	37.75
3. Ethanol switched off	70.01	0.48	2.39	1.90	5.55	4.14	3.39	25.62
4. 6% ethanol added	56.41	0.84	3.01	3.79	5.65	3.09	2.95	86.86
5. Ethanol switched off	65.49	0.49	2.50	2.70	5.44	3.91	3.39	26.13

***:** Carbon based selectivity.

(a)

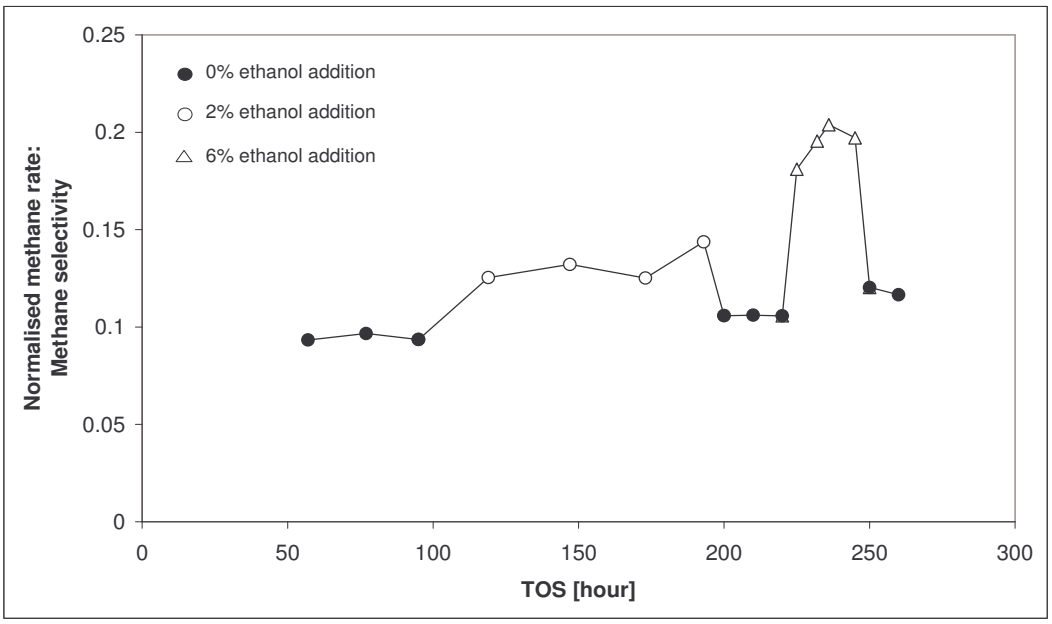

(b)

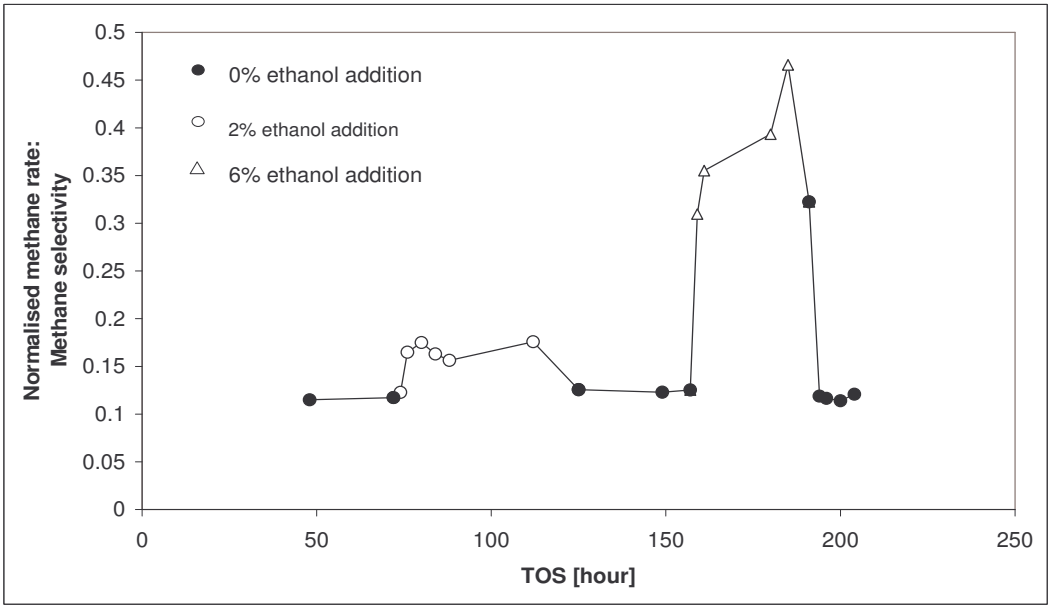

Figure 3.5 *Effect of ethanol addition on the methane selectivity (expressed as the ratio of methane formation rate over the rate of CO conversion): (a) high conversion FT runs; (b) low conversion FT runs*

Martinez et al.[42] have also reported a parallel relationship between the selectivities to methane and CO_2 on a Co/SBA-15 catalyst. They suggested that the higher methane selectivity observed with well-dispersed low-reducible catalysts could be due to a higher extent of the WGS reaction on unreduced cobalt species.

Khodakov et al[43] reported an inverse relationship between methane selectivity and the Co reduction extent for a series of cobalt supported mesoporous silica with different pores sizes. The higher methane selectivity was attributed to the presence of either unreduced species or to small particles, rather than to the WGS reaction. They could not measure significant formation of CO_2 over their catalysts. In the present study *no CO_2 was measured* in any of the runs suggesting that the WGS reaction was not significant.

By considering Figures 3.2 and 3.5 (a and b), it can clearly be seen that the methane selectivity increases with the catalyst deactivation and is thus related to the oxidation of cobalt metal to cobalt oxide species.

Although the reaction mechanism leading to the increase of methane formation on cobalt oxides is still unclear, the relationship between the methane selectivity and the catalyst activity observed in this study supports the above proposal.

As shown in Table 3.2 ethanol transformation over the cobalt FT catalyst also leads to the formation of methane. In the absence of syngas the rate of methane formation from ethanol transformation is about 3.5 μmol/min/gCo which is approximately 10% of the methane formation rate for the high conversion FT run before ethanol addition (see Table 3.3). The rate of methane formation from ethanol, in the presence of

(a)

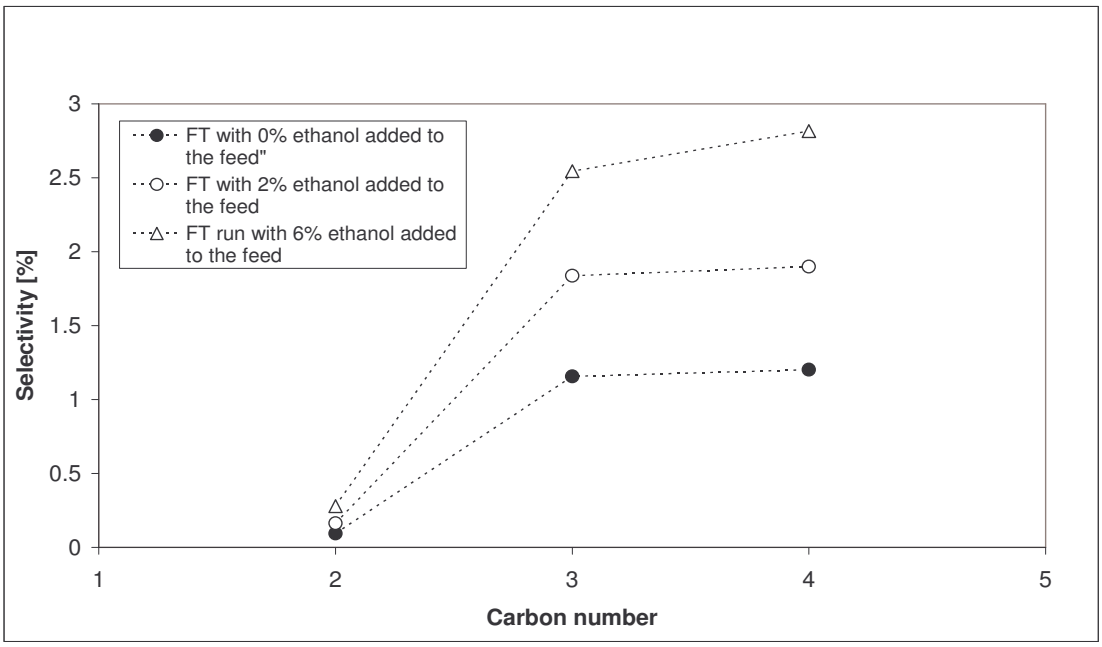

(b)

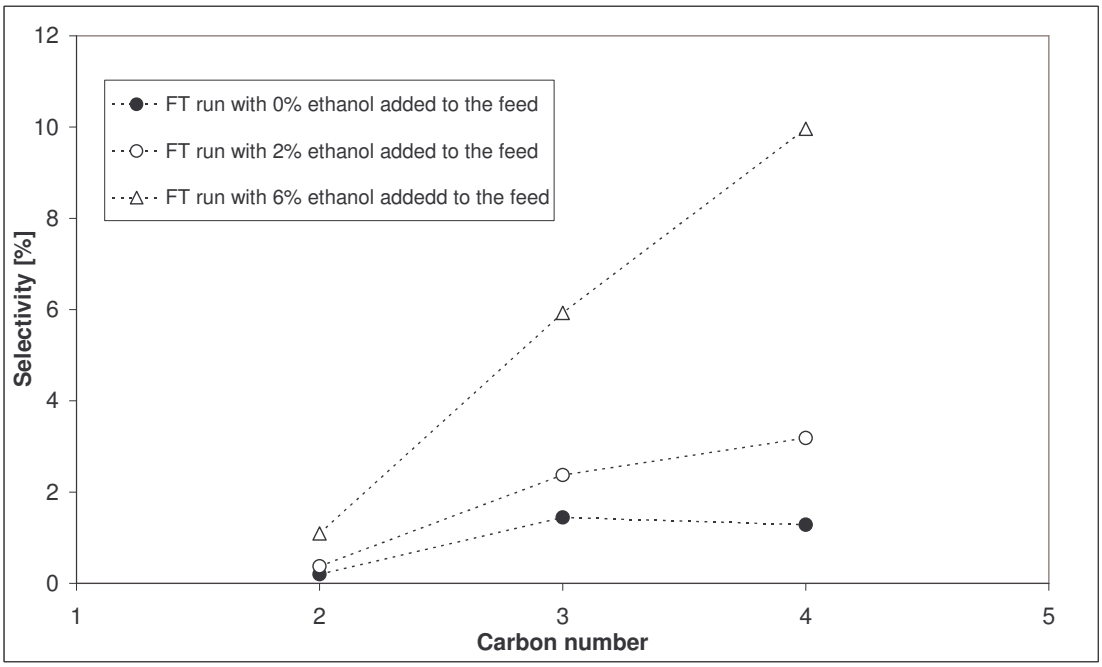

Figure 3.6 *Effect of ethanol addition on the light olefin selectivity (carbon based selectivity): (a) high conversion FT runs; (b) low conversion FT runs*

(a)

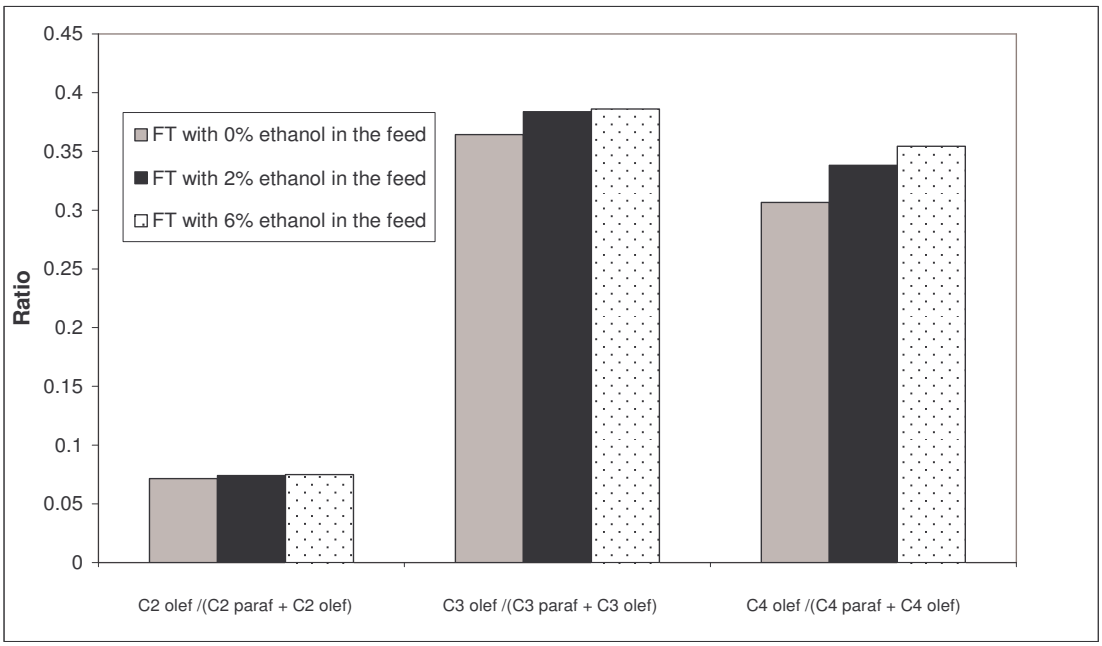

(b)

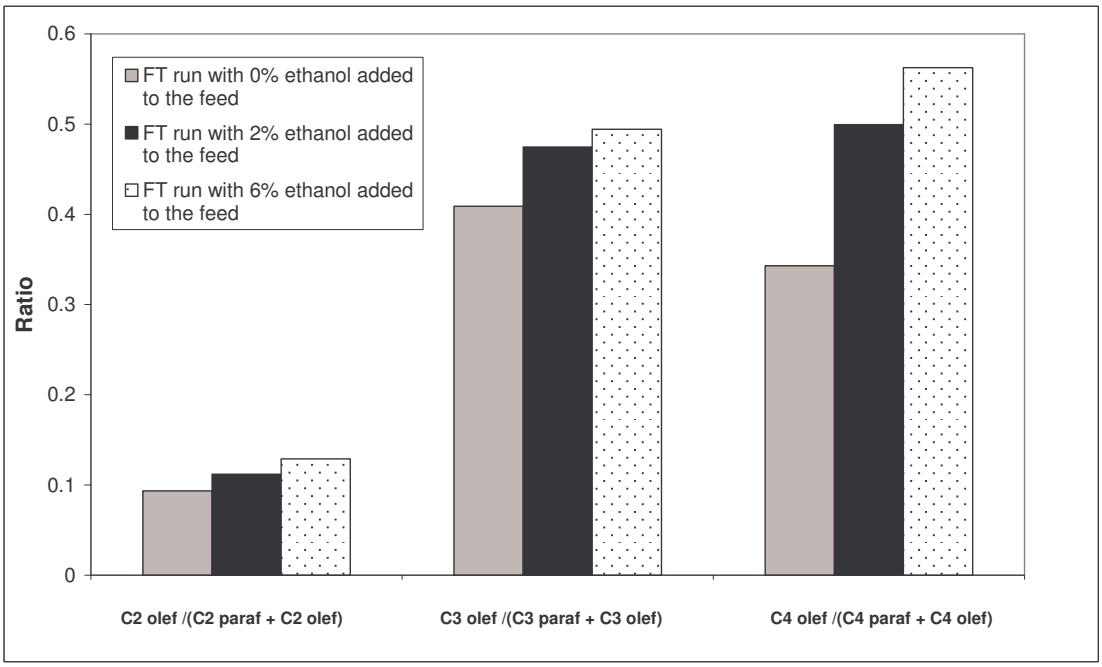

Figure 3.7 *Effect of ethanol addition on light olefins fraction: (a) at high conversion and (b) at low conversion*

syngas during the FT reaction cannot be predicted from the data presented in this study.

A high olefin to paraffin ratio after ethanol addition was also reported over an iron catalyst [27, 29]. This effect was attributed to the water vapour produced from the alcohol. The water was believed to be the real hydrogenation catalyst poison [27]. Hanlon et al.[29] suggested that the increase in olefin/paraffin ratios could also be due to the competitive adsorption of ethanol and α-olefins on the active sites, inhibiting the secondary reactions of the α-olefins.

The selectivity to olefins depends on the ability of α-olefins to re-adsorb on the catalyst surface and participate in the chain-growth process favouring the formation of high molecular mass products. It is suggested that the re-adsorption of α-olefins is high when the density of surface Co^o sites is high [44].

In our study the increase in olefin selectivity on the addition of ethanol during the FT reaction could be due to:

(i) The loss of some available Co^o sites as the result of catalyst deactivation under ethanol addition as well the competitive adsorption of ethanol. This would reduce the number of sites for secondary adsorption of olefins;

(ii) The olefin formation from ethanol transformation on the FT Co catalyst. In Table 3.2 it can be observed that the transformation of ethanol leads to the formation of more light olefins than paraffins.

C3 and C4 olefin formation rates from the reaction of ethanol in the absence of the syngas (Table 3.2) are comparable to those measured during the FT reaction (Table 3.3).

The above observations show that ethanol is transformed over the Co FT catalyst and leads to the formation of light hydrocarbons. The same behaviour can be assumed to take place even in the presence of the synthesis gas during FT reaction but to a smaller extent since most of the active sites are expected to be competitively occupied by CO. It can be observed that propane was not detected during ethanol transformation in the absence of syngas (Table 3.2). However during FT runs with ethanol addition (Table 3.3) the rate of formation of propane was similar to that of other light paraffins. This can suggest that the light paraffins are mainly formed from CO transformation and the contribution from ethanol transformation during FT reaction is very limited. The high selectivity to light products (Table 3.3) for runs where ethanol is thus added to the synthesis gas is believed to be a result of changes in the catalyst surface as well ethanol transformation reactions on the cobalt FT catalyst.

3.4 Conclusion

The effect of ethanol addition during FTS over 10%Co/TiO_2 catalyst was investigated at high and low CO conversion. To gain insight into the transformation of ethanol on the Co FT catalyst, further reactions were performed where only ethanol in nitrogen

was passed over the FT catalyst i.e. in the absence of syngas and under the same operating conditions as used as for the FT runs.

For low CO conversion runs the catalyst almost recovered its initial performance after the ethanol was switched off from the feed. This is explained by the reduction of the easy to reduce CoO species which resulted from the oxidation of Co by ethanol. The results of this study are the opposite of those reported by Kim et al.[1, 2] where water was added on a titania supported cobalt catalyst. This could be due to the difference in the ability to oxidize cobalt between water and ethanol.

References

1 C.J. Kim, *Eur. Appl. Patent.* No. EP 0 339 923 B1 (1989), to Exxon Res. Eng. Co.

2 C.J. Kim, *US patent* 5,227,407 (1993), to Exxon Res. Eng. Co.

3 E. Iglesia, S. Reyes, R. Madon, S. Soled, *Adv. Catal.* 39 (1993) 221.

4 H. Schulz, M. Claeys, S. Harms, *4th Int Natural Gas Convention Symp*., Kruger National Park, South Africa, 19-23 Nov 1995.

5 D. Schanke, A.M. Hilmen, E. Bergene, K. Kinnari, E. Rytter, E. Ådnanes, A. Holmen, *Cat. Lett.* 34 (1995) 269.

6 H. Schulz, M. Claeys, S. Harms, *Stud. Surf. Sci. Catal.* 107 (1997) 193.

7 M. Rothaemel, K.F. Hanssen, E.A. Blekkan, D. Schanke, A. Holmen, *Catal. Today*. 38 (1997) 79.

8 A.M. Hilmen, D. Schanke, K.F. Hanssen, A. Holmen, *Appl. Catal. A*: General 186 (1999) 169.

9 P.J. van Berge, J. van de Loosdrecht, S. Barradas, A.M. van der Kraan, *Catal. Today*. 58 (2000) 321.

10 J. Li, G. Jacobs, X. Zhan, Y. Zhang, T. Das, B.H. Davis, *Appl. Catal. A*: General 228 (2002) 203.

11 J. Li, G. Jacobs, T. Das, B.H. Davis, *Appl. Catal. A*: General 233 (2002) 255.

12 J. Li, G. Jacobs, T. Das, Y. Zhang, B.H. Davis, *Appl. Catal. A*: General 236 (2002) 67.

13 G. Jacobs, T.K. Das, P.M. Patterson, J. Li, L. Sanchez, B.H. Davis, *Appl. Catal. A*: General 247 (2003) 335.

14 G. Jacobs, P.M. Patterson, T.K. Das, M. Luo, B.H. Davis, *Appl. Catal. A*: General 270 (2004) 65.

15 S. Storsaeter, Ø. Borg, E.A. Blekkan, A. Holmen, *J. Catal.* 231 (2005) 405.

16 A.K. Dalai, T.K. Das, K.V. Chandhari, G. Jacobs, B.H. Davis, *Appl. Catal.* A: General 289 (2005) 135.

17 S. Storsaeter, Ø. Borg, E.A. Blekkan, B. Tøtdal, A. Holmen, *Catal. Today.* 100 (2005) 343.

18 T.K. Das, W.A. Conner, J. Li, G. Jacobs, M.E. Dry, B.H. Davis, *Energy and Fuels* 19 (2005) 1430.

19 B.H. Davis, G. Jacobs, K. Chandhari, M. Luo, T.K. Das, *AIChE Spring National Meeting, Conference Proceedings*, 2005, p 2005.

20 R.B. Anderson, Hydrocarbon synthesis, hydrogenation and cyclisation. In: *Emmett P, editor. Catalysis*, Vol. IV, Reinhold, New York, 1956, p. 1.

21 M.A. Vannice, *Catal. Rev.* 14 (1976) 153.

22 M.E. Dry, Fischer-Tröpsch synthesis. In: Anderson JR, Boudart M editors. *Catalysis Science Technology*, Vol. I, Springer, Berlin, 1981, p. 159.

23 C.N. Satterfield, R.T. Hanlon, S.E. Tung, Z.M. Zou, G.C. Papaefthymiou, *AIChE National Meeting* 1986; 55D: 1-36.

24 W.H. Zimmermann, D.B. Bukur, *Can. J. Chem. Eng*. 68 (1990) 292.

25 G.P. van der Laan, A.A.C.M. Beenackers, *Appl. Catal. A*: General 193 (2000) 39.

26 M. Claeys, E. van Steen, *Catal. Today*. 71 (2002) 419.

27 J.T. Kummer, P.H. Emmett . *J.Am.Chem.Soc*. 75 (1953) 5177.

28 L.M. Tau, H.A. Dabbagh, J. Halasz, B.H. Davis. *J. Mol. Catal.* 71(1992) 37.

29 R.T. Hanlon, C.N. Satterfield, *Energy Fuels* 2 (1988) 196.

30 H. Schulz, M. Claeys, *Appl. Catal A*: General 186 (1999) 71.

31 J. Patzlaff, Y. Liu, C. Graffmann, J. Gaube, *Appl. Catal. A*: General 186 (1999) 109.

32 C. Kibby, R. Panell, T. Kobylinsky, *Prepr. ACS-Div. Petr. Chem.* 29 (1984) 1113.

33 J. Li, *PhD thesis,* University of the Witwatersrand, Johannesburg, South Africa, 1999.

34 M. Kraum, M. Baerns, *Appl. Catal. A*: General 186 (1999) 189.

35 N.N. Madikizela, N. Coville, *J. Mol. Catal. A*: Chem. 181 (2002) 129.

36 M. Voβ, D.Borgmann, and G. Wedler, *J. Catal*. 212 (2002) 10.

37 L.F. Liotta, G. Pantaleo, G. Di Carlo, G. Marci, G. Deganello, *Appl. Catal. B*: Environmental 52 (2004) 1.

38 M. Del Arco and V. Rives, *J. Mat. Sc*. 21 (1986) 2938.

39 G. Jacobs, P.M. Patterson, Y. Zhang, T. Das, J. Li, B.H. Davis, *Appl. Catal. A*: General 233 (2002) 215.

40 T.K. Das, J. Jacobs, B.H. Davis, *Cat. Lett.* 101 (2005) 187.

41 R.C. Reuel, C.H. Bartholomew, *J. Catal.* 85 (1984) 63.

42 A. Martínez, C. López, F. Márquez, I. Díaz, *J. Catal*. 220 (2003) 486.

43 A.Y. Khodakov, A. Griboval-Constant, R. Bechara, V.L. Zholobenko, *J. Catal*. 206 (2002) 230.

44 E. Iglesia, S.L. Soled, R.A. Fiato, G.H. Via, *Stud. Surf. Sci. Catal.* 81 (1994) 433.

Chapter 4

Effect of cobalt carboxylate precursor chain length on Fischer-Tröpsch cobalt/alumina catalysts.

4.1 Introduction

The catalytic activity for the Fischer-Tröpsch (FT) reaction is a function of two conflicting parameters: metal dispersion and precursor reducibility and an ideal catalyst would involve an optimal combination of these two parameters. Highly dispersed catalysts generate a strong precursor-support interaction which tends to interfere with the reduction of precursors to the metal state [1].

Previous studies have shown [2-6] that the *type* of cobalt precursor used for the preparation of supported catalysts can affect the cobalt dispersion and reducibility. Van de Loosdrecht et al.[2] have shown that low-loaded cobalt catalysts (2.5 wt%) impregnated using cobalt EDTA and ammonium cobalt citrate precursors resulted initially in very small cobalt oxide particles which reacted with the support (alumina) during reduction. This reaction led to the formation of cobalt aluminates which were not active in the FT reaction. However, catalysts prepared from cobalt nitrate had larger particles which could easily be reduced to metallic cobalt and hence were active under reaction conditions. It was also found that higher loadings of cobalt

catalysts (5.0 wt.%) prepared using ammonium cobalt citrate showed a larger particle size than catalysts prepared with a lower loading (2.5 %) of the citrate precursor [2]. The use of oxalate, acetate and acetyl acetonate as cobalt precursors on titania have been studied and the synthesis resulted in catalysts with a higher activity compared to the reference catalyst prepared from cobalt nitrate. A slight correlation between the measured activities and an increasing cobalt dispersion which was affected by the preparation procedure and type of precursor was observed [3].

The effect of precursor type on SBA-15 and MCM-41 supported cobalt catalysts has also been reported [4, 5]. For Co/SBA-15 catalysts at similar cobalt loading (ca. 20%), a higher dispersion and a stronger cobalt-support interaction leading to the formation of poorly reducible cobalt silicates was observed for oxidized samples prepared from acetate and acetylacetonate precursors in comparison to that derived from cobalt nitrate [4].

Panpranot et al.[5] have found that for Co/MCM-41, use of an organic precursor such as cobalt acetate or cobalt acetylacetonate resulted in the generation of very small cobalt oxide particles. Further, the Co particles only exhibited low activities for CO hydrogenation and this observation was ascribed to the formation of cobalt silicate. The use of cobalt chloride has been reported to lead to the formation of very large cobalt particles and residual chloride ions that blocked metal sites that consequently lowered the active surface area. The use of cobalt nitrate resulted in the synthesis of

both small cobalt particles dispersed throughout MCM-41 and some larger particles located on the external surface of the MCM-41.

Most of these previous studies have compared catalysts prepared from a range of precursors that have been compared with catalysts prepared from cobalt nitrate as a reference. However, the Co precursors have been quite disparate and issues relating to the effect of the *counter ion* have not been studied in a systematic manner.

The present study aims at studying the effect that could originate from varying the cobalt carboxylate chain length during catalysts preparation. Little is known about the influence of cobalt precursors on the dispersion and reducibility of cobalt when different organic precursors with the same functional group are used. The dependency of the above effect with Co loading is also examined in this study.

4.2 Experimental

4.2.1 Synthesis of cobalt carboxylate complexes

Cobalt acetate was taken from the laboratory shelves (Aldrich 99%) and the other cobalt carboxylates were prepared by reacting $CoCO_3$ with excess of the appropriate carboxylic acid (pentanoic and nonanoic). Hot water (60ºC) was used as solvent

except in the preparation of cobalt nonanoate where hot distilled hexane (60ºC) was used. The carboxylic acid was added drop-wise to the carbonate solution and the reaction temperature was raised to 100ºC and held at this temperature until the volume of the solvent was reduced to 40% of its initial value. The solution was cooled, and held at room temperature for 24 hours. The solid formed was redissolved in hot distilled water, the solution filtered while still warm, and the filtrate was allowed to re-crystallize over several days. The obtained crystals were dried at 90ºC for 2 hours before they were used to prepare the supported catalyst.

In the case of cobalt nonanoate, instead of dissolving the solid that had formed after cooling, the solid was washed several times with cold, distilled hexane and then dried at 90ºC for 2 hours before being used in the catalyst preparation.

4.2.2 Catalyst preparation

Catalysts were prepared by incipient wetness impregnation of the γ-Al_2O_3 support (Laporte, surface area = 192 m^2/g) with the requisite cobalt carboxylate dissolved in methanol. The sample was dried for 24 hours at room temperature with occasional stirring and then dried at 120°C for 2 hours. The Co/Al_2O_3 was calcined in air at 400°C for 6 hours.

4.2.3 Catalyst characterization

TPR analyses were performed in the apparatus described in chapter 2. The calcined catalyst (0.1 g of 15 or 20% Co/Al_2O_3) or (0.2 g of 10% Co/ Al_2O_3) was placed in a U shaped quartz tube reactor and exposed to a flow of pure nitrogen at 150°C for 30 min prior to the reduction. The reduction was done using a 5% H_2 in Ar gas mixture. The gas flow-rate was kept at 20 ml/min for all the catalysts characterised in this study. The heating rate was set at 8°C/min. The maximum temperature for the analysis was 800ºC.

Catalysts were also characterized by XRD, H_2 chemisorption and O_2 titration described in chapter 2.

4.2.4 Catalyst designation

The new catalysts were designated as Co**X**-**Y**Al where **X** = Co wt.% in the catalyst and **Y** = Carbon number of the cobalt carboxylate used as catalyst precursor. Hence Co**10**-**9**Al will represent an alumina supported catalyst containing 10 wt.% Co prepared from cobalt nonanoate.

4.2.5 Catalyst testing

The FT reaction was carried out using the stirred basket reactor described in chapter 2. Before the FT reaction was commenced the catalyst was pre-treated in a pure hydrogen stream (T = 350°C, 18 hours, atmospheric pressure, flow rate 30 ml/min STP; exit conditions), during which time the cobalt oxide particles were reduced to cobalt metal, the active catalyst form for the FT reaction. To allow for comparison, in this study the reduction conditions used were the same for each run. After reduction the reactor was cooled and maintained at 220°C. The pure hydrogen was then replaced with synthesis gas (H_2:CO ratio of 2, 10% N_2 as internal standard for mass balance calculations). The space velocity was 0.225 SL.$(g_{cat}.h)^{-1}$ for all the runs. After the catalyst has stabilised the liquid and wax traps were emptied and the mass balance evaluation commenced.

4.3 Results and discussion

4.3.1 Purity of cobalt carboxylates

The purity of the prepared cobalt carboxylates was determined by TGA analysis in air. Figure 4.1 shows the TGA profile for cobalt pentanoate and cobalt nonanoate. The TGA profile for cobalt carbonate was also obtained for comparison in order to

confirm that new compounds (cobalt carboxylates), different from cobalt carbonate, were formed. An initial mass loss around 100°C was evident for all the three samples (figure 4.1). This was probably due to the removal of volatile impurities and the moisture in the samples. A mass loss due to the thermal decomposition of the sample was observed around 300°C for all the samples. As the thermal decomposition occurred in air, the residual mass of the sample at temperatures above 350°C was assumed to be Co_3O_4. The measured mass loss percentages agreed, within experimental error, with the theoretical mass loss percentages corresponding to cobalt carbonate, cobalt pentanoate and cobalt nonanoate transformation to Co_3O_4 respectively. The actual mass of cobalt contained in the analysed sample was calculated from the mass of Co_3O_4 formed during the TGA analysis. The purity of the sample was determined by comparing the actual mass of cobalt determined from Co_3O_4 by TGA analysis to the theoretical mass of cobalt that would have been contained in the sample before the TGA analysis if it was pure. 90.3 and 94.3 % purity were obtained for cobalt pentanoate and nonanoate respectively.

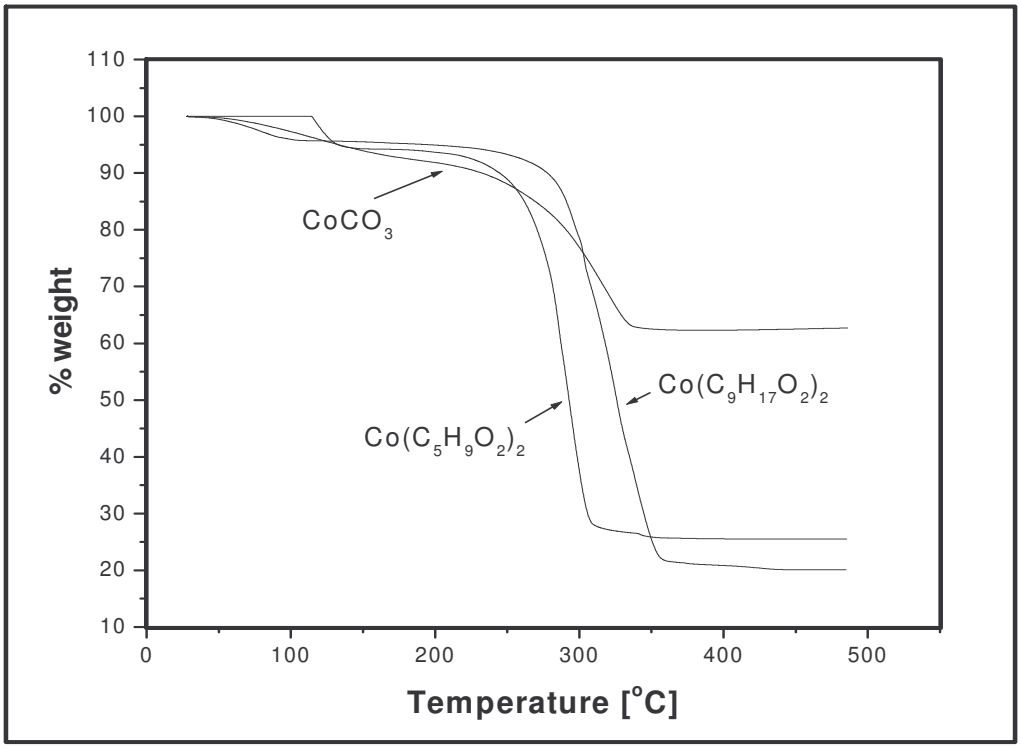

Figure 4.1 *TGA profile for cobalt salts*

4.3.2 TPR results

The TPR profiles for Co10-2Al, Co10-5Al and Co10-9Al are presented in Figure 4.2. All the catalysts show H_2 uptake peaks at low temperatures (below 500°C) and at high temperatures (above 500°C). The Co10-5Al and Co10-9Al show two major peaks below 500°C and a broad peak located between 450-750°C. In contrast the Co10-2Al sample presents only one minor peak below 500°C and a major peak at high temperature and another possible peak which starts around 700°C.

Two major peaks at ca. 350°C and between 400 and 800°C are usually reported for Co/Al_2O_3; The first peak for the two step reduction corresponds to the reduction of Co_3O_4 to CoO and CoO reduction to Co metal (around 350°C) and the second peak to the reduction of a highly dispersed material, Co_xO_y-Al_2O_3, to Co metal between 400 and 700°C [7-15]. An additional peak, sometimes observed around 200°C, is usually attributed to the reductive decomposition of the remaining cobalt nitrate left behind after incomplete calcination.

A high temperature peak (above 850°C) is also frequently reported for Co/Al_2O_3 catalysts [2, 7-9, 16]. It is assigned to a cobalt-aluminium oxide compound similar to cobalt aluminate ($CoAl_2O_4$) which reduces at around 950°C. The formation of this compound is a result of solid-state reactions with cobalt ions diffusing into the alumina lattice [8, 9]. Belambe et al.[17] have reported two separated peaks for the two steps of the reduction of Co_3O_4 to Co metal. However no broad peak between 400-700°C generally attributed to the reduction of highly dispersed and/or amorphous oxides was reported in their study. Voβ et al.[18] have reported that the calcined Co/Al_2O_3 showed four separate TPR peaks at 447, 547, 657 and 787 °C. The first peak was assigned to the reduction of CoO. The second and third peaks were assigned to the reduction of Co_3O_4 and the fourth peak was attributed to the reduction of $CoAl_2O_4$.

The TPR profiles of the *uncalcined* Co/Al_2O_3 prepared from Co carboxylates (not shown in this thesis) showed some negative peaks around 300°C which could certainly be assigned to the reductive decomposition of the carboxylates. These peaks have disappeared in the TPR profiles of the calcined catalyst suggesting a complete

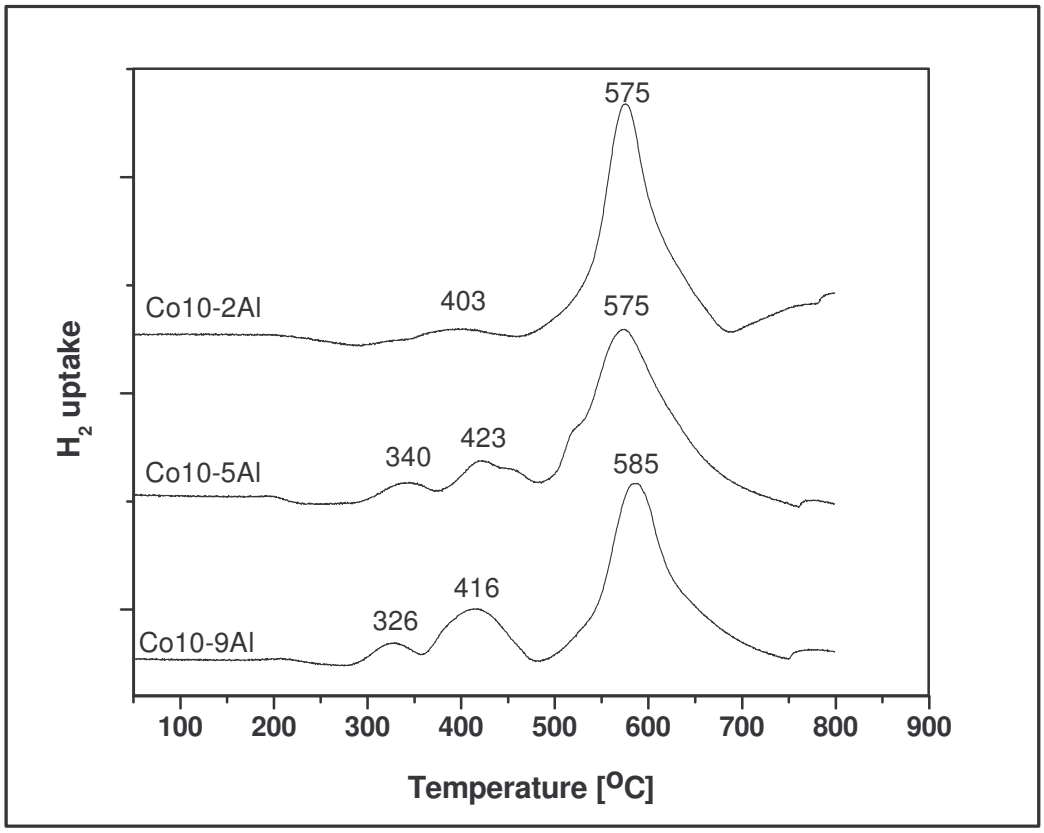

Figure 4.2 *TPR profiles for calcined alumina supported cobalt catalysts (10 wt.% Co) prepared from cobalt carboxylates of different chain lengths*

decomposition of the carboxylates during calcination. Thus, none of the TPR peaks obtained for the calcined catalysts in this study could be attributed to the reductive decomposition of the precursor (cobalt carboxylates). However it can be seen that the ratio of the area under the first peak to that of the second peak, for both the Co10-5Al and Co10-9Al catalysts is about 1:3 which is the stochiometric ratio for the two step

reduction of Co_3O_4 to Co metal. The first peak at 340 and 326°C for Co10-5Al and Co10-9Al catalyst respectively, is assigned to the reduction of Co_3O_4 to CoO and the second peak (423 and 416°C for Co10-5Al and Co10-9Al respectively) has been attributed to the reduction of CoO to Co^0 . The single peak at 403°C for the Co10-2Al was assigned to the unresolved reduction of Co_3O_4 to Co^o. For the latter catalyst, there is a peak which starts around 700°C. This peak can be assigned to the reduction of cobalt aluminates. The peaks around 580°C observed for all the three catalysts are attributed to the reduction of Co oxide particles in strong interaction with the support that are difficult to reduce.

Figure 4.3 shows TPR profiles for Co/Al_2O_3 with 20 wt.% Co loading. The following can be observed when comparing TPR profiles for catalysts with high cobalt loading (figure 4.3) to those with low cobalt loading (figure 4.2):

i) The increase in cobalt loading in the catalyst increases the area under the peaks corresponding to the two step reduction of Co_3O_4 to Co^o. These peaks grow bigger for the 20% cobalt loaded catalysts and are consequently less resolved (figure 4.3) compared to the low loaded catalysts (figure 4.2);

ii) The increase of cobalt loading in the catalyst induces a shift of reduction peaks to lower temperatures. In each case, when catalysts prepared from the same precursor are compared, it can be seen that reduction of Co_3O_4 to Co^0 and reduction of highly dispersed cobalt oxide species occur at lower temperatures for high loaded catalysts than for low loaded ones. For example: for catalyst prepared using cobalt nonanoate with 10% cobalt loading (Co10-9Al), the peaks assigned to reduction of CoO to Co^0 and to the reduction cobalt species in

strong interaction with the support occurred at 416 and 585°C respectively (figure 4.2). These reduction peaks shifted to 373 and 535°C respectively when the cobalt loading was increased to 20% (see Co20-9Al in figure 4.3);

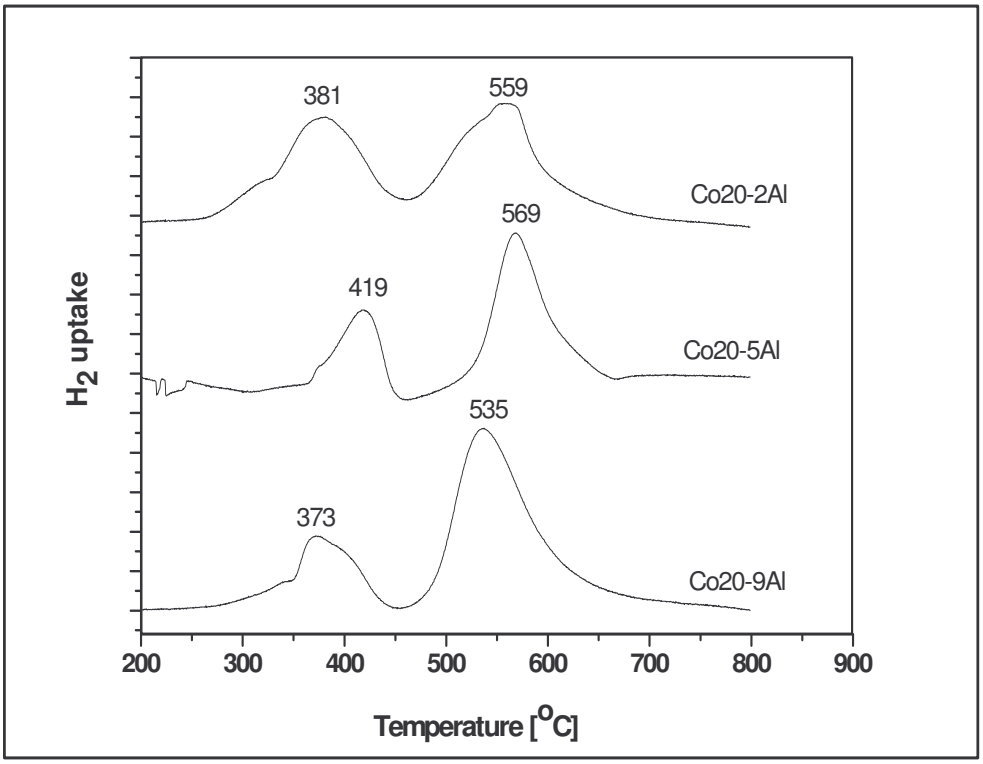

Figure 4.3 *TPR profiles for calcined alumina supported cobalt catalysts (20 wt.% Co) prepared from cobalt carboxylates of different chain lengths*

iii) The high reduction temperature peak (> 700°C) observed during the TPR for the 10% Co catalyst prepared from cobalt acetate has completely disappeared in the 20% cobalt loaded catalyst.

These observations show that the catalyst reducibility is improved with increasing cobalt loading in the catalyst.

The amount of cobalt reduced during TPR experiments was calculated for each catalyst after calibration with AgO. Calculations were based on the area under the peak around 400°C which was assigned to the reduction of CoO to Co^0. All species reduced above 500°C where not considered in calculations because of their unknown stochiometry. Thus, the relative position of peaks at ~ 400°C and 550°C and their magnitude can give an idea on the Co reduction process that is influenced by effects such as valency, cobalt oxide dispersion, metal-support interactions, etc.

It is generally agreed in the literature that the high temperature reduction peak (around 500 - 600°C) observed in the TPR for a Co/Al_2O_3 is due to the reduction of highly dispersed Co oxide particles strongly interacting with the support. Thus, the ratio of the area under this peak to that corresponding to the second step reduction of easily reducible cobalt oxide particles (around 400°C) would give an idea on the catalyst metal-support interaction. In this study the above ratio has been considered as the '*metal-support interaction factor*' and has been denoted by Φ. Therefore a very strong metal-support interaction would be expressed by a large value of Φ. Data are

summarized in figures 4.4 and 4.5. It can be seen for all the catalysts that the amount of Co reduced per gram of catalyst increases with Co loading in the catalyst.

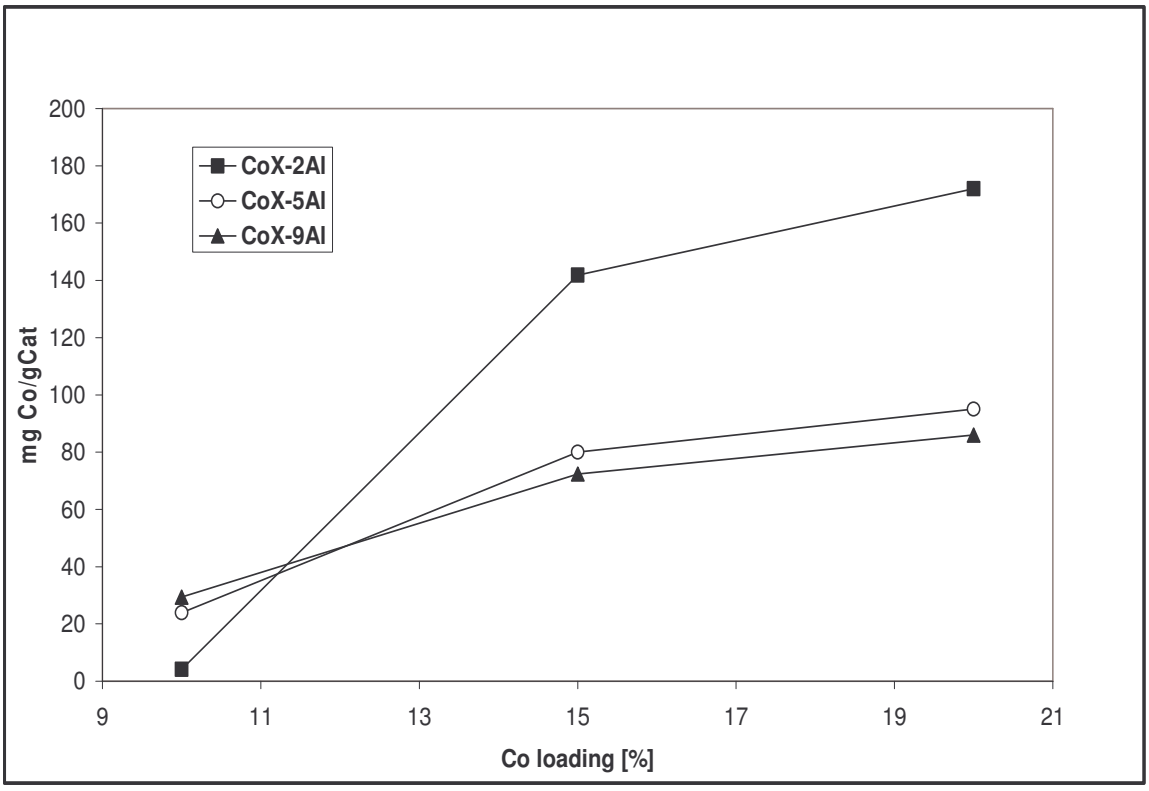

Figure 4.4 *Amount of reduced cobalt during TPR in function of Co loading for Co/Al_2O_3 catalysts prepared from Co carboxylates of different chain lengths*

With a Co loading around 10%, the reducibility of Co/Al_2O_3 increases in the order Co10-2Al < Co10-5Al<Co10-9Al. The catalyst prepared from Co acetate which was

the least reduced when Co loading was 10% becomes the most reduced at high Co loadings (figure 4.4).

The metal-support interaction factor Φ (see figure 4.5) was at its highest value for Co10-2Al and decreased with Co loading. The increase in Co loading did not significantly affect the Φ parameter in the range of 15-20% Co loading.

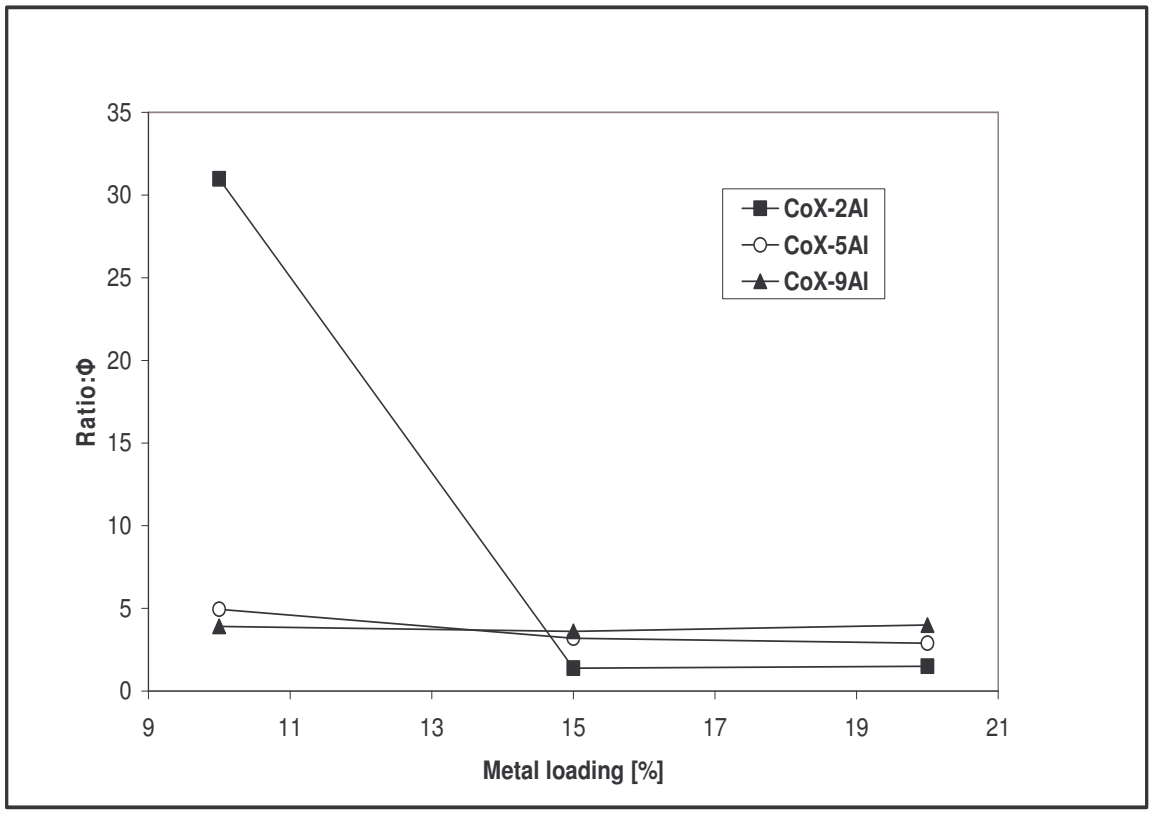

Figure 4.5 *Metal-support interaction factor Φ in function of Co loading for Co/Al_2O_3 catalysts prepared from Co carboxylates of different chain lengths*

Previous studies [4, 11, 19 - 22] have reported an increase in catalyst reducibility with metal loading. The increase in catalyst reducibility with the Co loading was explained by the increase in the average cluster size and the resulting loss of interaction with the support. It is believed that bigger cobalt particles can be readily reduced and facilitate the reduction of particles in strong interaction with the support by hydrogen spillover [23]. To gain more insight into this effect, XRD and H_2-chemisorption analysis was performed to complement the TPR study.

4.3.3 Results from H_2-Chemisorption

Jacobs et al.[22] have shown that cobalt species with strong support interactions are not completely reduced, even after 10 hours of reduction. To determine the cluster size by any chemisorption method for Co/Al_2O_3, the degree of reduction of cobalt should be considered [1, 22, 24, 25]. The dispersion percentage and the metal average particle size were calculated as indicated in chapter 2.

The results from the H_2-chemisorption analysis are presented in Table 4.1. It is shown in Table 4.1 that the metal dispersion for supported 10% Co catalysts prepared from Co carboxylates decreases with the carboxylate chain length. The calculated average metal crystallites diameter increases in the order Co10-2Al < Co10-5Al < Co10-9Al. By increasing the Co content on the catalyst, the average cobalt cluster size on the catalyst prepared from cobalt acetate is significantly increased while the average

cluster size on catalysts prepared from cobalt pentanoate and cobalt nonanoate is only slightly affected. By loading at the highest Co loading in this study (20 wt.% Co), the largest average cobalt particle size is obtained with Co20-2Al.

Table 4.1 Summary result from H_2-Chemisorption

Catalyst	Metal dispersion [%]	Average crystallite diameter [nm]
Co10-2Al	14.1	7
Co20-2Al	1.6	60
Co10-5Al	3.4	28
Co20-5Al	2.7	36
Co10-9Al	3.1	32
Co20-9Al	2.7	36

4.3.4 Results from XRD

The average Co_3O_4 particle size of the calcined catalysts was calculated using the Scherrer equation. The diameter of Co_3O_4 particles was used to calculate the diameter of metallic Co crystallite using the formula [10]:

$$d_v(Co^0) = 0.75\, d(Co_3O_4) \quad (3.1)$$

Figure 4.6 shows the XRD patterns of the Co/Al_2O_3 catalysts with 10% Co loading. No significant Co_3O_4 peak was detected in the XRD pattern of Co10-2Al suggesting very small particles. Table 4.2 summarizes the results obtained from XRD.

No peak for Co-Al_2O_4 was detected for all catalysts used in this study. Previous studies [8, 10] have also indicated that the Co/Al_2O_4 (on calcined Co/Al_2O_3) was also not detected by XRD analysis. This could suggest that the Co/Al_2O_4 attributed to the high temperature reduction peak (starting around 700°C during TPR analysis) for the Co10-2Al catalyst, did not form during calcination but rather during the TPR analysis. The average particle diameters calculated from XRD significantly differ from those obtained from chemisorption. This is probably due to the fact that the particle size determination from XRD was based on cobalt oxides peak detected around $2\theta = 31.4°$ instead of the most intense peak which was apparently situated at $2\theta = 37°$. The most intense peak could not be used in the calculation because of an overlap with an alumina diffraction peak. Although the sizes determined by the two methods (H_2 chemisorption and XRD) differ, the trends are the same. It can still be seen that there exists a dependency of the Co particle size with the carboxylate chain length.

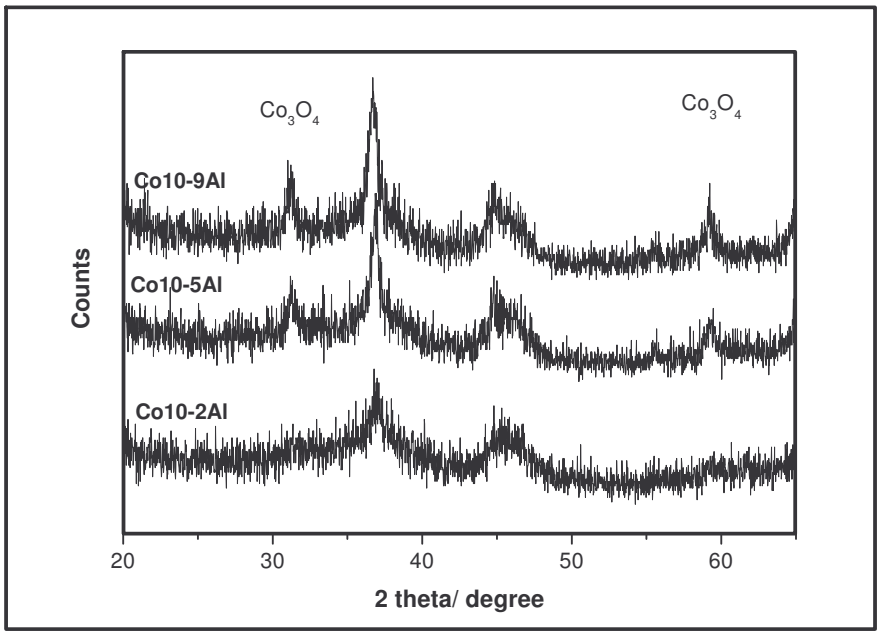

Figure 4.6 *XRD patterns for calcined 10%Co/Al_2O_3 catalysts prepared from Co carboxylates with different chain lengths.*

Table 4.2 Summary results from XRD

Catalyst	Average crystallite diameter [nm]
Co10-2Al	NPD*
Co15-2Al	10.3
Co20-2Al	9.7
Co10-5Al	7.0
Co15-5Al	7.9
Co20-5Al	7.1
Co10-9Al	7.5
Co15-9Al	7.0
Co20-9Al	7.6

NPD = No Co_3O_4 peak detected.*

At 10% Co loading, big cobalt particles are obtained when long chain precursors are used. However when the Co loading increases, cobalt particle sizes in the catalysts prepared using cobalt pentanoate and cobalt nonanoate stay comparable in size whereas the biggest cobalt particle sizes are measured on catalysts prepared from cobalt acetate which had the shortest chain length. A schematic diagram to show these effects is given below.

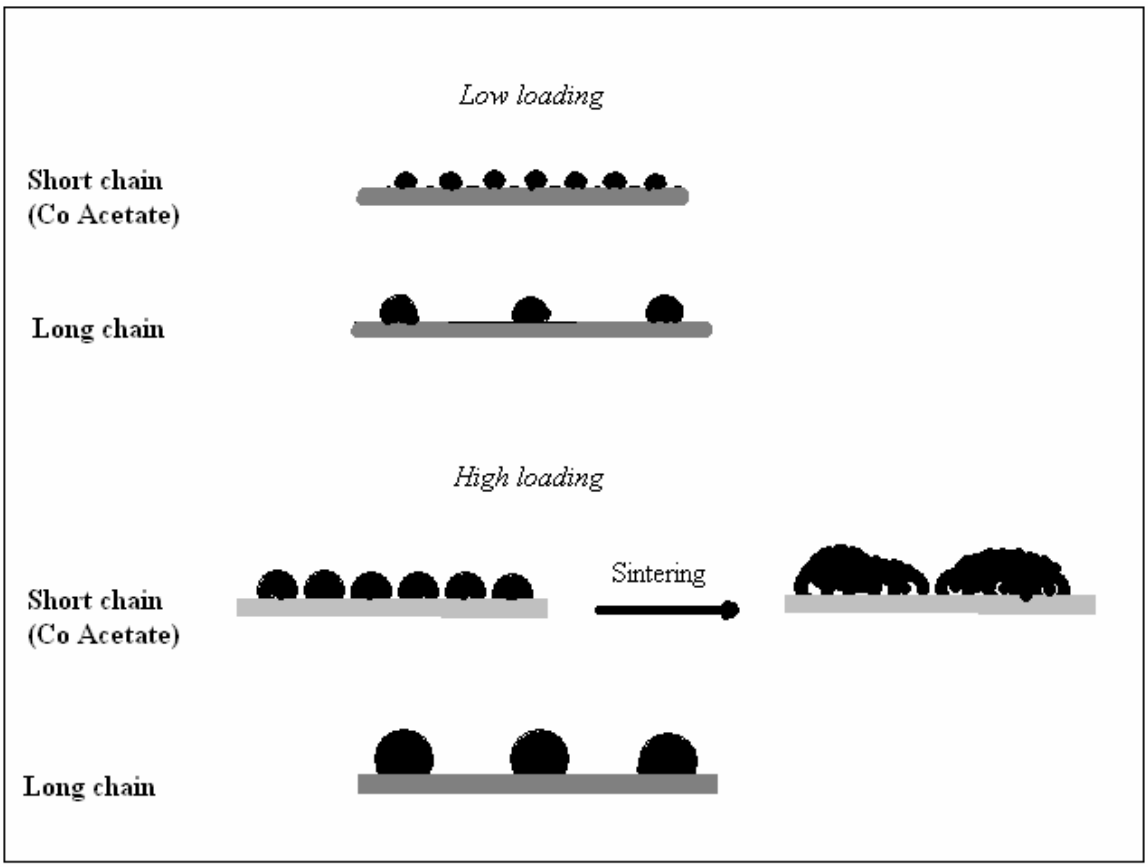

Figure 4.7 *Cartoon showing the proposed effect of cobalt carboxylate chain length on particle sizes*

During the formation of Co_3O_4 crystallites, the distance separating nuclei is believed to be proportional to the ligand chain length. At low loading, cobalt acetate leads to many nuclei which are closer to each other. This distribution leads to the formation of small particles as opposed to bigger particles obtained with longer chain cobalt carboxylates due to a small number of nuclei which are in this case far apart from each other. An increase in Co loading results in particle growth and reduction of the

distance between particles. Particles become significantly closer at a high loading of a short chain cobalt carboxylate. This favours sintering during thermal pre-treatment and can therefore explain the bigger average particle diameters measured in the catalysts prepared from cobalt acetate (short chain) at a high loadings. This agrees with the study by Cheung et al.[26] who showed that the formation of larger diameter iron nanoclusters by thermal decomposition of $Fe(CO)_5$ was favoured in the presence of shorter chain-length capping ligand, i.e. octanoic acid compared to lauric and oleic acid. Clearly HRTEM will be needed to further confirm our proposal.

4.3.5 Results from FT reactions

Table 4.3 summarizes the results from the FT reaction. The catalytic activity expressed as CO consumption rate per gram of catalyst with 10% Co loaded catalyst increases with increasing precursor chain length, i.e. Co10-2Al < Co10-5Al < Co10-9Al. By increasing the cobalt loading to 15 and 20% respectively catalysts prepared from cobalt pentanoate and cobalt nonoate display similar activities while higher activities are measured for catalysts prepared using cobalt acetate as precursor. When catalysts prepared from the same precursor are compared, the catalytic activity increases with cobalt loading. However the specific activity expressed as turnover frequency (TOF) for catalysts prepared from cobalt pentanoate and cobalt nonanoate are similar and are not affected by cobalt loading in the catalyst. A significant variation of the TOF with cobalt loading has been observed for catalysts prepared

Table 4.3 Summary of the FT results

Catalyst	Red. extent[a]	CO conv. rate[b]	10^3 x TOF[c]	CH_4 Select.[d]	C_{5+} Select.[e]	Olef. to paraf. ratio[f]
Co10-2Al	0.09	0.007	0.33	60	3	-
Co15-2Al		0.250		10	76	0.48
Co20-2Al	0.90	0.287	0.59	9	79	0.45
Co10-5Al	0.25	0.067	0.47	16	64	0.51
Co15-5Al		0.137		13	71	0.53
Co20-5Al	0.46	0.178	0.42	13	77	0.49
Co10-9Al	0.30	0.077	0.49	14	69	0.51
Co15-9Al		0.140		14	72	0.47
Co20-9Al	0.41	0.165	0.44	12	77	0.53

a: reduction extent determined by oxygen titration;

b: CO conversion rate in [$\mu mol.(g_{cat}.s)^{-1}$];

c: Turn over frequency in [s^{-1}], determined from chemisorption and FT reaction data;

d and e: carbon based selectivities in [%];

f: Olefin to paraffin ratio calculated from C_2 to C_4.

from cobalt acetate. A change in cobalt loading from 10% to 20% in these catalysts resulted in a significant increase of TOF from 0.33 x 10^{-3} to 0.59 x 10^{-3} s^{-1}.

As discussed earlier, an increase in cobalt loading in the catalyst significantly increased the cobalt particle size for catalysts prepared from cobalt acetate. An apparent correlation between the cobalt particle size and the TOF can therefore, be established: the TOFs decreases when Co particle size decreases. Catalysts prepared using cobalt pentanoate and cobalt nonanoate had comparable cobalt particle size leading to a comparable TOF. Previous studies have also reported a decrease in TOF with decreasing cobalt particle size (increasing dispersion) [19, 27]. This effect was explained by variations in the distribution of low and high coordination sites and by changes in the nature of the adsorbed CO species available for reaction [27]. These authors claimed that high specific activity is apparently favoured on sites to which CO is strongly coordinated. Other studies [4, 20, 28 - 35] have reported that the cobalt specific activity for CO hydrogenation reaction was not significantly affected by particle size. This apparent controversy suggests that the effect of cobalt particle size on catalytic behaviour is also affected by other parameters like particle size range, operating conditions, etc. Barbier et al.[36] have reported an increase of specific activity with increasing particle size up to 6 nm above which the specific activity was invariant with cobalt particle size. The explanation of the observed effect was based on a topological hypothesis suggesting that high index planes could favour highly coordinated chemisorbed CO. The most recent study [37] has also reported an increase of specific activity with increasing cobalt particle size up to a critical size of 6 and 8

nm when operating at 1 and 35 bar respectively. These effects were attributed to non classical structure sensitivity in combination with CO-induced surface reconstruction. Particular attention has been drawn to the particle size range where the Co specific activity has been reported to decrease with increasing dispersion [36, 37]. This corresponds to the range where Co metal crystallites reoxidize by water under typical FT reaction conditions [24, 32, 38]. Also, in most cases, specific activities reported in the literature are based on data collected on a catalyst which has reached a steady state, i.e. after the catalyst has been exposed to reacting molecules and to reaction products for a period of time during which an eventual deactivation can occur. As TOF calculations are based on the number of active sites usually determined by hydrogen or carbon monoxide chemisorption on a freshly reduced catalyst, an initial catalyst deactivation before reaching a steady state would lead to an underestimated value of TOF as a result of an unquantified loss of active sites. In the present study, catalysts with similar particle size exhibited comparable initial deactivation behaviour before reaching steady state and the initial deactivation was more significant on catalysts consisting of small cobalt particles. This deactivation behaviour was also observed by Iglesia [32] who had reported a rapid deactivation of small Co metal particles as a result of reoxidation in the presence of water reaction product under typical FTS conditions. Saib et al.[39] have recently established a connection between cobalt crystallites sizes and oxidation behaviour by water during the FT reaction. They used well-defined spherical Co/SiO_2 model catalysts with average cobalt crystallites sizes of 4, 13, and 28 nm. Their study showed that cobalt crystallites of average size of 4 nm did not oxidize with water due to their encapsulation with silica after reduction at

500°C in hydrogen. A maximum of 30 and < 2% cobalt oxidation by water was observed at 300°C for cobalt crystallites with average size of 13 and 28 nm respectively.

In the present study the loss of active sites on catalysts with small cobalt crystallite sizes is significant and this can explain the lower specific activity obtained for these catalysts. In the absence of catalyst deactivation, an invariant specific activity with cobalt particle size can be expected. Thus, changes in the rate of CO consumption per gram of catalyst in the present study can be interpreted as a result of changes in the number of active sites in the catalyst. The number of active sites is a function of metal dispersion and degree of reduction. From the results presented in table 4.3 one can see that the best cases for FT activity and methane selectivity are Co15_2Al and Co20_2Al which have the largest Co crystal sizes (table 4.1 and 4.2). Normaly this could mean that they have the lowest metal area (lowest dispersion) and therefore the lowest FT activity. However, the highest FT activities measured for these catalysts suggest that the degree of reduction is a key item as it increases with the FT activity. The general trend of the results shows a lower degree of reduction, consequently a lower FT activity for highly dispersed catalyst as a result of a high metal-support interaction.

The product selectivity was also affected by the catalyst particle effects induced by changing the catalyst precursor chain length and cobalt loading (see Table 4.3). With 10% Co loading the highest methane selectivity and lowest C_{5+} selectivity were measured on the catalyst prepared using cobalt acetate (Co10-2Al). By increasing the cobalt loading, no significant change in product selectivity was observed for catalysts

prepared using cobalt pentanoate and cobalt nonanoate. However a significant change in product selectivity was observed for catalysts prepared using cobalt acetate. An increase in cobalt loading from 10% to 20% resulted in a decrease of methane selectivity from 60% to 9%. These changes in selectivity are due to cobalt particle size changes in the catalyst. The general trend shows that methane selectivity is lower and C_{5+} selectivity higher on catalysts consisting of big cobalt particle sizes. Catalysts with similar particle sizes had a comparable product distribution.

Previous studies [4, 19, 27, 32, 33, 36, 37, 40] have also reported a decrease in methane selectivity and increase in C_{5+} products with an increasing cobalt particle size. Reuel et al.[19] had suggested that this effect may be due to stable oxides in the well-dispersed and poorly reduced catalysts which catalyze the water gas shift reaction leading to an increase of H_2/CO ratio at the surface. Iglesia [32] attributed this effect to the reversal of chain termination steps via diffusion-limited readsorption of α-olefins. Also Aaserud et al.[41] have recently shown that cobalt catalysts supported on low surface area supports exhibited the lowest activity for propene hydrogenation and that an increased selectivity to higher hydrocarbons would be a result of readsorbed olefins participating in the chain growth. Based on available data in the present study, it is not evident that the observed increase in C_{5+} selectivity is due to olefin readsorption. Olefins readsorption would result in a decrease of olefin to paraffin ratio with increase in C_{5+} selectivity. This trend was not observed with results presented in Table 4.3 where the olefin to paraffin ratio was, within experimental error, the same for all the catalysts except for Co10-2Al where the ratio could not be

determined. The latter catalyst was the least active and produced only a very small amount of products that made the determination of the olefin to paraffin ratio difficult. However results in Table 4.3 show a clear inverse relationship between catalyst reduction extent and methane selectivity and suggest that changes in product selectivity observed in this study are due to the presence of cobalt oxides in the catalysts [19]. The amount of cobalt oxides in the catalysts is affected by the chain length of the precursor used as well as the cobalt loading.

4.4 Conclusion

The effect of the chain length of the cobalt carboxylates used in the preparation of supported cobalt catalysts has been studied by TPR, XRD and hydrogen chemisoption techniques. The as prepared catalysts have been tested for CO hydrogenation activity. It has been shown that when a Co content of 10 wt.% was used, the highest activity was measured for catalysts prepared using longer chain Co carboxylates. However, when the Co loading was increased, the catalyst prepared from the short chain cobalt carboxylate proved to be the most active for the CO hydrogenation reaction. The chain length of Co carboxylates used as a catalyst precursor thus has an effect on the catalyst structure and this effect is dependent on the cobalt loading in the catalyst. The Co loading affects the average particle size and consequently the interaction between the precursor and the support.

References

1 S. Sun, N. Tsubaki, K. Fujimoto, *Appl. Catal. A*: General 202 (2000) 121.

2 J. van de Loosdrecht, M. van der Haar, A.M. van der Kraan, A.J. van Dillen, J.W. Geus, *Appl. Catal. A*: General 150 (1997) 365.

3 M. Kraum, M. Baerns, *Appl. Catal. A*: General 186 (1999) 189.

4 A. Martínez, C. López, F. Márquez, and I. Díaz, *J. Catal*. 220 (2003) 486.

5 J. Panpranot, S. Kaewkun, P. Praserthdam, and J.G. Goodwin, *Cat. Lett.* 91 (2003) 95.

6 S.L. Soled, E. Iglesia, R.A. Fiato, J.E. Baumgartner, H.B. Vroman, and S. Miseo. *Paper 293, 18th North American Catalysis Society Meeting*, Cancun, Mexico, 1-6 June 2003.

7 P. Arnoldy, J.A. Moulijin, *J. Catal.* 93 (1985) 38.

8 D. Schanke, S. Voda, E.A. Blekkan, A.M. Hilmen, A. Hoff, A. Holmen, *J. Catal*. 156 (1995) 85.

9 A.M. Hilmen, D. Schanke, A. Holmen, *Cat. Lett.* 38 (1996) 143.

10 A. Kogelbauer, J.G. Goodwin, and R. Oukaci, *J. Catal.* 160 (1996) 125.

11 M. Meng, P. Lin, Y. Fu, *J. Mol. Catal.* 11 (1997) 325.

12 B. Jongsomjit, J. Panpranot, J.G. Goodwin, *J. Catal.* 204 (2001) 98.

13 B. Jongsomjit, J. Panpranot, and J.G. Goodwin, *J. Catal.* 215 (2003) 66.

14 A. Sirijaruphan, A. Horvath, J.G. Goodwin, and R. Oukaci, *Cat. Lett.* 91 (2003) 89.

15 S.A. Hosseini, A. Taeb, F. Feyzi, F.Yaripour. *Cat. Comm*. 5 (2004) 137.

16 H.C. Tung, and C.T. Yeh, *J. Catal.* 122 (1990) 211.

17 A.R. Belambe, R. Oukaci, and J.G. Goodwin, *J. Catal*. 166 (1997) 8.

18 M. Voβ, D. Borgmann, and G. Wedler, *J. Catal*. 212 (2002) 10.

19 R.C. Reuel, C.H. Bartholomew, *J. Catal*. 85 (1984) 78.

20 S.W. Ho, M. Houalla, and D.M. Hercules, *J. Phys. Chem*. 94 (1990) 6396.

21 A. Barbier, A. Harrif, J.A. Dalmon, G.A. Martin, *Appl. Catal*. *A :* General 168 (1999) 333.

22 G. Jacobs, T.K. Das, Y. Zhang, J. Li, G. Racoillet, B.H. Davis. *Appl. Catal. A:* General 233 (2002) 263.

23 Y. Zhang, M. Koike, N. Tsubaki, *Catal. Lett.* 99 (2005) 193.

24 A.M. Hilmen, D. Schanke, K.F. Hanssen, A. Holmen, *Appl. Catal*. A: General 186 (1999) 169.

25 G. Jacobs, J.A. Chaney, P.M. Patterson, T.K. Das, B.H. Davis, *Appl. Catal. A*: General 264 (2004) 203.

26 C.L. Cheung, A. Kurtz, H. Park, and C.M. Lieber, *J. Phys. Chem*. B 106 (2002) 2429.

27 L. Fu, and C.H. Bartholomew, *J. Catal.* 92 (1985) 376.

28 M.I. Fernandez, R. A. Guerrero, G.F.J. Lopez, R.I. Rodriguez, C.C. Moreno, *Appl. Catal*. 14 (1985) 159.

29 B.G. Johnson, C.H. Bartholomew, D.W. Goodman, *J. Catal*. 128 (1991) 231.

30 E. Iglesia, S.L. Soled, R.A. Fiato, *J. Catal*. 137 (1992) 212.

31 E. Iglesia, S.L. Soled, R.A. Fiato, G.H. Via, *Stud. Surf. Sci. Catal*. 81 (1994) 433.

32 E. Iglesia, *Appl. Catal*. A: General 161 (1997) 59.

33 B. Ernst, C. Hilaire, A. Kiennemann, *Catal. Today*. 50 (1999) 413.

34 A.Y. Khodakov, A. Griboval-Constant, R. Bechara, V.L. Zholobenko, *J. Catal*. 206 (2002) 230.

35 W.P. Ma, Y.J. Ding, and L.W. Lin, *Ind. Eng. Chem. Res*. 43 (2004) 2391.

36 A. Barbier, A. Tuel, I. Arcon, A. Kodre, and G.A. Martin, *J. Catal*. 200 (2001) 106.

37 G.L. Bezemer, J.H. Bitter, H.P.C.E. Kuipers, H. Oosterbeek, J.E. Holewijn, X. Xu, F. Kapteijn, A.J. van Dillen, and K.P. de Jong, *J. Am. Chem. Soc*. 128 (2006) 3956.

38 D. Schanke, A.M. Hilmen, E. Bergene, K. Kimari, E. Rytter, E. Adnanes, A. Holmen, *Catal. Lett.* 34 (1995) 269.

39 A.M. Saib, A. Borgna, J. van de Loosdrecht, P.J. van Berge, J.W. Geus, J.W. Niemantsverdriet, *J. Catal*. 239 (2006) 326.

40 S. Storsaeter, B. Tϕtdal, J.C. Walmsley, B.S. Tanem, A. Holmen, *J. Catal.* 236 (2005) 139.

41 C. Aaserud, A.M. Hilmen, E. Bergene, S. Eric, D. Schanke, A. Holmen, *Catal. Lett.* 94 (2004) 171.

Chapter 5

Effect of the addition of Au on a Co/TiO_2 catalyst for use in the Fischer-Tröpsch reaction

5.1 Introduction

Titania supported Co catalysts have been reported to be more active for CO hydrogenation than cobalt catalysts supported on other supports i.e. Al_2O_3, SiO_2, etc [1]. However, one of the major problems associated with Co/TiO_2 catalysts is the formation of Co-titanates during a catalytic process. Soled et al.[2, 3] have reported that cobalt oxide (Co_3O_4) reacts with TiO_2 to form cobalt titanate ($CoTiO_3$) under regeneration conditions. The formed $CoTiO_3$ is very stable and does not have any Fischer-Tröpsch (FT) activity. The titanate can only be reduced at high temperatures and the resulting metal may not be accessible as it can be decorated by TiO_x species. To prevent the formation of $CoTiO_3$, Mauldin et al.[4, 5] have suggested the addition of promoters such as rhenium, hafnium, cerium, or zirconium to the Co/TiO_2 catalyst. Indeed, later studies have also shown that addition of a second metal to Co/TiO_2 system can change the catalyst behavior. Iglesia et al.[6] have reported that addition of small amounts of Ru to a Co/TiO_2 FT catalyst led to an increase in Co site density during reaction without modifying the chemical reactivity of the exposed Co surface atoms. A higher yield of a heavier and more paraffinic product was apparent on Co-Ru catalysts. The added Ru inhibited the deactivation of surface cobalt ensembles and facilitated the regeneration of Co-Ru catalysts by a hydrogen treatment at a

temperature as low as the reaction temperature. Price et al.[7] observed an increased reduction of surface Co in a Co/TiO_2 catalyst in presence of Ru. They also found that the CoRu catalyst was more active for the FT reaction than the Co catalyst. It has also been reported that the addition of Re or Ru to a Co/TiO_2 system improved the catalyst activity and selectivity for the FT reaction [8]. The noble metal promoted the reduction of Co oxide in the Co/TiO_2 catalyst [8, 9].

A similar effect was also observed by Leite et al.[10] who used Au to promote a Co/kaolin catalyst used for the synthesis of 2,3 –dihydrofuran. They reported that the addition of Au led to the formation of new cobalt species that were reducible at significantly lower temperatures when compared to the unpromoted catalyst. To the best of our knowledge, no other study of an Au promoting effect on a Co/TiO_2 catalyst has been reported in the literature to date. In the present study, the effect of Au addition on the structure of a Co/TiO_2 system and its performance in the FT reaction has been investigated. In particular, the effect of the Au/Co ratio has been evaluated by varying the amount of Au added to a 10% Co/TiO_2 catalyst.

5.2 Experimental

5.2.1 Preparation of catalyst supports

TiO_2 (Degussa P25, SA = 50 m^2g^{-1}) was mixed with distilled water (1 g TiO_2 with 1 ml distilled water), and dried at 120°C for one hour. The dried support was calcined in air (400°C, 16 h) in an oven and crushed and sieved to give particles with size < 100 µm size for use in the catalyst preparation.

5.2.2 Preparation of catalysts

A series of catalysts consisting of an undoped and Au doped (0.2 to 5 wt.% Au) titania supported cobalt catalyst was prepared by deposition-precipitation (undoped catalyst) and deposition-coprecipitation (Au doped catalysts).

For the undoped catalyst, the support (TiO_2) was mixed with a solution of $Co(NO_3)_2.6H_2O$ (3 g $Co(NO_3)_2.6H_2O$ in 50 ml H_2O). The amounts of support and precursor were combined to produce a catalyst containing 10 wt.% Co. Ammonia solution (ca. 4 M) was added dropwise to the mixture with stirring until a pH of around 8.5 was reached. The resulting sample was aged for one hour followed by filtration and drying at 120°C for 20 hours. For an Au doped catalyst, the preparation procedure was similar to that used to make the undoped catalyst except that an

appropriate amount of $HAuCl_4.3H_2O$ solution was added to the support-cobalt precursor mixture prior to coprecipitation. To achieve a good base for comparison, the amount of Co in all the catalysts was kept constant while the added Au only replaced a certain amount of the support. For example 100 g of totally reduced 5%Au/10%Co/TiO_2 contains 5 g Au, 10 g Co and 85 g TiO_2 (Au/Co atomic ratio = 0.15) . Also after filtration, the Au doped catalysts were washed several times with a large amount of distilled water to remove residual chloride ions. After drying, all the catalysts were calcined at 400°C in air (heating rate: 10°C/min and held at 400°C for 5 hours).

5.2.3 Catalyst characterization

Catalysts were characterized by Atomic adsorption (A.A) spectroscopy, X-ray diffraction (XRD) and X-ray photoelectron spectroscopy (XPS) analyses as described in chapter 2.

The temperature programmed reduction (TPR) analysis was also performed in the apparatus described in chapter 2. The analysis conditions were identical to those described in chapter 4 except that the mass of the sample was kept 200 mg for all the analysed catalysts.

5.2.4 Catalyst evaluation

The FT reaction was carried out in the Plug Flow Reactor (PFR) system described in chapter 2. To allow for comparison, all the FT runs were performed using the same amount of fresh catalyst (100 mg) diluted with silicon carbide (100 mg, 200 – 450 mesh). Before the FT reaction was commenced the catalyst was pre-treated in a pure hydrogen stream (heating rate 1°C/min). The reactor was maintained at 350°C for 10 hours (atmospheric pressure, GHSV=6 NL/(g_{cat}. h) referred to the feed), during which time the cobalt oxide particles were reduced to cobalt metal, the active catalyst form for the FT reaction. After reduction the reactor was cooled below 100°C and the pure hydrogen was then replaced with synthesis gas (H_2:CO ratio of 2, 10% N_2 as internal standard). The pressure in the reactor was increased and maintained at 20 bar for the FT reaction. The space velocity for the FT reaction was kept at 3 NL/(g_{cat}. h) referred to the reactor feed for all the runs unless otherwise specified. The temperature was gradually increased and maintain at 220°C (heating rate 10°C/min). Under these conditions no significant amount of wax could be collected at the bottom of the reactor. Thus, only one trap, maintained at ambient temperature, was mounted downstream of the reactor for oil and water collection. The analysis of the oil fraction was carried out using an off-line GC with a flame ionisation detector on a fused silica capillary column.

5.3 Results and discussion

5.3.1 Catalyst composition

Results from the AA analysis are shown in Table 5.1. These results were obtained on dried catalysts (120°C for 20 hours) before they were submitted to thermal treatment to decompose Co and Au hydroxides. This can explain the slightly lower values of Co and Au loadings reported in Table 5.1 compared to values which could have been expected from calcined and totally reduced catalysts. It can also be observed from the experimental data that the Co loading is the same for all the catalysts. The increase in Au loading in the catalysts agrees with the predicted trend.

Table 5.1 A A results

Catalyst	[a] % Co	[b] % Au
10%Co/TiO_2	9.0	-
0.2%Au/10%Co/ TiO_2	9.2	0.17
0.7%Au/10%Co/ TiO_2	9.0	0.60
2%Au/10% Co/ TiO_2	9.1	1.95
5%Au/10% Co/ TiO_2	8.9	4.19

a and b: weight percentage of dried uncalcined catalysts.

5.3.2 XRD analysis

Figure 5.1 shows XRD patterns of calcined 10%Co/TiO_2 catalysts doped with various amounts of gold. Diffraction peaks for Co_3O_4 are detected at 2θ = 31.6° and 59.01°. Au diffraction peaks characteristic of Au(1 1 1), Au(2 0 0), Au (2 2 0) and (2 2 2) and mostly corresponding to fcc metallic Au were detected at 38.4°, 44.5°, 64.1° and 77.1° [15, 16]. An overlap of the Au diffraction peak with the titania support at a diffraction angle around 2θ = 38° was observed. However, at high Au loadings this peak becomes bigger than that of titania and can be easily identified. No diffraction peak for Au was detected in catalysts at low loading (0.2 and 0.7 wt.% Au). However when the Au loading was further increased to 2 and 5% respectively, the intensity of the Au diffraction peaks increased with Au loading in the catalyst, thus suggesting an increase in the number of Au particles. The detection of very small Au nanoparticles by XRD is not possible.

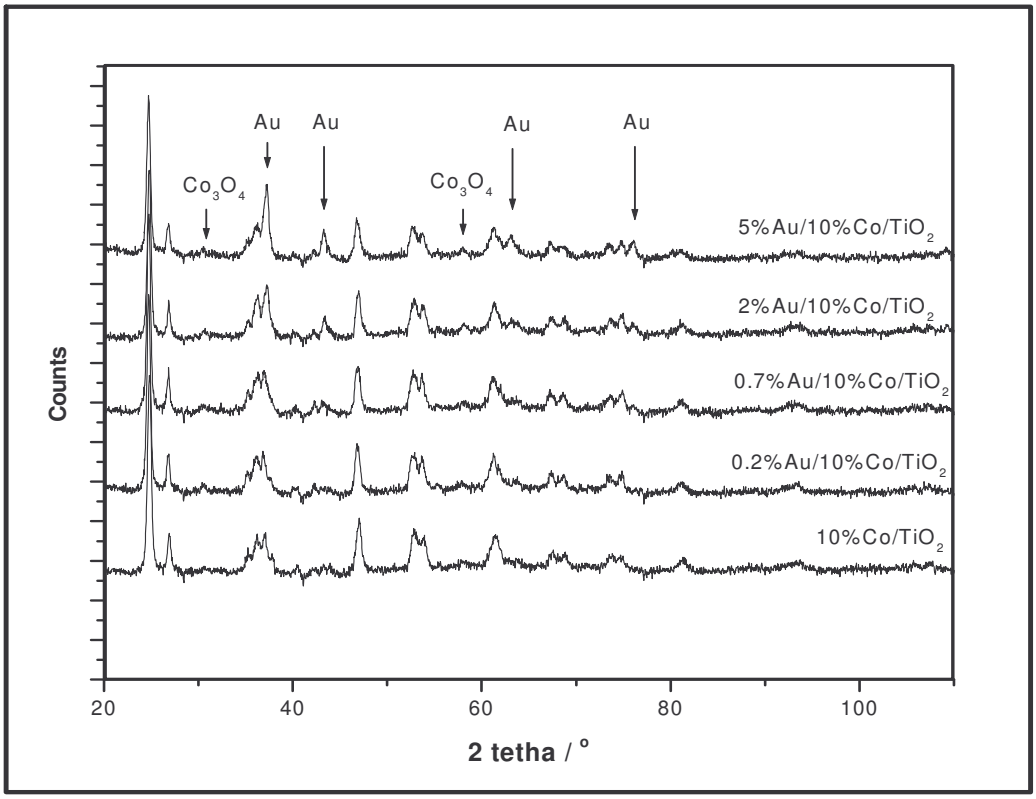

Figure 5.1 *XRD patterns for calcined, undoped and Au doped titania supported catalysts*

5.3.3 X-ray photoelectron spectroscopy (XPS) analysis

The analysis has been done by comparing XPS data for a calcined 5%Au/10%Co/TiO_2 catalyst to that of calcined 10%Co/TiO_2 and 5%Au/TiO_2 catalysts respectively. XPS peaks associated with cobalt (Co 2p) and oxygen (O 1s) binding energies for 5%Au/10%Co/TiO_2 and 10%Co/TiO_2 are shown in Figure 5.2

while the XPS spectra for gold (Au 4f binding energies) in the 5%Au/10%Co/TiO_2 and 5%Au/TiO_2 samples are shown in Figure 5.3. Co $2p_{3/2}$ peaks are detected at the binding energy of 779.8 eV and Co $2p_{1/2}$ at 795.8 eV for both the 5%Au/10%Co/TiO_2 and 10%Co/TiO_2 catalysts [Figure 5.2 and Table 5.2]. These peaks are attributed to the presence of Co_3O_4 on the calcined catalyst surface. This peak identification is in good agreement with reported literature values [17-21]. Also, XRD data obtained in this study only confirmed the presence of Co_3O_4 in the catalyst and no Co metal or CoO diffraction peaks were detected.

The Co/Ti ratio on the surface of 10%Co/TiO_2 and 5%Au/10%Co/TiO_2 catalysts are reported in Table 5.2. It can be seen that doping the 10%Co/TiO_2 catalyst with 5% Au results in a Co/Ti ratio increase from 0.115 to 0.262. This increase in Co/Ti suggests cobalt enrichment on the catalyst surface, which also means an increase in cobalt dispersion. Similar observations have been reported when Ru [8, 22-24] or Pt [25] was added to supported cobalt catalysts.

Oukachi et al.[26] have also reported that the addition of a noble metal or near-noble metal (Ru or Re) increased Co dispersion on a titania support by a factor of ca. 2. Pt and Pd were also reported to promote cobalt dispersion on a SiO_2 support [27]. This effect was explained by the dispersion of Pt or Pd in the form of a Pt-Co or Pd-Co alloy.

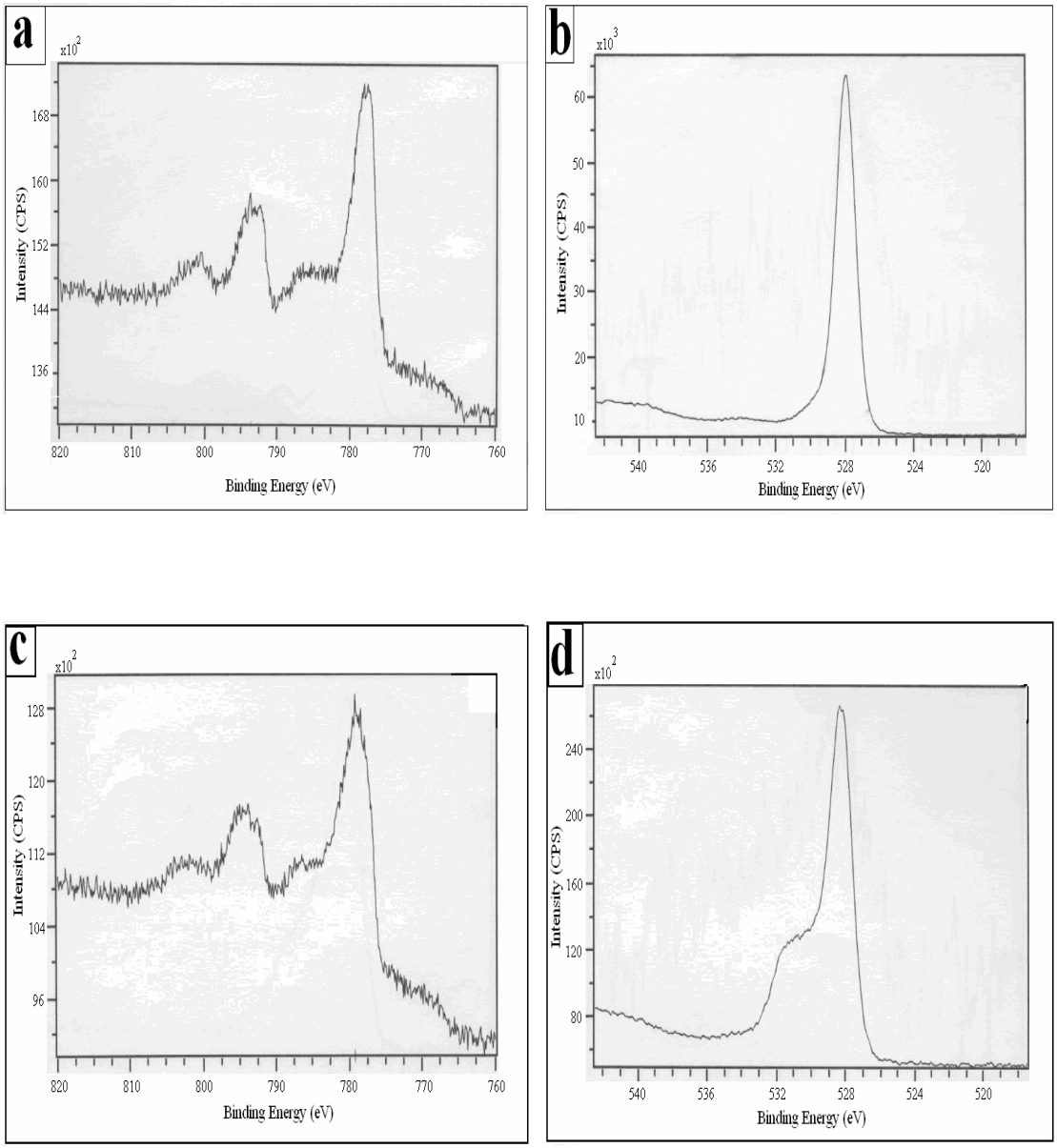

Figure 5.2 *XPS spectra at the Co 2p (a and c) and O 1s (b and d) energies for calcined 10%Co/TiO_2 and 5%Au/10%Co/TiO_2 catalysts respectively*

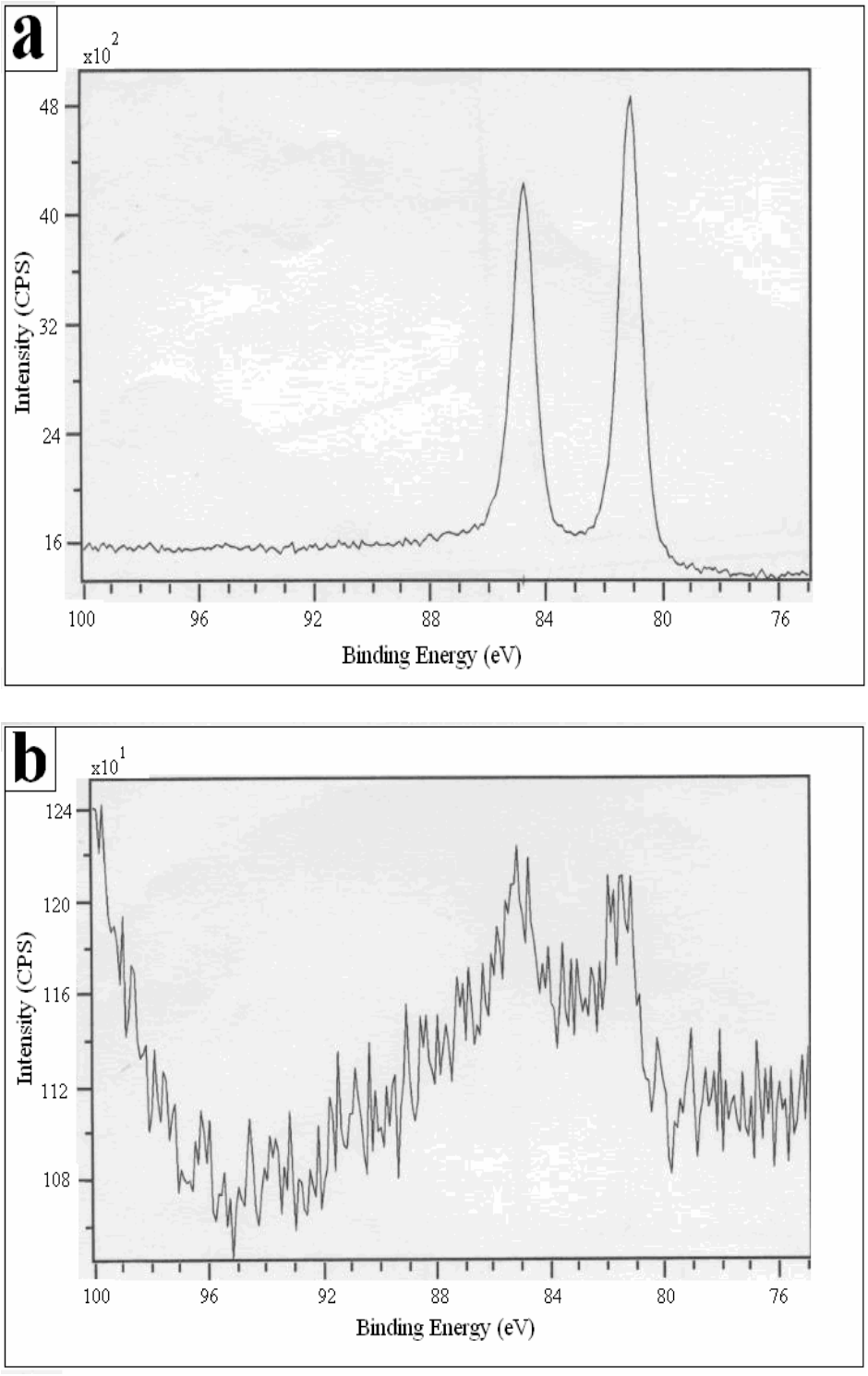

Figure 5.3 *XPS spectra at the Au 4f energies for calcined 5%Au/TiO_2 (a) and 5%Au/10%Co/TiO_2 (b) catalysts*

Table 5.2 Summary of XPS data

Catalyst	O 1s	[a]Co $2p_{3/2}$	[b]Co $2p_{1/2}$	[c]Au $4f_{7/2}$	[d]Au $4f_{5/2}$	[e]Co/Ti	[f]Au/Ti
10%Co/TiO_2	530.0	779.8	795.8	-	-	0.115	-
5%Au/10%Co/TiO_2	530.0	780.8	795.9	83.5	87.0	0.262	0.005
5%Au/TiO_2	530.0	-	-	83.6	87.3	-	0.034

a, b, c, d: corrected binding energy in eV.

e and f: atomic ratio.

Figure 5.3 shows that only a weak signal for doublets of Au 4f peaks were detected for 10%Co/5%Au/TiO_2 while these species are detected with a high intensity on 5%Au/TiO_2 catalyst. Previous studies involving Au species analysis by XPS have reported that peaks located around 83 and 87 eV are usually assigned to a Au(0) $4f_{7/2}$ and $4f_{5/2}$ doublet [14, 28, 29]. Some other studies have also reported an Au $4f_{7/2}$ peak for Au(0) at around 83-84 eV [30- 33]. Also the Au 4 $f_{7/2}$ peak position was reported to be particularly sensitive to changes in the chemical surroundings [14, 34]. In the present study two peaks in the Au 4f energy region have been detected at 83.5-83.6 and 87.0-87.3 eV respectively [Figure 5.3 and Table 5.2]. These peaks were attributed to metallic Au. This peak attribution is consistent with XRD data which showed the presence of fcc metallic Au particles in calcined Au containing catalysts.

Table 5.2 also shows the Au/Ti ratio on the 5%Au/10%Co/TiO_2 and 5%Au/TiO_2 catalyst surface. The ratio is very low (0.005) for 5%Au/10%Co/TiO_2 compared to the Au/Ti surface ratio of 0.034 on the 5%Au/TiO_2. Su et al.[33] had observed a decrease of Au/Ti ratio of a 1%Au/TiO_2 catalyst after thermal pretreatment. They did not give an unambiguous explanation of this effect but did consider the possible transport of Au species, thought to be very mobile, deeper into the pores of the support. The authors also considered the presence of a possible TiO_x decorating layer in catalysts reduced at high temperatures but this could not explain the near zero Au/Ti ratio for catalysts submitted to a high temperature reduction followed by flowing O_2 calcination which would, in principle remove the decorating layer. In the present study, XPS analysis has only been done on calcined catalysts which were not submitted to a high temperature hydrogen thermal treatment known to lead to a metal decoration by TiO_x species [33, 35 - 37]; therefore the presence of a TiO_x decorating layer can be excluded. A possibility of Au species migrating into the pores of the support can still be considered but this alone cannot explain why this migration would be far more pronounced for 5%Au/10%Co/TiO_2 than a 5%Au/TiO_2 catalyst having the same Au loading on the identical support. Thus, the near-zero Au/Ti ratio in 5%Au/10%Co/TiO_2 could be due to Au species coverage by cobalt particles. Similar behavior has been observed by Epling et al.[38]. Using XPS analysis, they reported an Au surface enrichment on Au/Fe_3O_4 with an Au surface composition of 20 atom % as opposed to an Au surface composition of 1.4 atom % in an Au/Co_3O_4 system containing a similar Au loading (nominal 10 atom % Au).

5.3.4 TPR analysis

The effect of Au on the reducibility of titania supported cobalt catalysts has been studied using TPR analysis. Figure 5.4 shows TPR profiles for a 10%Co/TiO_2 catalyst doped with various amounts of Au. The profile for the undoped catalyst (10%Co/TiO_2) constitutes the base case for comparison. Three major peaks at 344°, 373° and 545°C are evident for the TPR profile of the base case. The area under the reduction peaks at 344°C is approximately a third of the area under the reduction peak at 373°C. This ratio corresponds to the stochiometry of the two step reduction of Co_3O_4. Thus, reduction peaks at 344° and 373°C can be attributed to the two step reduction of Co_3O_4 to CoO and CoO to Co^0. The broad high temperature reduction peak with maximum around 545°C can be attributed to the reduction of Co species in interaction with the titania support which is difficult to reduce. This peak assignment is in agreement with other studies which have also reported the presence of a broad peak at higher temperatures indicating the presence of Co surface species in interaction with the titania support [9, 20, 39-41]. By adding Au to the titania supported cobalt catalysts the peaks corresponding to the two step reduction of Co_3O_4 become unresolved and slightly shift to higher reduction temperatures. Also, the high temperature peak attributed to the reduction of difficult to reduce Co species significantly shifts to lower reduction temperatures. A decrease of 68°C and 116°C

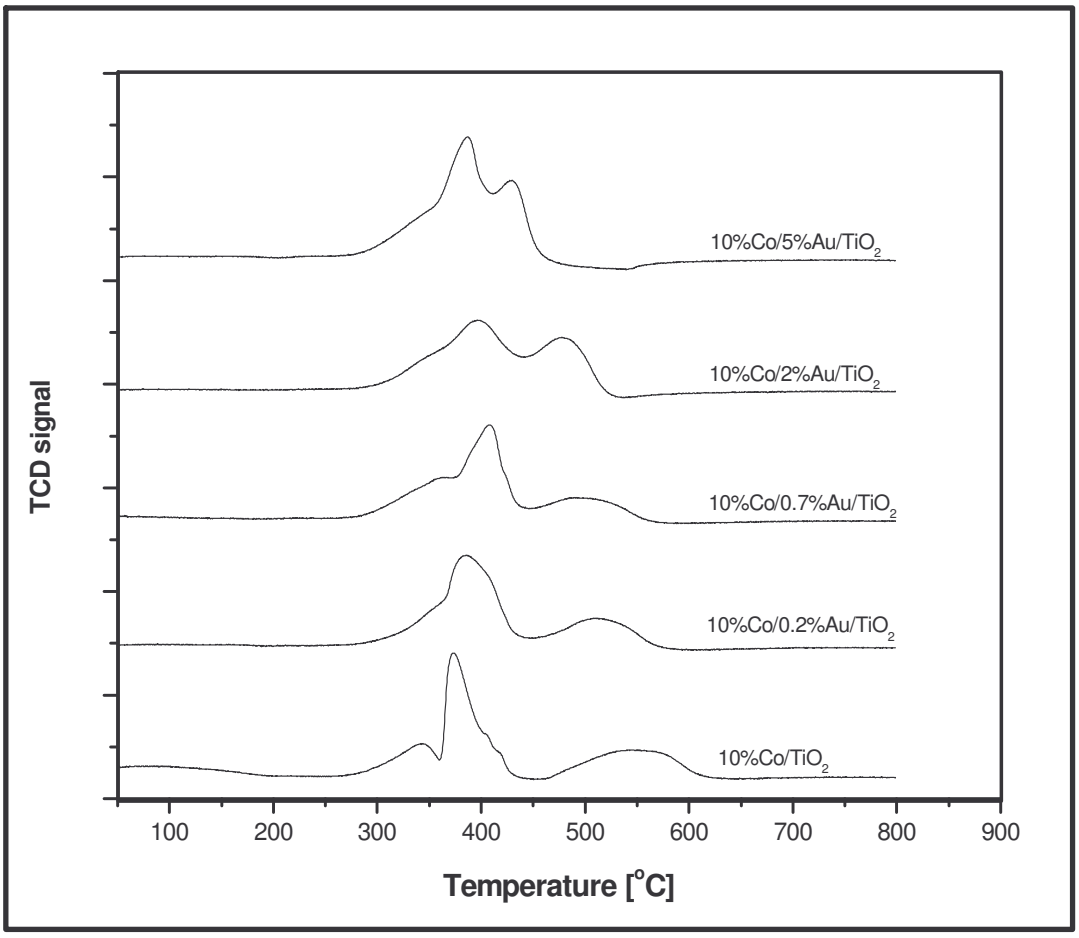

Figure 5.4 *Summary TPR results for calcined catalysts*

for the high temperature peak (around 545° in the undoped titania supported catalyst) can be observed when the catalyst is doped with 2% and 5% of Au respectively. This effect suggests that Au either promotes the reduction of Co species in interaction with the support or more likely prevents their formation during the catalyst pretreatment. Similar behavior was also observed by Nagaoka et al.[40] who reported that the number of Co oxides species interacting strongly with the TiO_2 was decreased by the

addition of Pt to a titania supported cobalt catalyst even at a Pt/Co ratio as low as 0.005.

Many studies involving Co reduction promotion by noble metals have suggested either a H_2 spillover mechanism where H_2 dissociates on a noble metal surface and becomes reactive enough to reduce cobalt oxide particles [22, 23, 25, 40, 42 - 45] or a direct Co-noble metal interaction to produce facile Co reduction [23, 45-47].

A metallic state of a noble metal has been reported to be a prerequisite for the H_2 spillover mechanism [44, 45]. Guzman and Gates [48] have reported that a reduction peak for Au^{3+} in supported Au complexes to metallic Au was observed at 207°C. In the present study no reduction peak for Au was observed in any of the Au doped and calcined cobalt catalysts. The absence of a gold reduction peak was further confirmed by recording another TPR profile of a calcined catalyst sample containing only 5%Au on TiO_2. The sample was submitted to similar conditions of pretreatment and analysis as other catalysts. This implies that a metallic form of gold was produced in calcined catalysts before reduction as confirmed by XRD and XPS data. This is probably due to the reduction of Au hydroxide to metallic gold during calcination at 400°C as was also observed by others [29, 49]. The promotion of the two step reduction of Co_3O_4 by H_2 spillover was not observed suggesting that Au does not dissociate H_2, at least in the range of conditions used and Au particles sizes obtained in this study. This is in agreement with a study by Hammer and Nørskov [50] who had mentioned the high dissociation energy of hydrogen molecule and the low chemisorption energy

on Au surface to illustrate the nobility of Au. H_2 spillover from Au particles is very unlikely to explain the effect that Au has on Co_3O_4 reducibility.

The shift to lower temperatures with an increase in Au loading in the catalyst observed for peaks corresponding to the reduction of Co species in interaction with the support can be explained *by a direct* Co-Au *contact*. These Au particles are located between Co oxides particles and the TiO_2 support as indicated in the XPS analysis.

5.3.5 Catalyst evaluation

Results on the effect of Au doping of titania supported cobalt catalysts on the catalytic performance in the FT reaction are summarized in Table 5.3. The CO conversion increased with Au loading up to 1 wt.% Au in the titania supported cobalt catalysts. When the Au loading was further increased, the CO conversion decreased slightly but still remained higher than that of the undoped catalyst. The methane and light hydrocarbon selectivity increased with Au loading but, no consistent trend in the olefin to paraffin ratio was noted. Jacobs et al.[45] have indicated that a direct relationship between the Co activity in the FT reaction and the number of surface active cobalt atoms is always obtained.

Table 5.3 Summary FT reaction results

Catalyst ratio	[a]CO conv	[b]CO conv rate	[c]HC Select.			Olefin to paraffin ratio				H_2/CO
			CH_4	C_2 - C_4	C_{5+}	C_2	C_3	C_4	C_5	
10%Co/TiO_2	13	1.451	12	8	80	0.15	1.28	1.23	0.64	1.93
0.2%Au/10%Co/TiO_2	16	1.786	14	7	79	0.09	1.12	1.03	0.35	1.91
0.7%Au/10%Co/TiO_2	16	1.786	15	7	78	0.09	1.31	0.98	0.43	1.90
1%Au/10%Co/TiO_2	22	2.455	18	16	66	010	1.49	1.59	1.10	1.88
2%Au/10%Co/TiO_2	18	2.009	24	20	56	0.16	1.56	1.56	0.97	1.90
5%Au/10%Co/TiO_2	15	1.674	28	23	49	0.10	1.45	1.60	1.00	1.90

a: percentage CO conversion; b: rate of CO consumption [µmol.(g_{cat}.s)$^{-1}$]; c: hydrocarbons selectivity based on CO moles converted; no CO_2 was measured

P=20bar; T=220°C; H_2/CO=2; SV=3NL/gCat/h

The density of surface cobalt atoms available for reaction (i.e. the active site density) is higher in catalysts with a high Co dispersion and extent of reduction. The total area under the TPR peaks is, within experimental error, the same for all the catalysts, thus suggesting that there is no significant difference in extent of reduction. However the Co dispersion was enhanced by the presence of Au in the catalyst as shown by XPS analysis. The increase in CO conversion with the increase of Au loading relative to the base case can thus be explained by the increase of Co dispersion on the surface of Au doped catalyst.

The slight decrease in CO conversion at high loading of Au ≥ 1 wt.% in the catalyst cannot unambiguously be explained with the present data. A significant increase in CO conversion might have been expected for the 5%Au/10%Co/TiO_2 catalyst when compared to the undoped catalyst (10%Co/TiO_2) related to the differences in the Co/Ti ratios (0.264 for 5%Au/10%Co/TiO_2 and only 0.110 for10%Co/TiO_2 catalyst) on the surface of the two catalysts with similar Co reduction extents. This was not the case.

It can be speculated that a high Au content in catalysts can affect the redistribution of Au and Co particles *during the reduction and reconstruction phases* on the cobalt surface during the early stage of the FT reaction. Similar behavior was reported by Zhang et al.[51] who studied the effect of magnesia on alumina supported Co FTS catalysts. They proposed that a high MgO content inhibited the process of Co catalyst

reassembly under FT reaction conditions. This also explained the high methane selectivity that they had measured on MgO promoted Co catalysts. Sun et al.[52] have also reported an increase in methane and light product selectivity on Pt or Pd promoted cobalt FT catalysts. The proposed explanation for this effect included the strong hydrogen activation ability of the noble metal, which introduced hydrogen to the catalyst surface, enhancing the methane formation and terminating the chain growth process. Hydrogen activation cannot explain the increase of methane selectivity in doped Au catalysts as Au does not have the ability to activate hydrogen under FTS conditions. Other studies have also reported an increase in methane selectivity and decrease in selectivity to higher hydrocarbon with increase in cobalt dispersion [1, 43, 53-56]. This effect was explained by the presence of unreduced cobalt oxides in catalysts which are active for the Water-Gas-Shift (WGS) reaction leading to a local increase of H_2 partial pressure on the catalyst surface [1, 53]. A direct comparison of the catalytic performance of 10%Co/TiO_2 and 5%Au/10%Co/TiO_2 shows that methane selectivity was high over a catalyst with a high dispersion of Co, i.e. 5%Au/10%Co/TiO_2.

The presence of unreduced cobalt oxides is unlikely to explain differences in methane selectivity as all the catalysts had a similar Co reduction extent. However, a possible WGS reaction catalyzed by Au particles in the catalyst can be envisaged to explain this effect. No CO_2 was detected in any of the FT runs reported in Table 5.3. This suggests that the WGS reaction under conditions used for these runs produced CO_2 below the limit of detection. To gain more insight on the WGS reaction, 10%Co/TiO_2

and 1%Au/10%Co/TiO_2 catalysts were tested in the FT reaction at a CO conversion approaching 30%. The measured CO_2 selectivity with time on stream is shown in figure 5.5. The CO_2 selectivity for the Au doped catalyst was almost three times as high as that formed for the undoped catalyst, suggesting Au activity for the WGS reaction under typical FT conditions. This is in agreement with a study by Andreeva et al.[57] who measured a high activity for the WGS reaction on Au supported on Co_3O_4 and TiO_2 in a range of temperatures typically used in the FT reaction. The increase in methane and light product selectivity measured in the present study can hence be explained by the extra H_2 produced in the Au catalysed WGS reaction on the surface of Au doped titania supported cobalt FT catalysts.

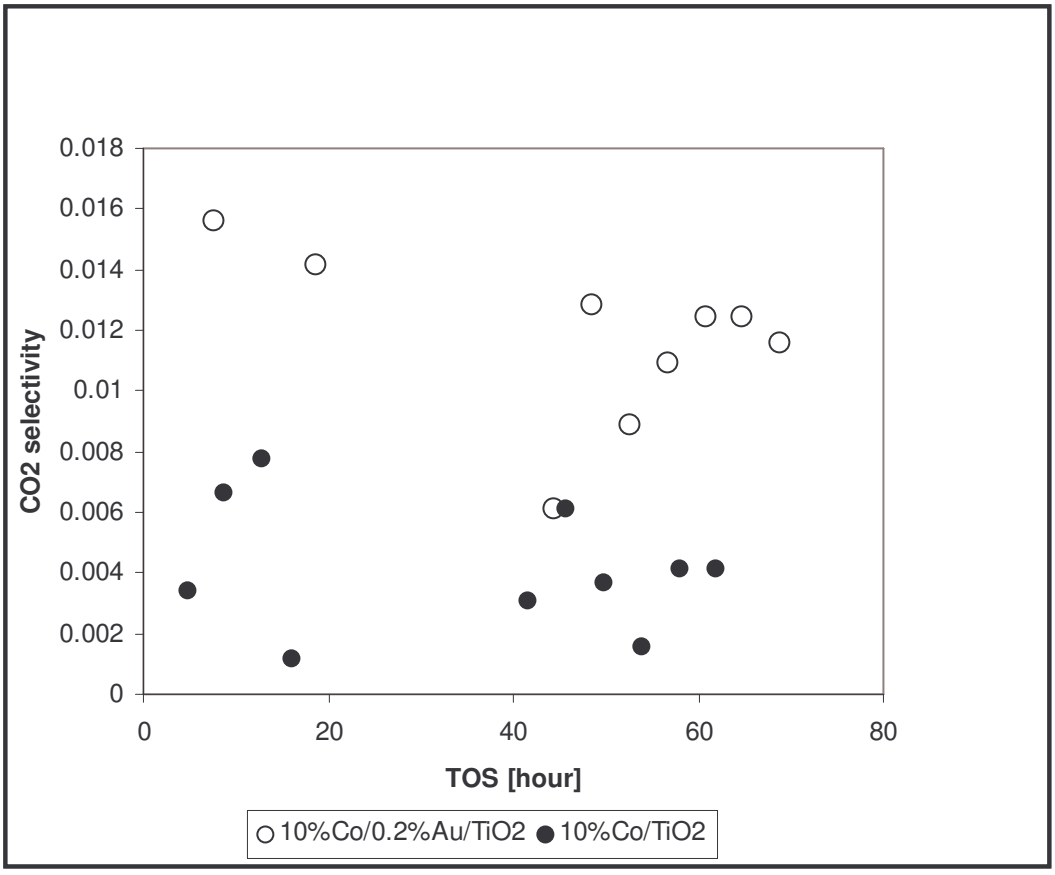

Figure 5.5 *CO_2 selectivity during FT reaction at 28% CO conversion over 10%Co/TiO_2 and 1%Au/10%Co/TiO_2 catalysts. The CO_2 selectivity is expressed as the fraction of CO converted to CO_2.*

5.4 Conclusions

XRD, XPS and TPR analysis have suggested that most or all the Au added (0 – 5% Au) to a 10%Co/TiO_2 exists in metallic form after catalyst calcination in air. The shift of reduction temperature of cobalt oxides in interaction with the support to lower temperatures is explained by a direct Co-Au contact with the metallic gold particles located between the cobalt particles and the titania support. The increase of Au content in the catalyst improved the Co dispersion and consequently the catalytic activity in the FT reaction. However, further increase of Au loading above 1wt.% for the Co/TiO_2 catalyst leads to an increase in methane selectivity, believed to be due to a WGS reaction catalyzed by Au particles in the catalysts.

References

1 R.C. Reuel, C.H. Bartholomew, *J. Catal*. 85 (1984) 78.

2 S.L. Soled, E. Iglesia, R.A. Fiato, G.B. Ansell, *U.S. Patent*, 5,169,821 (1992).

3 S.L. Soled, E. Iglesia, R.A. Fiato, G.B. Ansell, *U.S. Patent*, 5,397,806 (1995).

4 C.H. Mauldin, S.M. Davis, K.B. Arcuri, *U.S. Patent*, 4,663,305 (1987).

5 C.H. Mauldin, S.M. Davis, K.B. Arcuri, *U.S. Patent*, 4,755,536 (1988).

6 E. Iglesia, S.L. Soled, R.A. Fiato, G.H. Via, *J. Catal*. 143 (1993) 345.

7 J.G. Price, D. Glasser, D. Hildebrandt and N.J. Coville, *Stud. Surf. Sc. Cat*. 107 (1997) 243.

8 J. Li, G. Jacobs, Y. Quig., T. Das, B.H. Davis, *Appl. Catal. A*: General 223 (2002) 195.

9 J. Li, G. Jacobs, T. Das, B.H. Davis, *Appl. Catal. A*: General 233 (2002) 255.

10 L. Leite, V. Stonkus, L. Ilieva, L. Plyasova, T. Tabakova, D. Andreeva, E. Lukevics, *Catal. Comm.* 3 (2002) 341.

11 M. Oku, K. Hirokawa and S. Ikeda, *J. Electron. Spectrosc. & Related Phenomena.* 7 (1975) 465.

12 C.R. Brundle, T.J. Chuang and K. Wandelt, *Surf. Sci.* 68 (1977) 459.

13 U. Lindner and H. Papp, *Appl. Surf. Sci.* 32 (1988) 75.

14 J. Garcia-Serrano, A.G. Galindo, U. Pal, *Solar En. Mat & Solar Cells* 82 (2004) 291.

15 D.B. Akolekar, S. K. Bhargava, *J. Mol. Catal. A: Chem*. 236 (2005) 77.

16 V.G. Pol, A. Gedanken, and J. Calderon-Moreno, *Chem. Mat.* 15 (2003) 1111.

17 Y. Okamoto, N. Hajime, T. Imanaka, S. Teranishi, *Bull. Chem. Soc. Jpn.* 48 (1975) 1163.

18 T.J. Chuang, C.R. Brundle, D.W. Rice, *Surf. Sci*. 59 (1976) 413.

19 W.J. Wang, Y.W. Chen, *Appl. Catal.* 77 (1991) 223.

20 R. Riva, H. Miessner, R. Vitali, G. Del Piero, *Appl. Catal. A*: General 196 (2000) 111.

21 L. Ji, J. Lin, and H.C. Zeng, *J. Phys. Chem. B* 104 (2000) 1783.

22 A. Kogelbauer, J.G. Goodwin Jr, and R. Oukaci, *J. Cat*. 160 (1996) 125.

23 S.A. Hosseini, A. Taeb, F. Feyzi, F. Yaripour, *Catal. Comm*. 5 (2004) 137.

24 S.A. Hosseini, A. Taeb, F. Feyzi, *Catal. Comm*. 6 (2005) 233.

25 D. Schanke, S. Vada, E.A. Blekkan, A.M. Hilmen, A, Hoff, and A, Holmen, *J. Catal.* 156 (1995) 85.

26 R. Oukachi, A.H. Singleton, J.G. Goodwin Jr, *Appl. Catal. A*: General 186 (1999) 129.

27 N. Tsubaki, S. Sun, and K. Fujimoto, *J. Catal*. 199 (2001) 236.

28 B. Koslowski, H.G. Boyen, C. Wilderotter, G. Kastle, P. Ziemann, R. Wahrenberg, P. Oelhafen, *Surf. Sci*. 475 (2001) 1.

29 J.R. Mellor, A.N. Palazov, B.S. Grigorova, J.F. Greyling, K. Reddy, M.P. Letsoalo, J.H. Marsh, *Catal. Today*. 72 (2002) 145.

30 D. Briggs and M.P. Seah, *Practical Surface Analysis*, 2nd Ed. (Ellis Horwood, Chichester, 1990).

31 A. Fernnadez, A. Caballero, A.R. Gonzalez-Elipe, J. M. Herrmann, H. Dexpert and F. Villain, *J. Phys. Chem*. 99 (1995) 3303.

32 T.M. Salama, T. Shido, H. Minagawa and M. Ichikawa, *J. Catal.* 152 (1995) 322.

33 Y.S. Su, M. Y. Lee and S.D. Lin, *Cat. Lett.* 57 (1999) 49.

34 C. Ocal, and S. Ferrer, *Surf. Sci*. 191 (1987) 147.

35 S. Takatani, Y.W. Chung, *J. Catal*. 90 (1984) 75.

36 S. Takatani, Y.W. Chung, *Appl. Surf. Sci*. 19 (1984) 341.

37 S.J. Tauster, *Acc. Chem. Res.- Am. Chem. Soc*. 20 (1987) 389.

38 W.S. Epling, G.B. Hoflund, J.F. Weaver, S. Tsubota and M. Haruta, *J. Phys. Chem.* 100 (1996) 9929.

39 G. Jacobs, T.K. Das, Y. Zhang, J. Li, G. Racoillet, B.H. Davis, *Appl. Catal. A*: General 233 (2002) 263.

40 K. Nagaoka, K. Takanabe, K. Aika, *Appl. Catal. A*: General 268 (2004) 151.

41 S. Storsaeter, Ø. Borg, E.A. Blekkan, A. Holmen, *J. Catal.* 231 (2005) 405.

42 A. Sarkany, Z. Zsoldos, Gy. Stefler, J.W. Hightower, and L. Guczi, *J. Catal.* 157 (1995) 179.

43 E. Iglesia, *Appl. Catal. A*: General 161 (1997) 59.

44 T.K. Das, G. Jacobs, P.M. Patterson, W.A. Conner, J. Li, B.H. Davis, *Fuel.* 82 (2003) 805.

45 G. Jacobs, J.A. Chaney, P.M. Patterson, T.K. Das, B.H. Davis, *Appl. Catal*. A: General 264 (2004) 203.

46 M. Ronning, D.G. Nicholson, A. Holmen, *Catal. Lett*. 72 (2001) 141.

47 L. Guczi, D. Bazin, I. Kovacs, L. Borko, Z. Schay, J. Lynch,P. Parent, C. Lafon, G. Stefler, Z. Koppany, I. Sajo, *Top. Catal*. 20 (2002) 129.

48 J. Guzman and B.C. Gates, *J. Phys. Chem*. B 107 (2003) 2242.

49 D.B. Akolekar, S.K. Bhargava, G. Foran, M. Takahashi, *J. Mol. Catal.A*: Chem. 238 (2005) 78.

50 B. Hammer and J.K. Nørskov, *Nature*. 376 (1995) 238.

51 Y. Zhang, H. Xiong, K. Liew, J. Li, *J. Mol. Catal. A*: Chem 237 (2005) 172.

52 S. Sun, K. Fujimoto, Y. Yoneyama, N. Tsubaki, *Fuel.* 81 (2002) 1583.

53 L. Fu, and C.H. Bartholomew, *J. Catal*. 92 (1985) 376.

54 B. Ernst, C. Hilaire, A. Kiennemann, *Catal. Today.* 50 (1999) 413.

55 A. Martínez, C. López, F. Márquez, and I. Díaz, *J. Catal*. 220 (2003) 486.

56 S. Storsaeter, B. Tϕtdal, J.C. Walmsley, B.S. Tanem, A. Holmen, *J. Catal*. 236 (2005) 139.

57 D. Andreeva, V. Idakiev, T. Tabakova, R. Giovanoli, *Bulg. Chem. Comm*. 30 (1998c) 59.

Chapter 6

Effect of the addition of Au on a Co/Al_2O_3 catalyst for use in the Fischer-Tröpsch reaction

6.1 Introduction

Alumina supported catalysts are often used for the FTS reaction because of favourable mechanical properties associated with alumina as a support. However, one of the major problems associated with the Co/Al_2O_3 system is a limited reducibility of Co due to a strong interaction between the support and the Co oxides [1-5]. Water vapor has been found to promote the formation of Co-support compounds [6-11]. It was suggested that water affects the reducibility of alumina supported cobalt catalyst by possibly increasing the cobalt-support interaction and by facilitating the migration of cobalt ions into the tetrahedral sites of γ-Al_2O_3 to form nonreducible cobalt aluminate [8, 10]. Sirijaruphan et al.[11] have reported that the presence of partially reduced cobalt in a well-dispersed form is required for the formation of cobalt aluminate. They found that water vapor promotes cobalt aluminate formation probably by either hydrating the alumina or partially reoxidizing highly dispersed cobalt. The formation of Co-alumina compounds causes a loss in active cobalt metal needed for the FT reaction.

Several studies have been done by different groups to overcome this problem by adding a second metal or a metal oxide to modify the catalyst properties. Modification of the alumina supported cobalt catalysts by ZrO_2 [12, 13] and MgO [14, 15]

have been reported in the literature. Schanke et al.[4] have shown that addition of a small amount of Pt (0.4 wt.%) strongly improved the reducibility of Co/Al_2O_3 catalysts. The highly dispersed and difficult to reduce surface cobalt oxides were reduced at normal reduction temperatures (350˚C) in the presence of Pt. Promotion with Pt also increased metallic cobalt dispersion and the rate of CO hydrogenation. Li et al.[16] and Jacobs et al.[17] have also observed a significant improvement of catalyst reducibility after addition of Pt (0.5 wt.%) to a Co/Al_2O_3 catalyst. Cobalt dispersion was similar for both Pt promoted and unpromoted alumina supported cobalt catalysts. Re [17 - 19] and Ru [5, 20] were also reported to increase the reducibility and the catalytic activity of alumina supported cobalt catalysts. Au/Co catalytic systems have also been reported in the literature but highly dispersed Au on Co_3O_4 was reported to be active for CO oxidation [21- 26], oxidative destruction of dichloromethane [27], selective catalytic oxidation of NO in flue gases at low temperature of 120°C [28], automotive pollution abatement [29], etc.

Leite et al.[30] used Au to promote a Co/kaolin catalyst used for 2,3–dihydrofuran synthesis. They reported that the addition of Au led to the formation of new cobalt species reducible at significantly lower temperatures compared to the unpromoted catalyst. To the best of our knowledge, no other study of an Au promoting effect on a Co/Al_2O_3 catalyst has been reported to date.

In the present study, the effect of Au addition on the structure of a Co/Al_2O_3 system and its performance in the FT reaction has been investigated. In particular, the effect

of the Au/Co ratio has been determined by varying the amount of Au added to a 10% Co/Al_2O_3 catalyst.

6.2 Experimental

6.2.1 Preparation of catalysts

A series of catalysts consisting of an undoped and Au doped (0.2 to 5 wt.% Au) alumina supported cobalt catalyst (10 wt.% Co) was prepared by deposition-precipitation (undoped catalyst) and deposition-coprecipitation (Au doped catalysts). The support (γ-Alumina, Condea Vista Catalox B, SA = 150 $m^2.g^{-1}$) was first calcined in air at 500˚C for 10 hours before being used for catalyst preparation.

The catalyst preparation procedure was identical to that used for the preparation of titania supported catalysts (see chapter 5).

6.2.2 Catalyst characterization and evaluation for the FT reaction

Catalysts were characterised by atomic absorption (AA) spectroscopy, X-ray diffraction (XRD), X-ray photoelectron spectroscopy (XPS) and temperature programmed reduction (TPR) as for the titania supported catalysts (chapter 5).

The FT reaction study was carried out using the same reactor system and operating conditions as for titania supported catalysts described in chapter 5.

6.3 Results and discussion

6.3.1 Catalyst composition

Results from the AA analysis are shown in Table 6.1. These results are comparable to those obtained in chapter 5 with titania supported catalysts as they were also obtained on dried catalysts (120°C for 20 hours) before they were submitted to thermal treatment to decompose Co and Au hydroxides. All the catalysts had the same Co

Table 6.1 A A results

Catalyst	[a] % Co	[b] % Au
10%Co/Al_2O_3	9.1	-
0.5%Au/10%Co/Al_2O_3	9.2	0.47
1.5%Au/10%Co/Al_2O_3	9.0	1.30
2%Au/10% Co/Al_2O_3	9.3	1.90
5%Au/10% Co/Al_2O_3	8.8	4.30

a and b: weight percentage of dried uncalcined catalysts.

loading and an increase in Au loading in the catalysts was observed as intended.

6.3.2 XRD analysis

Figure 6.1 shows XRD patterns of calcined 10%Co/Al_2O_3 catalysts doped with various amounts of gold. The broad diffraction peaks with weak signal detected at 2θ = 31.6° and 59.01° are due to the presence of small Co_3O_4 particles. Au diffraction peaks were detected at around 2θ = 38°; 44.9° and 77.3° for catalysts containing 1.5 and 2% Au loading. An overlap of the Au diffraction peak with the alumina support at diffraction angles around 2θ = 38°; 44.5° can be observed. Previous studies have reported that diffraction peaks characteristic of Au(1 1 1), Au(2 0 0), Au (2 2 0) and (2 2 2) mostly corresponding to fcc metallic Au were detected around 38.4°, 44.5°, 64.1° and 77.1° [31, 32]. In this study, the Au diffraction peak at around 64° was not observed because of the overlap with the alumina support. Thus, diffraction peaks detected at around 2θ = 38°; 44.9° and 77.3° have been attributed to metallic Au in the catalyst. It can also be observed that the intensity of the Au diffraction peaks increased with Au loading in the catalyst, thus suggesting an increase in the number of Au particles.

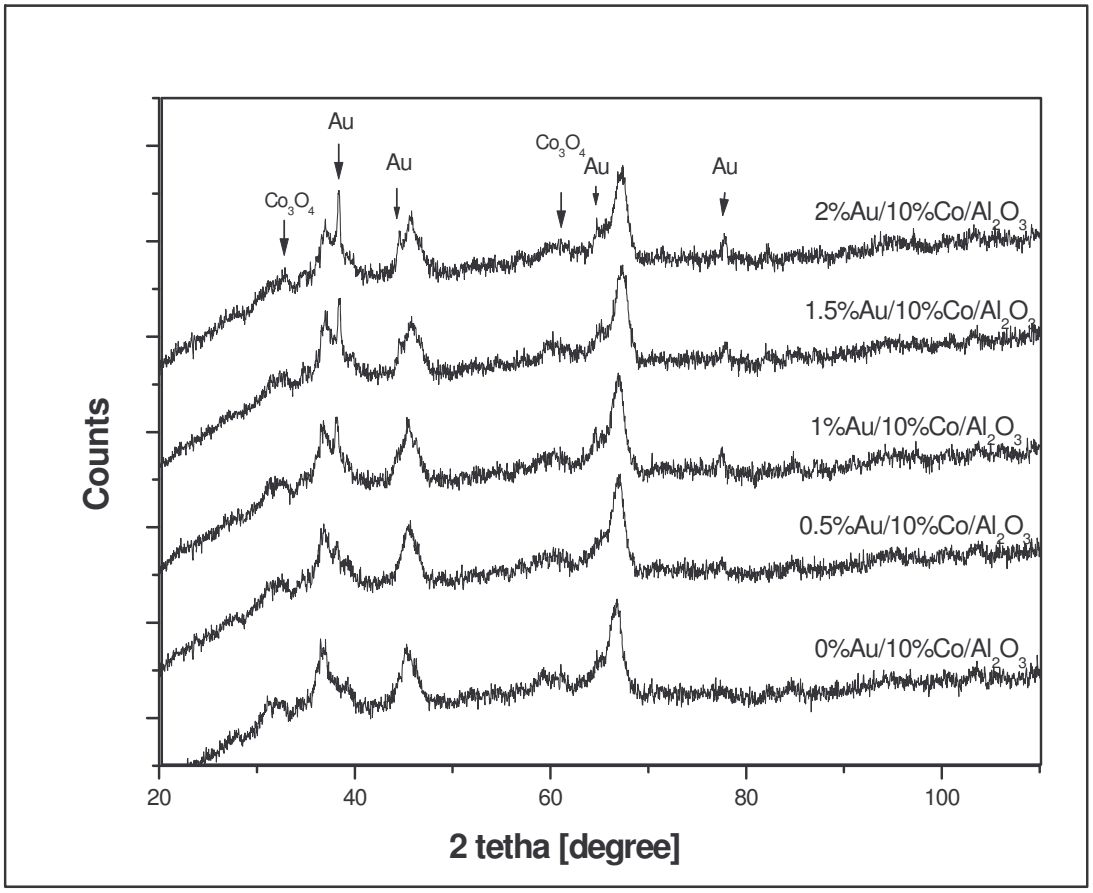

Figure 6.1 *XRD patterns for calcined, undoped and Au doped alumina supported catalysts*

6.3.3 X-ray photoelectron spectroscopy (XPS) analysis

The analysis has been done by comparing XPS data for a calcined 5%Au/10%Co/Al_2O_3 catalyst to that of calcined 10%Co/Al_2O_3 and 5%Au/Al_2O_3 catalysts respectively. XPS spectra at the Co 2p and O1s binding energies for 10%Co/Al_2O_3 and 5%Au/10%Co/Al_2O_3 are shown in figures 6.2 and 6.3 respectively while the XPS spectra at the Au 4f binding energies for 5%Au/Al_2O_3 and 5%Au/10%Co/Al_2O_3 are shown in figure 6.4.

Co $2p_{3/2}$ peaks are detected at the binding energy around 779.4 eV and Co $2p_{1/2}$ at around 795.4 eV for both the 5%Au/10%Co/Al_2O_3 and 10%Co/Al_2O_3 catalysts [Figures 6.2 and 6.3 and Table 6.2]. These peaks have been attributed to the presence of Co_3O_4 on the calcined catalyst surface. This peak identification has been discussed in chapter 5 and was in good agreement with the literature [33-37]. Table 6.2 also reports the Co/Al ratio on the surface of 10%Co/Al_2O_3 and 5%Au/10%Co/Al_2O_3 catalysts. It can be seen that doping the 10%Co/Al_2O_3 catalyst with 5% Au has little or no effect on the Co/Al ratio which is around 0.254 and 0.264 for10%Co/Al_2O_3 and 5%Au/10%Co/Al_2O_3 catalysts respectively. Thus, the addition of Au does not significantly affect the Co dispersion on the alumina support.

Figure 6.4 shows that only a weak signal for doublets of Au 4f peaks was detected for 10%Co/5%Au/ Al_2O_3 while these species are detected with a high intensity on the 5%Au/ Al_2O_3 catalyst. Au peak identification was discussed in chapter 5 [38 - 45]. In the present study two peaks in the Au 4f energy region have been detected at 83.2-83.3

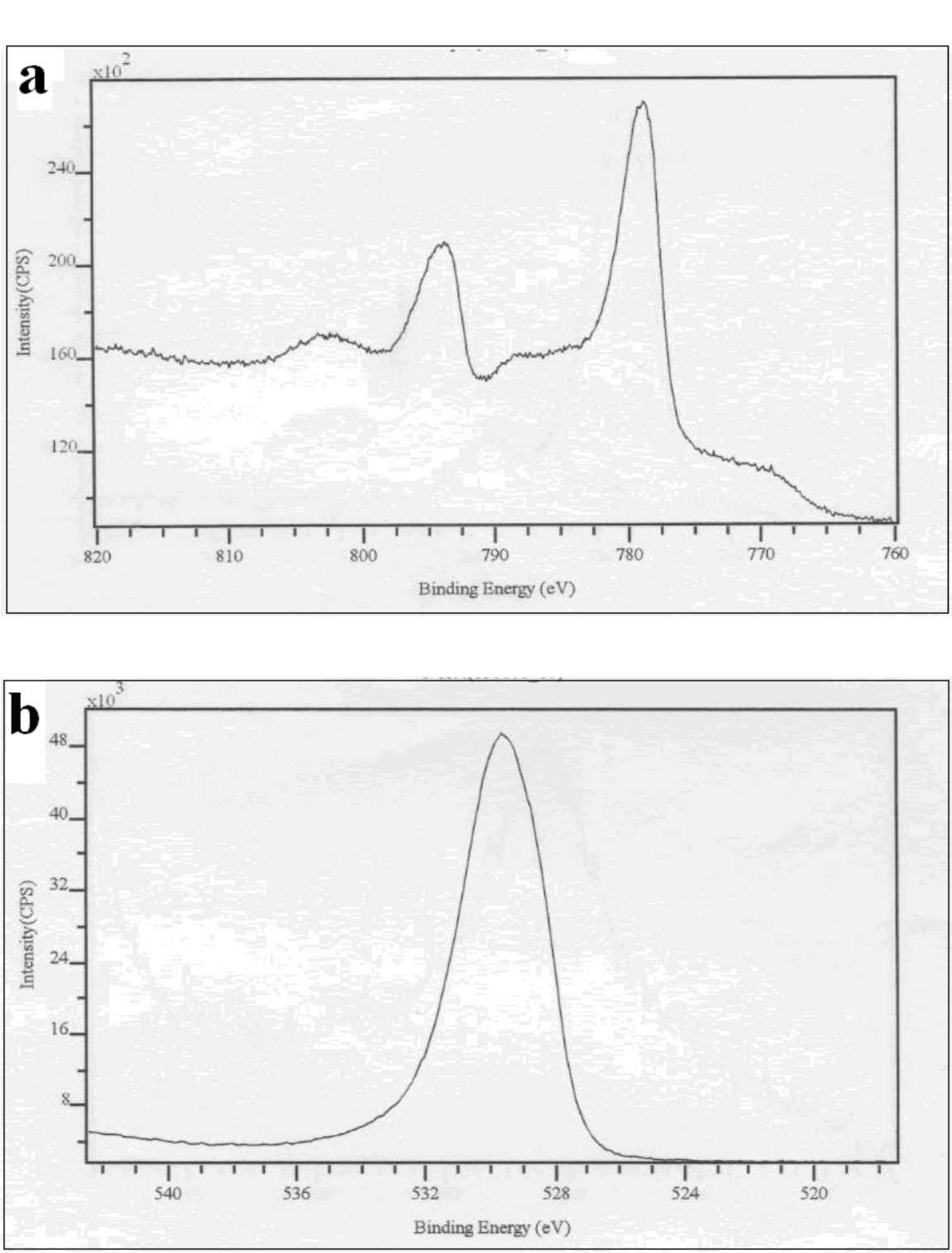

Figure 6.2 *XPS spectra at the (a) Co 2p and (b) O 1s energies for the calcined 10%Co/Al_2O_3 catalyst*

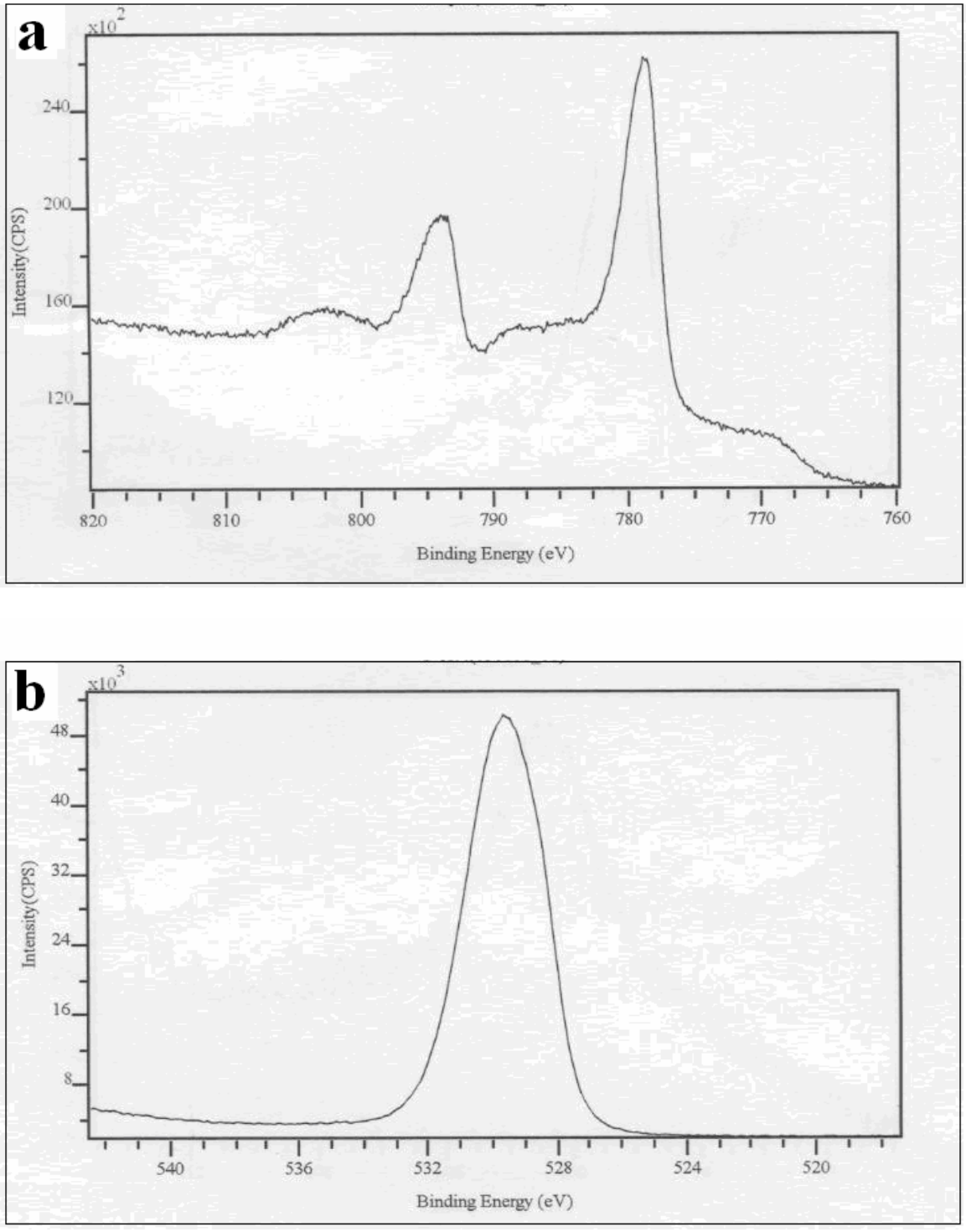

Figure 6.3 *XPS spectra at the (a) Co 2p and (b) O 1s energies for the calcined 5%Au/10%Co/Al_2O_3 catalyst*

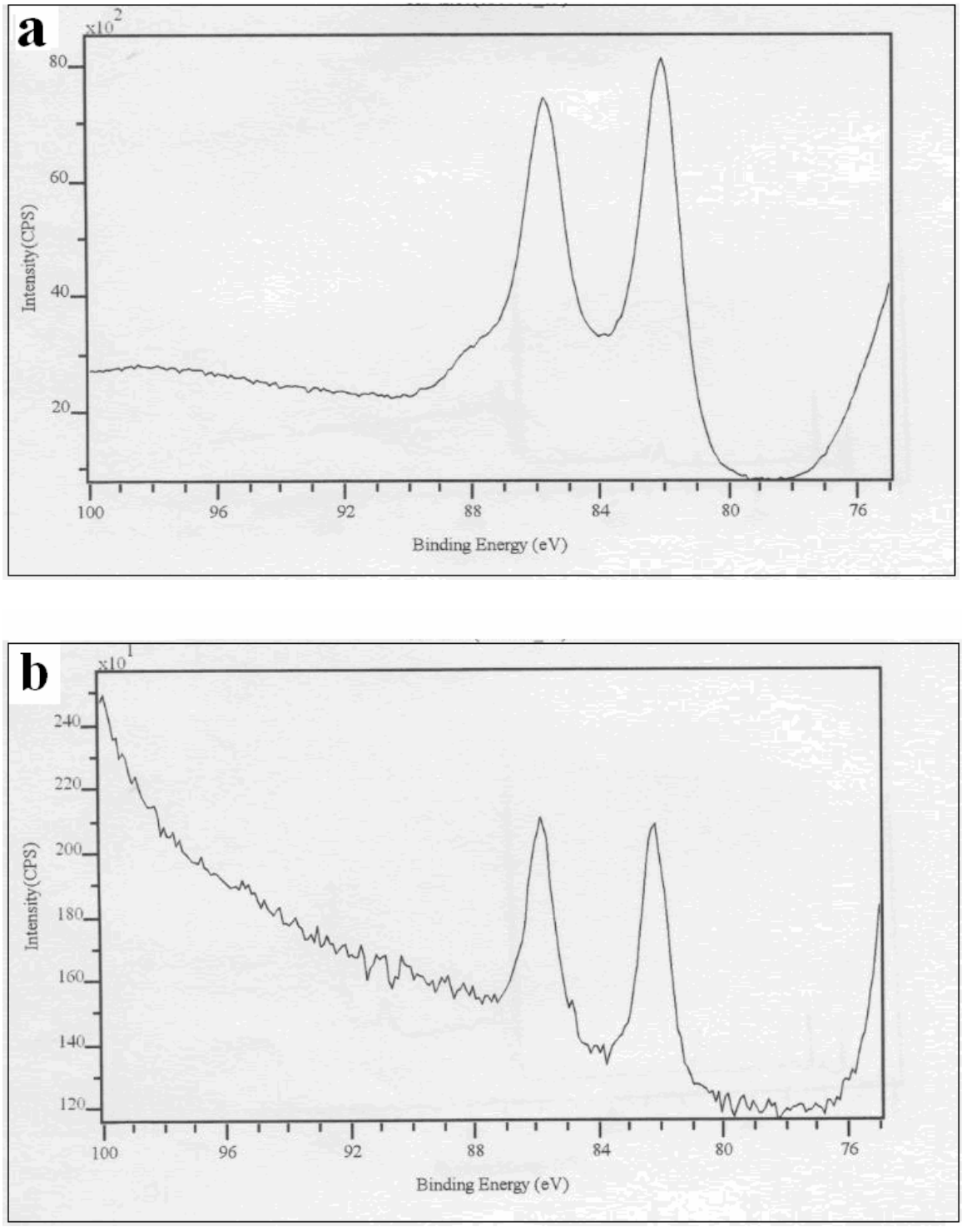

Figure 6.4 *XPS spectra at the Au 4f energies for (a) calcined 5%Au/Al_2O_3 and (b) 5%Au/10%Co/Al_2O_3 catalysts*

and 86.8-86.9 eV respectively [Figure 6.4 and Table 6.2]. These peaks are attributed to metallic Au. The Au/Al ratio on the 5%Au/10%Co/ Al_2O_3 and 5%Au/ Al_2O_3 catalyst surface is also reported in Table 6.2. The ratio is very low (0.003) for 5%Au/10%Co/Al_2O_3 compared to the Au/Al surface ratio of 0.039 on the 5%Au/Al_2O_3. Similar behaviour was observed with titania supported catalysts (chapter 5) and suggests that the low Au/Al ratio in 5%Au/10%Co/Al_2O_3 could be due to Au species coverage by cobalt oxide particles.

Table 6.2 Summary of XPS data

Catalyst	O 1s	[a]Co $2p_{3/2}$	[b]Co $2p_{1/2}$	[c]Au $4f_{7/2}$	[d]Au $4f_{5/2}$	[e]Co/Al	[f]Au/Al
10%Co/Al_2O_3	530.0	779.4	794.5	-	-	0.254	-
5%Au/10%Co/Al_2O_3	530.0	780.3	794.4	83.3	86.8	0.262	0.003
5%Au/Al_2O_3	530.0	-	-	83.2	86.9	-	0.039

a, b, c, d: corrected binding energy in eV.

e and f: atomic ratio.

6.3.4 TPR analysis

The effect of Au on the reducibility of alumina supported cobalt catalysts has been studied using TPR analysis. Figure 6.5 shows TPR profiles for a 10%Co/Al_2O_3 catalyst doped with various amounts of Au. The profile for the undoped catalyst (10%Co/Al_2O_3) constitutes the base case for comparison. All the profiles present reduction peaks below 400°C and also at high temperatures. The peaks with maxima below 400°C are attributed to the two step reduction of Co_3O_4 to CoO and CoO to Co^0. The broad high temperature reduction peak with maximum above 600°C can be attributed to the reduction of Co species in interaction with the alumina support which is difficult to reduce [46 - 48].

Addition of Au to the alumina supported cobalt catalysts caused the high temperature peaks, corresponding to the reduction of difficult to reduce Co species, to shift to lower reduction temperatures. A shift of 30°C toward low temperatures has been observed for the high temperature peak when the Au loading in the alumina supported cobalt catalyst has been increased from 0% to 5 wt.% (Figure 6.5).This effect suggests that Au either promotes the reduction of Co species in interaction with the support or prevents their formation during the catalyst pre-treatment. A quantitative analysis of the TPR profiles presented in figure 6.5 was difficult particularly because the baseline was not well defined for all the profiles. To allow a quantitative analysis of the effect of Au addition on the alumina supported cobalt catalyst, another TPR

study was done using the two samples representing the two Au loading extremes in the series of catalysts that were studied, i.e. 10%Co/Al_2O_3 and 5%Au/10%Co/ Al_2O_3. The amount of sample has been halved (100 mg) compared to the profiles reported in figure 6.5. This was done to improve the baseline and the peak resolution. The temperature was raised by 10°C/min and was then maintained at 350°C for the rest of the analysis to get closer to conditions used during the catalyst activation process

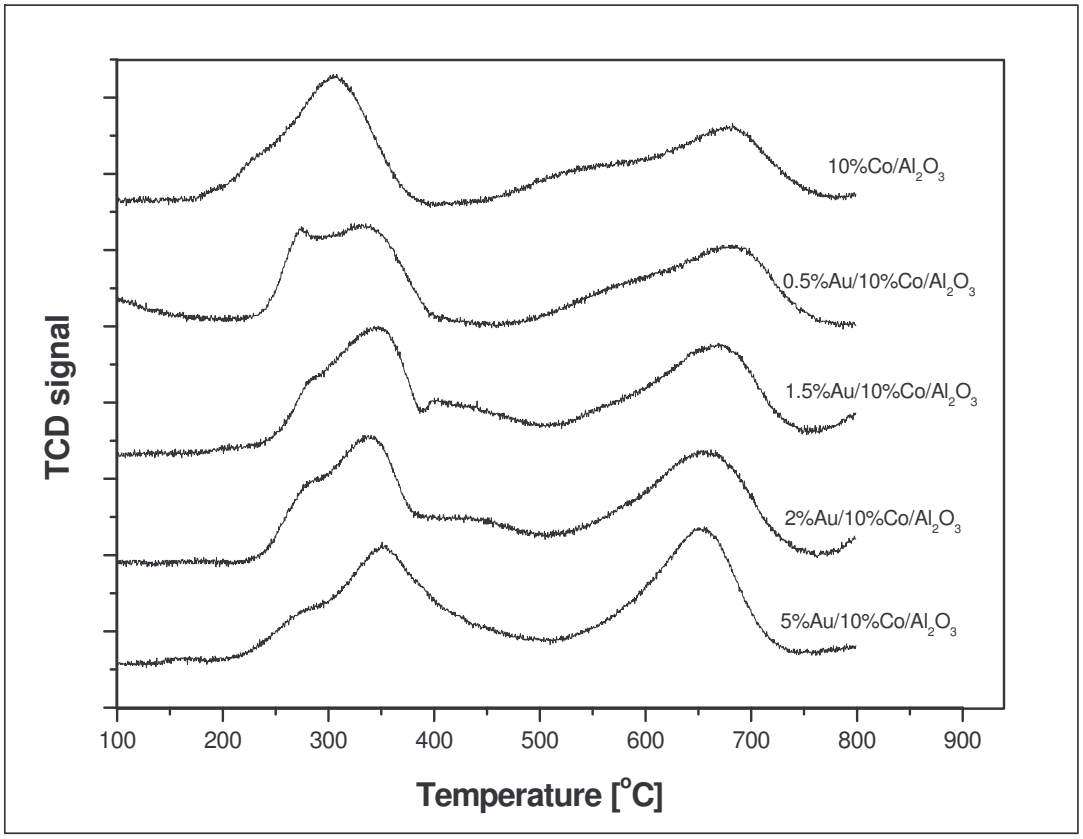

Figure 6.5 *Summary TPR results for calcined catalysts*

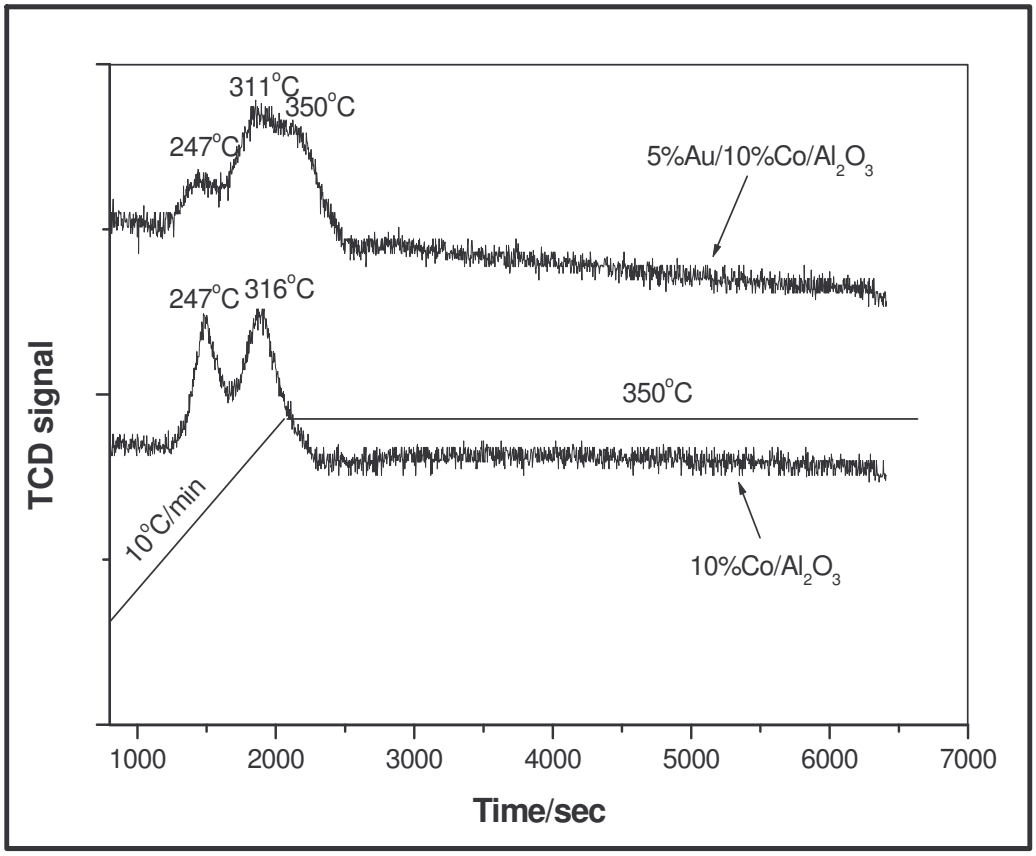

Figure 6.6 *TPR profiles for 10%Co/Al_2O_3 and 5%Au/10%Co/Al_2O_3 catalysts*

before the FT reaction. The obtained TPR profiles are presented in figure 6.6. The two profiles present peaks below 350°C which were attributed to the two step reduction of Co_3O_4 to CoO and to Co^0. The TPR profile for the 5%Au/10%Co/Al_2O_3 catalyst presented an extra peak as a shoulder to the peak at ~ 312°C around 350°C. This indicates that an additional cobalt oxide species has now been reduced. This effect is also shown in figure 6.5 and is indicated by the extended sloping baseline between 350 and 500°C (compare 10%Co/Al_2O_3 with 5%Au/10%Co/Al_2O_3 profile). It is possible that the broad ill defined peak at ~ 550°C in 10%Co/Al_2O_3 (Figure 6.5) is the source of the new reduced peak shown in figure 6.6.

The integration of the area under the two TPR profiles in figure 6.6 revealed that the hydrogen consumption (proportional to the measured area) for the Au doped catalyst was 23% higher than that of the undoped catalyst. These results indicate that the addition of Au to alumina supported cobalt catalysts increased the degree of reduction of cobalt oxides in the catalyst. Similar behaviour was observed by adding noble metals to a Co/Al_2O_3 catalyst [4, 5, 19, 20, 47, 49-52].

As was also discussed in chapter 5 for titania supported catalysts, the promotion of the reduction of alumina supported Co oxide species by adding Au is proposed to be due to *a direct contact* between Co and Au and not to a hydrogen spillover from Au particles.

6.3.5 Catalyst evaluation

Results for the FT reaction are summarized in table 6.3. It can be seen that by adding Au to a 10%Co/Al_2O_3 catalyst: (i) A synergetic effect was observed on the catalyst activity. The catalyst activity nearly doubled when the catalyst contained around 0.7 wt.% Au. Near six times the activity of the undoped catalyst was measured when 1.5% Au was added to the catalyst. Further increase of the amount of Au in the catalyst did not show any significant effect; (ii) The methane and light product selectivities passed through a maximum at around 0.7 wt.% Au loading in doped supported Co catalysts; (iii) The olefin to paraffin ratio for C_2 decreased and other light olefin to paraffin ratios were not significantly affected by increasing the amount of Au up to around 0.7 wt.% Au in the catalyst. For catalysts containing 1 wt.% Au and above, the general trend showed that the olefin to paraffin ratio decreased with an increase of Au loading; (iv) The CO_2 selectivity increased with Au loading in the catalysts.

In earlier studies [4, 5, 16 - 20] an increase in the activity of alumina supported Co catalysts after the addition of a noble metal has been reported. This was explained by an increase in the number of active sites as a result of an increase in cobalt reduction extent and dispersion due to the presence of a noble metal in the catalyst. Our XPS results have indicated that the addition of Au (5 wt.%) to a 10%Co/Al_2O_3 catalyst does not affect Co dispersion on alumina supported cobalt catalysts. This suggests that the increase in catalyst activity measured on Au doped alumina supported Co

Table 6.3 Summary FT reaction results

Catalyst ratio	[a]CO conv	[b]CO conv rate	[c]HC Select.			[d]CO_2 Select.	Olefin to paraffin ratio				H_2/CO
			CH_4	C_2 - C_4	C_{5+}		C_2	C_3	C_4	C_5	
10%Co/Al_2O_3	2.6	0.290	11.0	8.1	80.6	-	0.89	3.23	2.51	1.31	1.98
0.5%Au/10%Co/Al_2O_3	3.4	0.379	13.1	10.8	75.2	-	0.71	3.23	3.31	1.95	1.98
0.7%Au/10%Co/Al_2O_3	4.8	0.536	15.9	11.5	72.1	-	0.29	3.51	3.10	1.57	1.97
1%Au/10%Co/Al_2O_3	7.1	0.792	14.1	12.9	72.2	0.6	0.20	3.22	2.74	1.58	1.96
1.5%Au/10%Co/Al_2O_3	14.7	1.641	10.6	8.0	80.1	0.9	0.12	2.26	2.10	1.03	1.93
2%Au/10%Co/Al_2O_3	14.9	1.663	10.1	7.1	81.1	1.3	0.20	2.75	2.17	1.06	1.92
5%Au/10%Co/Al_2O_3	16.4	1.830	10.2	7.4	80.1	2.1	0.10	2.23	1.42	0.64	1.90

a: percentage CO conversion; b: rate of CO consumption [µmol.$(g_{cat}.s)^{-1}$]; c: hydrocarbons selectivity based on (CO+CO_2) moles converted; d: CO_2 selectivity defined as percentage of CO converted to CO_2

P=20bar; T=220°C; H_2/CO=2; SV=3NL/gCat/h

catalyst is mainly explained by a cobalt reduction enhancement by Au. This could be because Au shields Co from Al_2O_3. TPR studies have shown that by increasing the amount of Au in the catalyst, more Co species in interaction with the alumina support get reduced to metallic Co and therefore, increase the number of metallic surface Co atoms in the catalyst.

The change in methane and light product selectivity is usually explained by changes of hydrogen concentration on the catalyst surface. Changes in hydrogen concentration can be due to the water gas shift reaction on the unreduced cobalt oxides in the catalyst [53 - 55] or to hydrogen activation on a noble metal [56]. As discussed in chapter 5, our TPR results suggested that, Au did not enhance Co reduction by a hydrogen spillover mechanism which is explained by the ability of a metal to activate hydrogen. Hydrogen activation on Au is therefore, very unlikely to explain the change in product selectivity observed in this study.

On the other hand if unreduced cobalt oxides were responsible for the change in methane selectivity, the highest methane selectivity would have been measured on the undoped Co catalyst which contained more unreduced Co species (due to a lower reduction extent) as shown by TPR results. As this was not observed, the presence of unreduced cobalt oxides is also unlikely to explain the increase of methane and light product selectivity that occurs with an increase of Au loading observed in catalysts containing $\leq$ 0.7 wt.% Au. However, the increase in CO_2 selectivity (see table 6.2) with an increase in Au loading in the catalysts is suggestive of an Au catalyzed water gas shift reaction taking place during FT reaction. This is in agreement with a study

by Andreeva [57] who reported that an Au/Al_2O_3 system was active for the water gas shift reaction under typical conditions used for the FT reaction. Thus, Au particles in the doped alumina supported Co catalysts catalyse the WGS reaction which increases the local concentration of hydrogen. The extent of the WGS reaction increases with an increasing amount of Au in the catalyst and in the meantime an increase in CO conversion is observed. As the residence time during catalyst evaluation was the same for all the catalysts, a decrease of H_2/CO ratio on the catalyst surface due to an increase in CO conversion would lead to a decrease in methane selectivity. The two opposite trends i.e. the increase of hydrogen concentration due to the WGS reaction and the decrease of hydrogen partial pressure on a catalyst surface due to the increase in CO conversion can explain the maximum in methane and light product selectivity observed at around a 0.7 wt.% Au loading.

The decrease in olefin to paraffin ratio with the increase of Au loading in the catalyst can be explained by two factors: i) an increase in hydrogen concentration on the catalyst surface due to the Au catalysed WGS reaction. The increase in local concentration will favour the hydrogenation of olefins; ii) olefin readsorption as a result of an increase of Co^0 site density [58].

6.4 Conclusion

XRD, XPS and TPR analysis have suggested that most or all the Au added to the 10%Co/Al_2O_3 existed in metallic form after catalyst calcination in air. The increased reduction of cobalt in interaction with the alumina support is explained by a direct contact between Co and Au possibly due to the Au acting as a sandwich between the Co and the Al_2O_3, i.e. the metallic gold particles are located between cobalt particles and the alumina support. The increase in the Au content in the catalyst did not change the Co dispersion and the increase in the number of surface Co^0 sites with an increase of Au loading was mainly due to the reduction of Co oxides in interaction with the support. The change in product selectivity can be explained by the change in hydrogen concentration on the catalyst surface due to the Au catalyzed water-gas-shift reaction and the change in CO conversion due to the change in Co^0 site density with Au loading in the catalyst.

References

1 R.L. Chin, D.M. Hercules, *J. Phys. Chem*. 86 (1982) 360.

2 P. Arnoldy, M.C. Franken, B. Cheffer, J.A. Moulijin, *J. Catal*. 96 (1985) 381.

3 E. Iglesia, S.L. Soled, R.A. Fiato, G.H. Via, *J. Catal*. 143 (1993) 345.

4 D. Schanke, S. Vada, E.A. Blekkan, A.M. Hilmen, A. Hoff, A. Holmen, *J. Catal.* 156 (1995) 85.

5 A. Kogelbauer, J.G. Goodwin Jr, R. Oukaci, *J. Catal.* 160 (1996) 125.

6 A. Kogelbauer, J.C. Weber and J.G. Goodwin Jr, *Catal. Lett*. 34 (1995) 259.

7 D. Schanke, A.M. Hilmen, E. Bergene, K. Kinnari, E. Rytter, E. Ednanes and A. Holmen, *Catal. Lett*. 34 (1995) 269.

8 Y. Zhang, D. Wei, S. Hammache and J.G. Goodwin Jr, *J. Catal*. 188 (1999) 281.

9 A.M. Hilmen, D. Schanke, K.F. Hanssen, A. Holmen, *Appl. Catal. A*: General 186 (1999) 169.

10 B. Jongsomjit, J. Panpranot, J.G. Goodwin Jr, *J. Catal*. 204 (2001) 98.

11 A. Sirijaruphan, A. Horváth, J.G. Goodwin Jr., and R. Oukaci, *Catal. Lett*. 91 (2003) 89.

12 G.R. Moradi, M.M. Basir, A. Taeb, A. Kiennemann, *Catal. Comm*. 4 (2003) 27.

13 F. Rohr, O.A. Linväg, A. Holmen and E.A. Blekkan, *Catal. Today*. 58 (2000) 247.

14 P.A. Chernavskii, G.V. Pankina, V.V. Lunin, *Catal. Lett*. 66 (2000) 121.

15 Y. Zhang, H. Xiong, K. Liew and J. Li, *J. Mol. Catal. A*: Chem. 237 (2005) 172.

16 J. Li, X. Zhan, Y. Zhang, G. Jacobs, T. Das, B.H. Davis, *Appl. Catal. A*: General 228 (2002) 203.

17 Jacobs, P.M. Patterson, Y. Zhang, T. Das, J. Li, B.H. Davis, *Appl. Catal. A*: General 233 (2002) 215.

18 T.K. Das, G. Jacobs, P.M. Patterson, W.A. Conner, J. Li, B.H. Davis, *Fuel.* 82 (2003) 805.

19 G. Jacobs, J.A. Chaney, P.M. Patterson, T.K. Das, B.H. Davis, *Appl. Catal. A*: General 264 (2004) 203

20 S.A. Hosseini, A. Taeb, F. Feyzi, F. Yaripour, *Catal. Comm*. 5 (2004) 137.

21 M. Haruta, *Catal. Today*. 36 (1997) 153.

22 M.A.P. Dekkers, M.J. Lippits, B.E. Nieuwenhuys, *Catal. Today*. 54 (1999) 381.

23 W.S. Epling, G.B. Hoflund, J.F. Weaver, S. Tsubota, and M. Haruta, *J. Phys. Chem*. 100 (1996) 9929.

24 M. Haruta, N. Yamada, T. Kabayashi, S. Lijima, *J. Catal*. 115 (1989) 301.

25 M. Haruta, S. Tsubota, T. Kabayashi, H. Kageyama, M.J. Genet, B. Delmon, *J. Catal.* 144 (1993) 175.

26 R.J.H. Grisel, B.E. Nieuwenhuys, *Catal. Today*. 64 (2001) 69.

27 B. Chen, C. Bai, R. Cook, J. Wright, C. Wang, *Catal. Today*. 30 (1996) 15.

28 H. Wang, J. Wang, W.D Xiao, W.K. Yuan, *Powd. Techn*. 111 (2000) 175.

29 J.R. Meller, A.N. Palazov, B.S. Grigorova, J.F. Greyling, K. Reddy, M.P. Letsoalo, J.H. Marsh, *Catal. Today.* 72 (2002) 145.

30 L. Leite, V. Stonkus, L. Ilieva, L. Plyasova, T. Tabakova, D. Andreeva, E. Lukevics, *Catal. Comm*. 3 (2002) 341.

31 D.B. Akolekar, S. K. Bhargava, *J. Mol. Catal. A*: Chem. 236 (2005) 77.

32 V.G. Pol, A. Gedanken, and J. Calderon-Moreno, *Chem. Mat.* 15 (2003) 1111.

33 Y. Okamoto, N. Hajime, T. Imanaka, S. Teranishi, *Bull. Chem. Soc. Jpn.* 48 (1975) 1163.

34 T.J. Chuang, C.R. Brundle, D.W. Rice, *Surf. Sci*. 59 (1976) 413.

35 W.J. Wang, Y.W. Chen, *Appl. Catal.* 77 (1991) 223.

36 R. Riva, H. Miessner, R. Vitali, G. Del Piero, *Appl. Catal. A*: General 196 (2000) 111.

37 L. Ji, J. Lin, and H.C. Zeng, *J. Phys. Chem. B* 104 (2000) 1783.

38 J. Garcia-Serrano, A.G. Galindo, U. Pal, *Solar En. Mat. & Solar Cells.* 82 (2004) 291.

39 B. Koslowski, H.G. Boyen, C. Wilderotter, G. Kastle, P. Ziemann, R. Wahrenberg, P. Oelhafen, *Surf. Sci*. 475 (2001) 1.

40 J.R. Mellor, A.N. Palazov, B.S. Grigorova, J.F. Greyling, K. Reddy, M.P. Letsoalo, J.H. Marsh, *Catal. Today.* 72 (2002) 145.

41 D. Briggs and M.P. Seah, *Practical Surface Analysis*, 2nd Ed. (Ellis Horwood, Chichester, 1990).

42 A. Fernandez, A. Caballero, A.R. Gonzalez-Elipe, J. M. Herrmann, H. Dexpert and F. Villain, *J. Phys. Chem*. 99 (1995) 3303.

43 T.M. Salama, T. Shido, H. Minagawa and M. Ichikawa, *J. Catal.* 152 (1995) 322.

44 Y.S. Su, M. Y. Lee and S.D. Lin, *Cat. Lett.* 57 (1999) 49.

45 C. Ocal, and S. Ferrer, *Surf. Sci.* 191 (1987) 147.

46 G. Jacobs, T.K. Das, Y. Zhang, J. Li, G. Racoillet, B.H. Davis, *Appl. Catal. A*: General 233 (2002) 263.

47 S. Storsaeter, Ø. Borg, E.A. Blekkan, A. Holmen, *J. Catal.* 231 (2005) 405.

48 A.M. Hilmen, D. Schanke, A. Holmen, *Cat. Lett.* 38 (1996) 143.

49 L. Guczi, T. Hoffer, Z. Zsoldos, S. Zyade, G. Maire and F. Garin, *J. Phys. Chem.* 95 (1991) 802.

50 Z. Zsoldos, T. Hoffer and L. Guczi, *J. Phys. Chem*. 95 (1991) 795.

51 Z. Zsoldos and L. Guczi, *J. Phys. Chem*. 96 (1992) 9393.

52 S.A. Hosseini, A. Taeb, F. Feyzi, F. Yaripour, *Catal. Comm*. 5 (2004) 137.

53 R.C. Reuel, C.H. Bartholomew, *J. Catal*. 85 (1984) 78.

54 L. Fu, and C.H. Bartholomew, *J. Catal*. 92 (1985) 376.

55 A. Martinez, C. Lopez, F. Marquez, I. Diaz, *J. Catal*. 220 (2003) 486.\

56 S. Sun, K. Fujimoto, Y. Yoneyama, N. Tsubaki, *Fuel.* 81 (2002) 1583.

57 D. Andreeva, V. Idakiev, T. Tabakova, R. Giovanoli, *Bulg. Chem. Comm*. 30 (1998c) 59.

58 E. Iglesia, S.L. Soled, R.A. Fiato, G.H. Via, *Stud. Surf. Sci. Catal*. 81 (1994) 433.

Chapter 7

Effect of the addition of Au on a Co/SiO_2 catalyst for use in the Fischer-Tröpsch reaction

7.1 Introduction

Co catalytic activity for the Fischer-Tröpsch (FT) reaction is determined by the number of surface Co atoms available for reaction. The final surface density of Co^0 depends on the cobalt reducibility and dispersion. To increase the surface Co^0 density a cobalt precursor is typically dispersed on a support. Al_2O_3, TiO_2 and SiO_2 are the supports most used for Co FT catalysts. Al_2O_3 and TiO_2 present a strong metal-support interaction leading to high dispersion and to the formation of nonreducible Co-support compounds. SiO_2 presents a weak interaction with Co leading to a high reducibility of Co oxides and a low dispersion of Co^0 on a silica support [1]. To improve Co dispersion on SiO_2 organic Co precursors have been used for the catalyst preparation [1 - 7]. The high dispersion of the catalyst has however led to formation of poorly-reducible cobalt silicates [5 -7]. Addition of small amounts of a noble metal has been shown to improve Co/SiO_2 catalyst properties. Okabe et al.[8] have reported that noble metal addition (0.01 – 1wt% of Ir or Ru) enhanced the reducibility of a Co/SiO_2 catalyst. Similar results were also reported by Jacobs et al.[9] after the addition of Ru or Pt to a Co/SiO_2 catalyst. Sun et al.[10] have reported that the addition of a small amount of Ru to a Co/SiO_2 catalyst remarkably increased the reduction degree and

the catalytic activity while Pt or Pd promoted cobalt dispersion and decreased the TOF. Girardon et al.[11] have reported that Ru addition to a Co/SiO_2 prepared using Co nitrate increased Co dispersion while maintaining high reducibility. Promotion with Ru increased the fraction of the Co_3O_4 crystalline phase and decreased the concentration of Co silicates in Co/SiO_2 catalysts prepared via low temperature decomposition of cobalt acetate.

Leite et al.[12] used Au to promote a Co/kaolin catalyst used for 2,3–dihydrofuran synthesis. They reported that the addition of Au led to the formation of new cobalt species reducible at significantly low temperatures compared to the unpromoted catalyst. To the best of our knowledge, no other study of a Au promoting effect on a Co/SiO_2 catalyst has been reported to date.

In the present study, the effect of Au addition on the structure of a Co/SiO_2 system and its performance in the FT reaction has been investigated. In particular, the effect of the Au/Co ratio has been determined by varying the amount of Au added to a 10% Co/SiO_2 catalyst.

7.2 Experimental

Undoped and Au doped (0.5 to 5 wt.% Au) silica supported cobalt catalyst were prepared by deposition-precipitation (undoped catalyst) and deposition-coprecipitation (Au doped catalysts). The preparation procedure was the same as for

titania supported catalysts (chapter 5) and alumina supported catalysts (chapter 6). The support used for catalyst preparation was Matrex silica 60, 35 – 70 micron, pore size = 60 Å (SA = 300 m^2g^{-1}).

Catalyst characterisation and testing for the FT reaction were done according to procedures described for titania and alumina supported catalysts in chapter 5 and 6 respectively.

7.3 Results and discussion

7.3.1 Catalyst composition

The verification of catalysts composition was done by AA analysis and the results are shown in Table 7.1. These results were obtained on dried catalysts (120°C for 20 hours) before they were submitted to thermal treatment to decompose Co and Au hydroxides. Co loading was found to be, within experimental error, the same for all the catalysts. The increase in Au loading in the catalysts agreed with the expected trend.

Table 7.1 A A results

Catalyst	[a] % Co	[b] % Au
10%Co/SiO_2	9.3	-
0.5%Au/10%Co/ SiO_2	9.2	0.49
1.5%Au/10%Co/SiO_2	9.1	1.23
2%Au/10% Co/SiO_2	9.0	1.79
5%Au/10% Co/SiO_2	9.1	4.43

a and b: weight percentage in dried catalysts.

7.3.2 XRD analysis

Figure 7.1 shows XRD patterns of calcined 10%Co/SiO_2 catalysts doped with various amounts of gold. The silica support was essentially amorphous and no diffraction peak for Co_3O_4 particles was detected most probably because of their small sizes. Au diffraction peaks were detected at diffraction angles around 2θ = 38°; 44.9°; 64.5 and 77.5° characteristic of Au (1 1 1), Au (2 0 0), Au (2 2 0) and (2 2 2) and mostly corresponding to fcc metallic Au [13, 14]. It can also be observed that the intensity of the Au diffraction peaks increased with an increase in Au loading in the catalyst, thus suggesting an increase in number of Au particles.

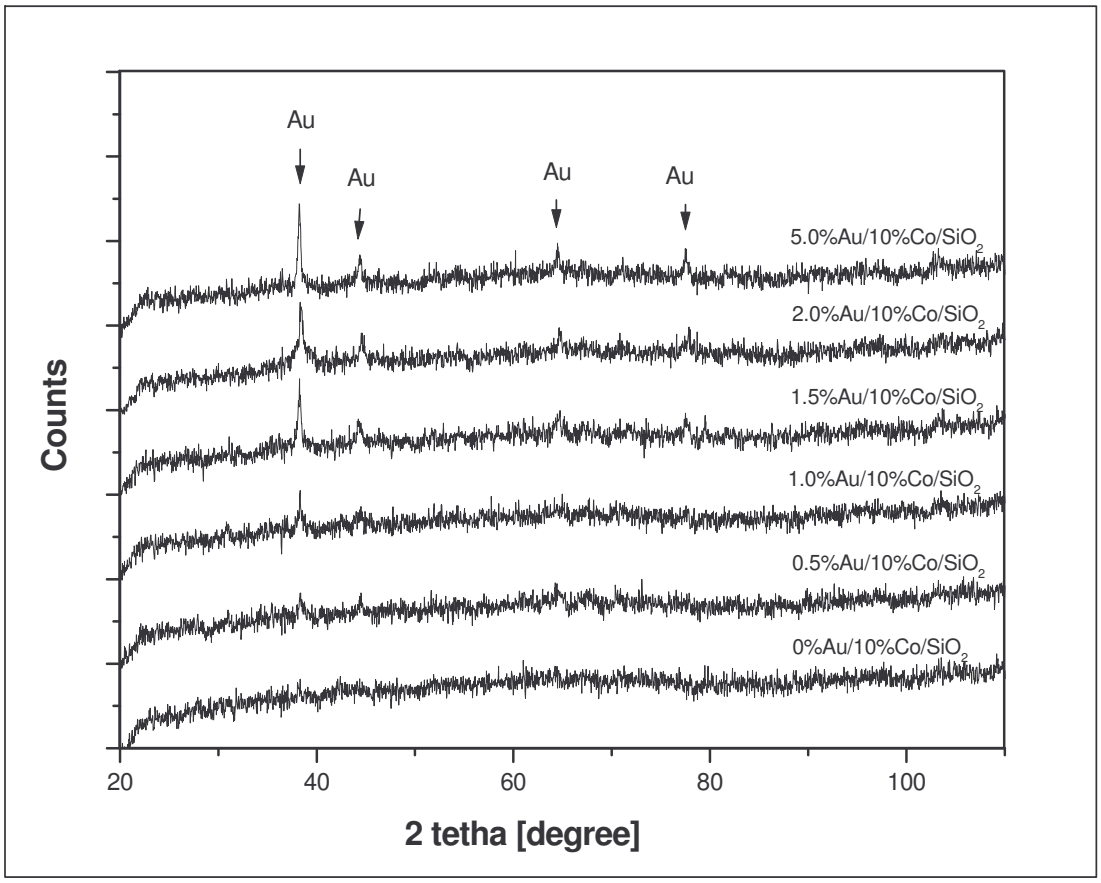

Figure 7.1 *XRD patterns for calcined, undoped and Au doped silica supported catalysts*

7.3.3 X-ray photoelectron spectroscopy (XPS) analysis

The analysis has been done by comparing XPS data for a calcined 5%Au/10%Co/SiO_2 catalyst to that of calcined 10%Co/SiO_2 and 5%Au/SiO_2 catalysts respectively. XPS spectra at the Co 2p and O1s binding energies for 10%Co/SiO_2

and 5%Au/10%Co/SiO_2 are shown in Figures 7.2 and 7.3 while the XPS spectra at the Au 4f binding energies for 5%Au/10%Co/SiO_2 and 5%Au/SiO_2 are shown in figure 7.4. Co $2p_{3/2}$ peaks are detected at the binding energy around 779 eV and Co $2p_{1/2}$ at around 795.4 eV for both the 5%Au/10%Co/SiO_2 and 10%Co/SiO_2 catalysts [figure 7.2 and 7.3 and Table 7.2]. These peaks have been attributed to the presence of Co_3O_4 on the calcined catalyst surface [15 - 19]. The Co/Si ratio on the surface of 10%Co/ SiO_2 and 5%Au/10%Co/ SiO_2 catalysts are reported in table 7.2. Addition of Au (5 wt.%) to the 10%Co/ SiO_2 catalyst increased the Co/Si ratio from 0.676 in the undoped catalyst to 0.718 in the doped catalyst. Thus, this suggests that the addition of Au to a Co/SiO_2 catalyst increases Co dispersion on the silica support. Similar behaviour was also reported by earlier studies [20-26] where a noble metal was added to supported cobalt catalysts.

The XPS spectra for 5%Au/10%Co/ SiO_2 and 5%Au/ SiO_2 catalysts both showed two peaks in the Au 4f energy region at around 83 and 86.6 eV respectively [Figure 7.4 and Table7.2]. These peaks were attributed to metallic Au [27-33]. The peak attribution is consistent with XRD data which showed the presence of fcc metallic Au particles in calcined Au containing catalysts. Au/Si atomic ratios are also reported in Table 7.2. The Au/Si atomic ratio on the catalyst surface was very low (Au/Si = 0.006) for 5%Au/10%Co/SiO_2 compared to that on the 5%Au/Al_2O_3 catalyst (Au/Si = 0.137). This suggests that only a small amount of Au was present on the surface of Au doped supported cobalt catalyst. The low Au/Si ratio in 5%Au/10%Co/SiO_2 catalyst compared to the 5%Au/SiO_2 catalyst is thought to be mainly due to Au species coverage by cobalt particles as discussed in chapter 5 and 6.

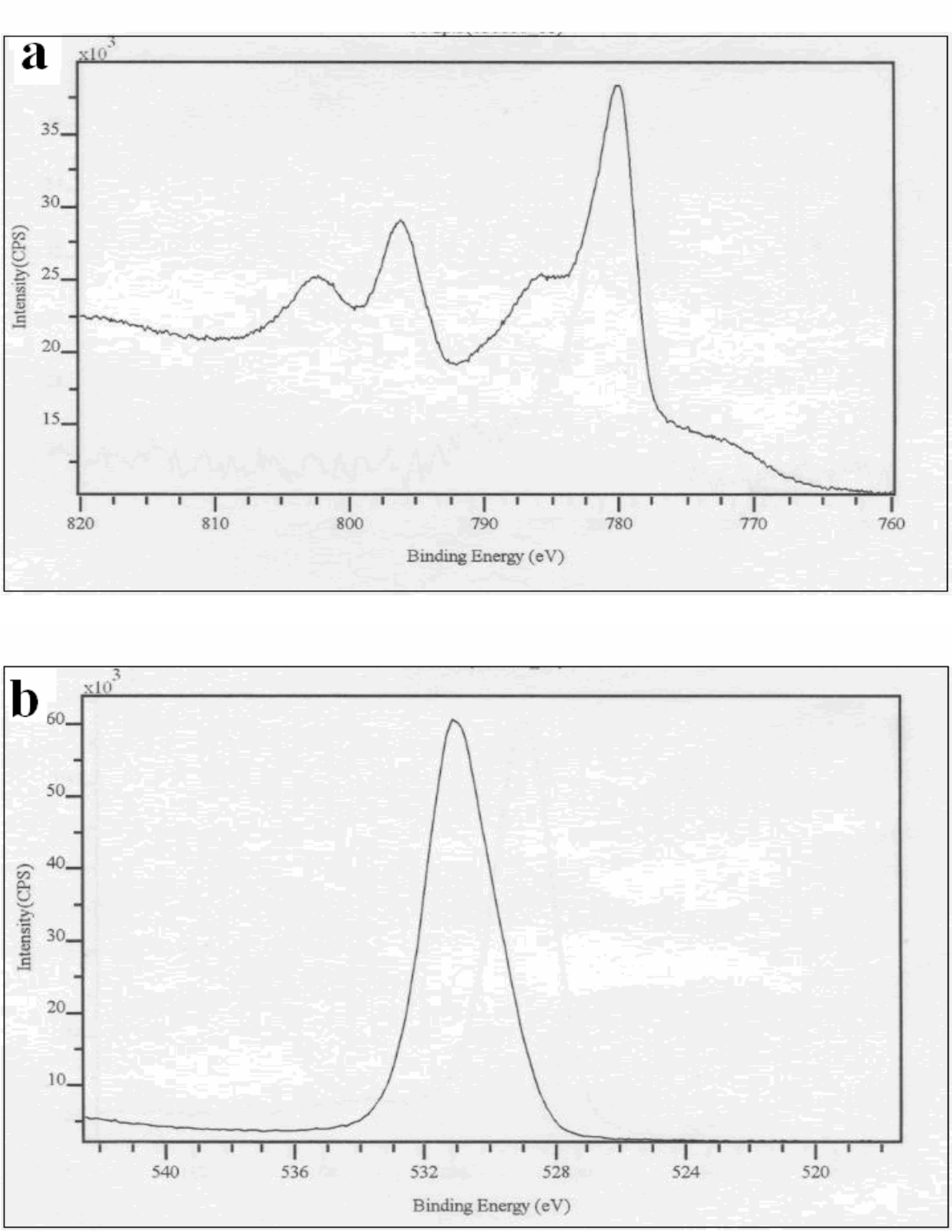

Figure 7.2 *XPS spectra at the Co 2p (a) and O 1s (b) energies for the calcined 10%Co/Al_2O_3 catalyst*

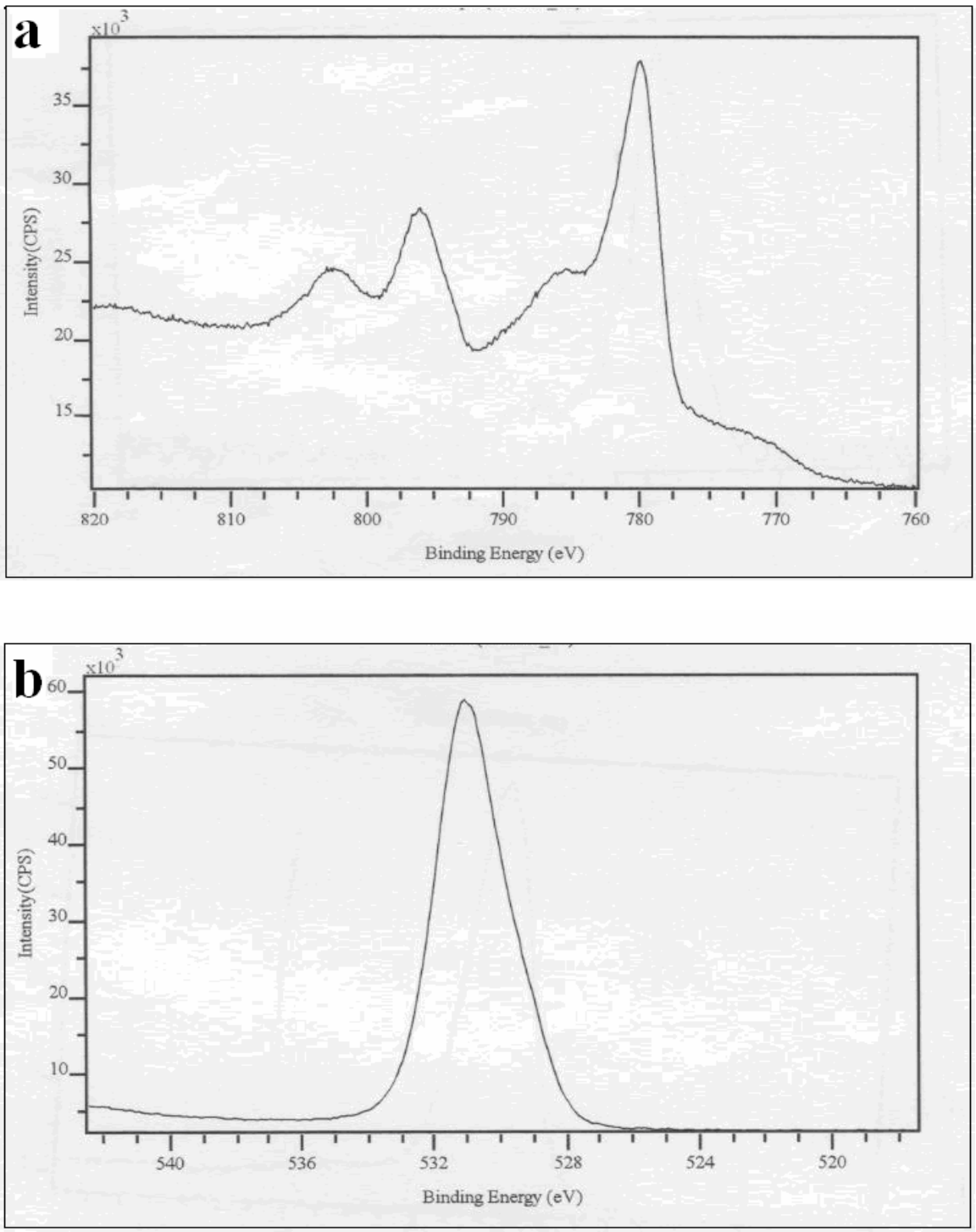

Figure 7.3 *XPS spectra at the Co 2p (a) and O 1s (b) energies for the calcined 5%Au/10%Co/Al_2O_3 catalyst*

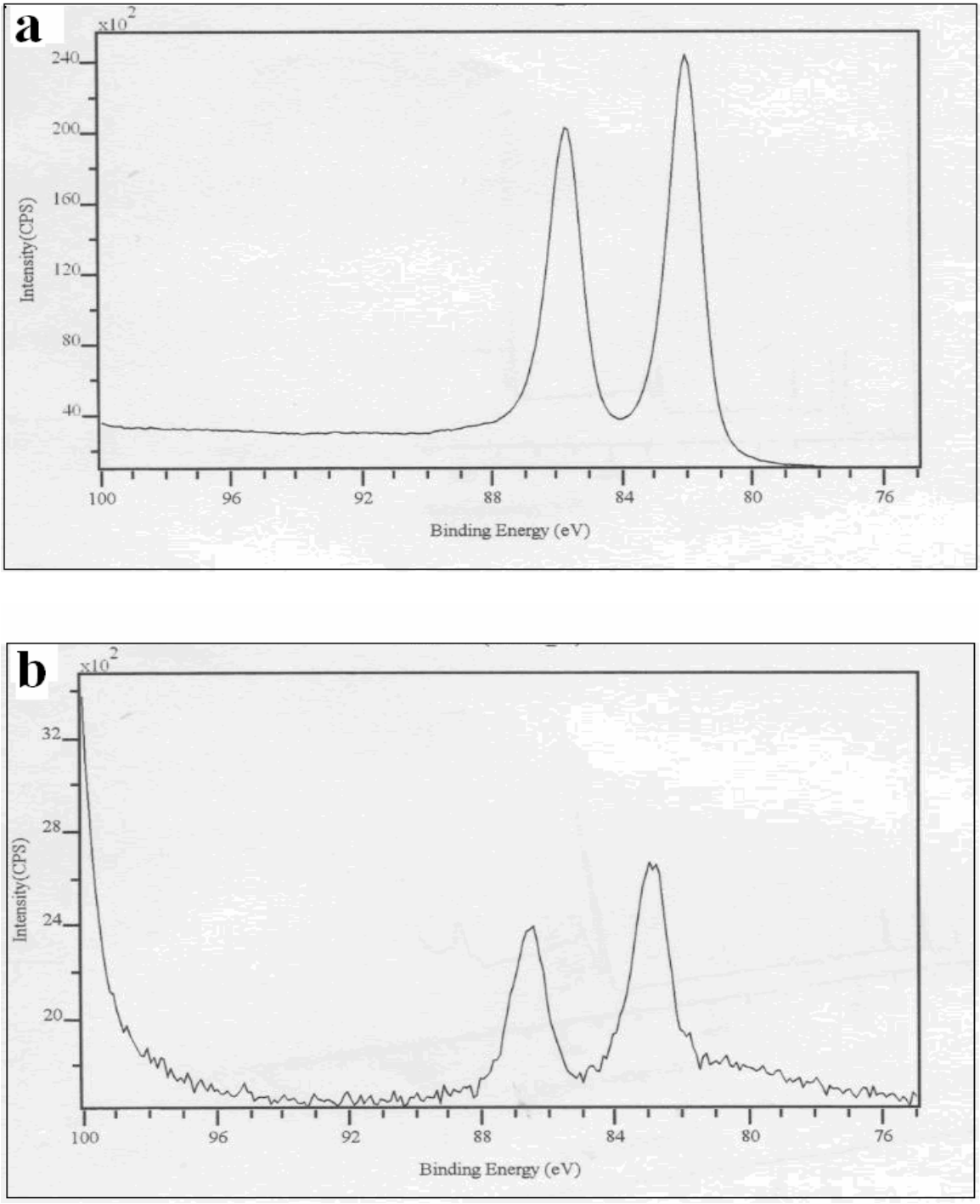

Figure 7.4 *XPS spectra at the Au 4f energies for calcined 5%Au/Al_2O_3 (a) and 5%Au/10%Co/Al_2O_3 (b) catalysts*

Table 7.2 Summary of XPS data

Catalyst	O 1s	[a]Co $2p_{3/2}$	[b]Co $2p_{1/2}$	[c]Au $4f_{7/2}$	[d]Au $4f_{5/2}$	[e]Co/Si	[f]Au/Si
10%Co/SiO_2	530.0	779.1	795.5	-	-	0.676	-
5%Au/10%Co/SiO_2	530.0	779.1	794.9	83.3	86.8	0.719	0.006
5%Au/ SiO_2	530.0	-	-	83.1	86.7	-	0.137

a, b, c, d: corrected binding energy in eV.

e and f: atomic ratio.

7.3.4. TPR analysis

The effect of Au on the reducibility of silica supported cobalt catalysts has been studied using TPR analysis. TPR profiles for a 10%Co/SiO_2 catalyst doped with various amounts of Au are presented figure 7.5. The profile for the undoped catalyst (10%Co/SiO_2) constitutes the reference for comparison and presents two major peaks; a low temperature peak starting around 215˚C and ending around 360˚C attributed to the two step reduction of Co_3O_4 to CoO and CoO to Co^0 and a broad high temperature peak starting above 500˚C. This peak could be due to the reduction of cobalt oxide species in interaction with the silica support [34] or to the reduction of the fraction of cobalt that is contained in the inner cavity of the silica support [18]. The reducibility of this fraction of Co is thought to be limited by the diffusion through the

pores of the water formed during the reduction. It can be seen that the high temperature peak is not symmetrical and presents a shoulder around 640˚C suggesting the existence of cobalt oxides with different degrees of interaction with the support. An addition of 1.5 wt.% of Au to Co/SiO_2 increased the area under the low temperature peak and shifted the maximum of the high temperature peak from 776˚ to 685˚C. When Au was added at a content of ca. 5wt.% (profile c), the peak corresponding to the two step reduction shifted to lower temperatures and the presence of a second peak in the low temperature range became evident. The maximum of the high temperature peak also shifted with ca. 100˚C to lower temperatures compared to that of the undoped catalyst. When the amount of Au was increased in the silica supported cobalt catalyst the general trend revealed an increase in the area under the peaks corresponding to the Co oxides reducible at low temperatures concomitant to a decrease in the area corresponding to the reduction of Co oxides in interaction with the support. This effect suggests that Au either promoted the reduction of Co species in interaction with the support or prevented their formation during the catalyst pre-treatment.

Similarly to the titania and alumina supported cobalt catalysts discussed in chapter 5 and 6 respectively, the positive effect of Au addition on silica supported cobalt catalysts is thought to be due to a direct contact between Co and Au.

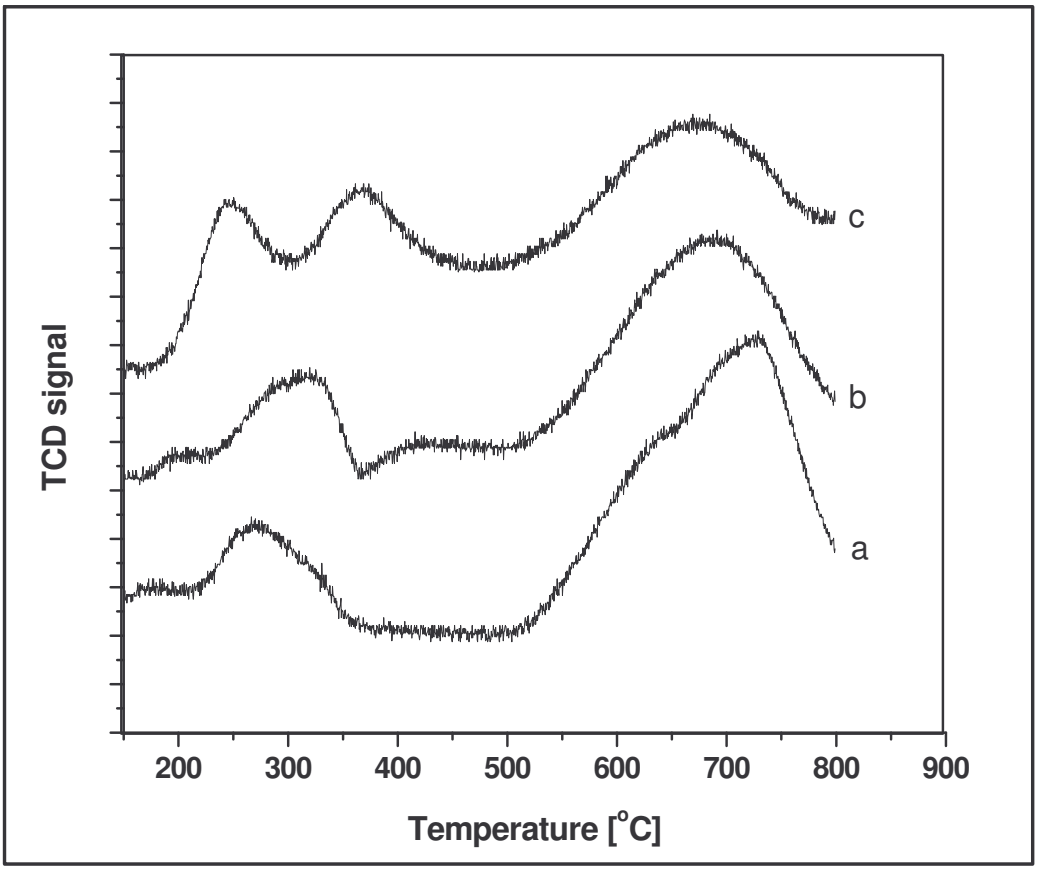

Figure 7.5 *Summary TPR results for 10%Co/SiO_2 (a), 1.5%Au/10%Co/SiO_2 (b) and 5%Au/10%Co/SiO_2 (c) calcined catalysts*

7.3.5 Catalyst evaluation

FT reaction results are summarized in Table 7.3. The CO conversion increased with an increase in Au loading in the silica supported Co catalysts. Addition of 0.5 and 1.5 wt.% increased the CO conversion by a factor of 2.7 and 3.6 respectively. Further increase in Au loading led to a slight increase in CO conversion. The methane selectivity increased from ca. 8% to 17% after adding 0.5 wt% Au in the catalyst and stayed at this value without changing when Au loading was further increased up to 5% Au. The light product selectivity also followed the same trend as that of methane. However, the olefin to paraffin ratio for C_2 decreased all the way with the addition of Au and the $C_3 - C_5$ olefin to paraffin ratio was found to increase when 0.5 wt.% Au was added to catalyst and decreased with further increase in Au loading above 0.5 wt.%. It can also be observed that ethanol selectivity increased with an increase in Au loading in the catalyst. For the undoped catalyst no ethanol was detected suggesting that a very limited amount of ethanol was produced during the FT reaction. By adding 0.5 wt.% Au to the catalyst, ethanol was detected with a selectivity around 1.1% and further increase in Au loading slightly increased the ethanol selectivity. Matsuzaki and co-workers [35, 36] have shown that the main active site for the formation of oxygenates from syngas on a Co/SiO_2 catalyst was a highly dispersed Co metal site. The observed increase in ethanol selectivity with Au loading in the catalyst confirmed that the addition of Au increases the Co dispersion on silica as established by XPS analysis.

Table 7.3 Summary FT reaction results

Catalyst	[a]CO conv	[b]CO conv rate	[c]HC Select.			[d]C_2H_6O Select.	Olefin to paraffin ratio				H_2/CO ratio
			CH_4	C_2 - C_4	C_{5+}		C_2	C_3	C_4	C_5	
10%Co/SiO_2	1.6	0.179	7.8	3.6	88.6	-	0.63	0.76	0.88	0.49	1.99
0.5%Au/10%Co/SiO_2	4.4	0.491	17.2	16.0	65.7	1.09	0.40	2.76	1.30	0.54	1.97
1%Au/10%Co/SiO_2	5.4	0.603	16.6	15.8	66.5	1.11	0.29	2.41	0.94	0.37	1.97
1.5%Au/10%Co/SiO_2	5.8	0.647	16.3	16.6	65.8	1.16	0.13	1.89	0.73	0.28	1.90
2%Au/10%Co/SiO_2	5.9	0.658	16.5	16.1	65.4	1.17	0.14	1.66	0.31	0.11	1.96
5%Au/10%Co/SiO_2	6.1	0.681	16.2	16.6	65.2	1.48	0.13	1.57	0.32	0.10	1.96

a: percentage CO conversion; b: rate of CO consumption [µmol.(g_{cat}.s)$^{-1}$]; c: hydrocarbons selectivity based on CO moles converted, no CO_2 was measured; d: defined as percentage of CO converted to C_2H_6O

P=20bar; T=220°C; H_2/CO=2; SV=3NL/gCat/h

The increase in CO conversion with Au loading in the catalyst was due to an increase in surface Co^0 atoms as a result of an improvement of Co dispersion and catalyst reduction due to the presence Au particles in the catalyst. Early studies involving the addition of a noble metal to a supported Co catalyst have also reported a similar behaviour [8-11, 20, 21, 25, 37 - 40]. The change in methane and light product selectivity is usually explained by changes of hydrogen concentration on the catalyst surface.

Reasons explaining the changes in hydrogen concentration on catalyst surface include the water gas shift reaction on the unreduced cobalt oxides in the catalyst [1, 41] and hydrogen activation on a noble metal [10]. The unreduced cobalt oxides are not likely to explain the increase in methane selectivity on Au doped catalysts in this study because Au doped catalysts showed a better reducibility than the undoped catalyst, and therefore the highest methane selectivity would have been obtained on the undoped catalyst. Instead, an opposite trend was observed. However, the possibility of the water gas shift reaction catalysed by Au particles in the catalyst during the FT reaction can be considered to explain the observed trend. As shown in chapter 5 and 6 where $Au/Co/TiO_2$ and $Au/Co/Al_2O_3$ systems were respectively used as catalysts, the methane selectivity was influenced by the water gas shift reaction catalysed by Au particles in the catalyst. The observation was in agreement with a study by Andreeva et al.[42] who reported that Au/Co_3O_4 system was active for the water gas shift reaction under typical conditions for the FT reaction. The increase in methane and light product selectivity by hydrogen activation on Au is still uncertain as we could not establish, from the data in this study, the ability of Au to activate hydrogen.

Schulz et al.[43] have reported that FT Co catalysts undergo an in-situ reconstruction which is addressed as surface segregation through strong CO chemisorption. By this process a disproportionation of sites into sites of lower and higher coordination at the expense of plane sites takes place. They proposed that the chain growth is related to top sites (low coordination sites) and CO dissociation to sites of higher coordination. The remaining plane sites of the Co catalysts are widely poisoned through CO chemisorption, but are still available to some extent for minor reactions, such as olefin isomerisation, olefin hydrogenation and methane formation. Thus, it is proposed that the type of Au-Co interaction in Au doped Co catalysts can affect the process of self-organization on the catalyst surface and therefore alter the catalyst behaviour. The increase in methane selectivity in Au doped Co catalyst can also suggest that Au prevented the Co catalyst surface disproportionation to some extent and kept a high proportion of plane sites in the catalyst structure during the FT reaction. Similar behaviour was also observed by Zhang et al.[44] who measured an excessive methane formation on higher magnesia-modified cobalt catalysts. They also proposed that magnesia hindered the process of catalyst reassembling under FTS conditions.

Olefin selectivity is determined by the ability of α-olefins to readsorb on the catalyst surface and participate in the chain growth process. Iglesia et al.[45] had reported that the readsoption of olefins is high when the Co^0 site density is high. Also, Schulz et al. [46] have suggested that the olefin selectivity could be explained by the probability of olefins readsorption on the on-top (growth) sites. As discussed above, it is thought that an Au-Co interaction prevents Co surface reconstruction during the FT reaction,

thus leading to less growth sites in Au doped catalyst compared to the undoped catalyst. This suggests that the probability for olefins to readsorb on growth sites was higher on the undoped catalyst which consequently exhibited a lower olefin to paraffin ratio compared to the Au doped catalysts. On the other hand, the Co^0 density was shown to increase with an increase in Au loading in the catalyst suggesting that more olefins were readsorbed on Au doped catalysts. It is hence suggested that the trend of the olefin to paraffin ratio measured on different catalysts in the present study indicates that olefins readsorption is related to the number of the on-top sites in the catalyst. This depends on the Co reconstruction process during FT reaction and on the initial Co^0 density which is a function of Co dispersion and Co reduction extent in the catalyst.

7.4. Conclusion.

XRD and XPS analysis have revealed that most or all the Au added to the 10%Co/SiO_2 existed in metallic form after catalyst calcination in air. The metallic gold particles were located between cobalt oxides particles and the silica support. The location of Au particles and the type of Co oxide-Au interactions are thought to decrease the interaction of Co oxides with the silica support and can explain the improvement of the catalyst reduction with an increase in Au loading in the catalyst. The change in product selectivity after the addition of Au to the Co/SiO_2 is thought to be due to the Au catalyzed water gas shift reaction and to the Au induced changes in

Co surface reconstruction process during the FT reaction. The increase in CO conversion with an increase in Au loading in the catalyst was due to changes in Co^0 site density as a result of an improvement in Co oxides reduction and Co dispersion on the silica support.

References

1 A. Martínez, C. López, F. Márquez, and I. Díaz, *J. Catal*. 220 (2003) 486.

2 M.P. Rosynek, and C.A. Polansky, *Appl. Catal*. 73 (1991) 97.

3 T. Matsuzaki, K. Takeuchi, T. Hanaoka, H. Arakawa, Y. Sugi, *Catal. Today*. 28 (1996) 251.

4 S. Sun, N. Tsubaki, K. Fujimoto, *Appl. Catal. A*: General. 202 (2000) 121.

5 Y. Wang, M. Noguchi, Y. Takahashi, Y. Ohtsuka, *Catal. Today.* 68 (2001) 3.

6 J. Panpranot, S. Kaewkun, P. Praserthdam, and J.G. Goodwin Jr, *Cat. Lett*. 91 (2003) 95.

7 J.S. Girardon, A.S. Lermontov, L. Gengembre, P.A. Chernavskii, A. Griboval – Constant, A.Y. Khodakov, *J. Catal*. 230 (2005) 339.

8 K. Okabe, X. Li, T. Matsuzaki and H. Arakawa, *J. Sol-Gel. Sc. And Techn*. 19 (2000) 519-523.

9 G. Jacobs, T.K. Das, Y. Zhang, J. Li, G. Racoillet, B.H. Davis, *Appl. Catal. A*: General 233 (2002) 263.

10 S. Sun, K. Fujimoto, Y. Yoneyama, N. Tsubaki, *Fuel.* 81 (2002) 1583.

11 J.S. Girardon, A. Griboval – Constant, L. Gengembre, P.A. Chernavskii, A.Y. Khodakov, *Catal. Today*. 106 (2005) 161.

12 L. Leite, V. Stonkus, L. Ilieva, L. Plyasova, T. Tabakova, D. Andreeva, E. Lukevics, *Catal. Comm*. 3 (2002) 341.

13 D.B. Akolekar, S. K. Bhargava, *J. Mol. Catal. A*: Chem. 236 (2005) 77.

14 V.G. Pol, A. Gedanken, and J. Calderon-Moreno, *Chem. Mat*. 15 (2003) 1111.

15 Y. Okamoto, N. Hajime, T. Imanaka, S. Teranishi, *Bull. Chem. Soc. Jpn.* 48 (1975) 1163.

16 T.J. Chuang, C.R. Brundle, D.W. Rice, *Surf. Sci*. 59 (1976) 413.

17 W.J. Wang, Y.W. Chen, *Appl. Catal.* 77 (1991) 223.

18 R. Riva, H. Miessner, R. Vitali, G. Del Piero, *Appl. Catal. A*: General 196 (2000) 111.

19 L. Ji, J. Lin, and H.C. Zeng, *J. Phys. Chem. B* 104 (2000) 1783.

20 D. Schanke, S. Vada, E.A. Blekkan, A.M. Hilmen, A, Hoff, and A, Holmen, *J. Catal.* 156 (1995) 85.

21 A. Kogelbauer, J.G. Goodwin Jr, and R. Oukaci, *J. Catal.* 160 (1996) 125.

22 R. Oukachi, A.H. Singleton, J.G. Goodwin Jr, *Appl. Catal. A*: General 186 (1999) 129.

23 N. Tsubaki, S. Sun, and K. Fujimoto, *J. Catal.* 199 (2001) 236.

24 J. Li, G. Jacobs, Y. Quig., T. Das, B.H. Davis, *Appl. Catal. A*: General 223 (2002) 195.

25 S.A. Hosseini, A. Taeb, F. Feyzi, F. Yaripour*, Catal. Comm*. 5 (2004) 137.

26 S.A. Hosseini, A. Taeb, F. Feyzi, *Catal. Comm*. 6 (2005) 233.

27 D. Briggs and M.P. Seah, *Practical Surface Analysis*, 2nd Ed. (Ellis Horwood, Chichester, 1990).

28 A. Fernnadez, A. Caballero, A.R. Gonzalez-Elipe, J. M. Herrmann, H. Dexpert and F. Villain, *J. Phys. Chem*. 99 (1995) 3303.

29 T.M. Salama, T. Shido, H. Minagawa and M. Ichikawa, *J. Catal.* 152 (1995) 322.

30 Y.S. Su, M. Y. Lee and S.D. Lin, *Cat. Lett.* 57 (1999) 49.

31 B. Koslowski, H.G. Boyen, C. Wilderotter, G. Kastle, P. Ziemann, R. Wahrenberg, P. Oelhafen, *Surf. Sci.* 475 (2001) 1.

32 J.R. Mellor, A.N. Palazov, B.S. Grigorova, J.F. Greyling, K. Reddy, M.P. Letsoalo, J.H. Marsh, *Catal. Today.* 72 (2002) 145.

33 J. Garcia-Serrano, A.G. Galindo, U. Pal, *Solar En. Mat & Solar Cells* 82 (2004) 291.

34 A.M. Saib, M. Claeys, E. van Steen, *Catal. Today*. 71 (2002) 395.

35 T. Matsuzaki, K. Takeuchi, T. Hanaoka, H. Arawaka and Y. Sugi, *Appl. Catal. A*: General 105 (1993) 159.

36 T. Matsuzaki, T. Hanaoka, K. Takeuchi, H. Arakawa, Y. Sugi, K. Wei, T. Dong, M. Reinikainen, *Catal. Today.* 36 (1997) 311.

37 T.K. Das, G. Jacobs, P.M. Patterson, W.A. Conner, J. Li, B.H. Davis, *Fuel.* 82 (2003) 805.

38 G. Jacobs, J.A. Chaney, P.M. Patterson, T.K. Das, B.H. Davis, *Appl. Catal. A*: General 264 (2004) 203.

39 J. Li, X. Zhan, Y. Zhang, G. Jacobs, T. Das, B.H. Davis, *Appl. Catal. A*: General 228 (2002) 203.

40 G. Jacobs, P.M. Patterson, Y. Zhang, T. Das, J. Li, B.H. Davis, *Appl. Catal. A*: General 233 (2002) 215.

41 R.C. Reuel, C.H. Bartholomew, *J. Catal*. 85 (1984) 78.

42 D. Andreeva, V. Idakiev, T. Tabakova, R. Giovanoli, *Bulg. Chem. Comm*. 30 (1998c) 59.

43 H. Schulz, Z. Nie, F. Ousmanov, *Catal. Today.* 71 (2002) 351.

44 Y. Zhang, H. Xiong, K. Liew, J. Li, *J. Mol. Catal. A*: Chem. 237 (2005) 172.

45 E. Iglesia, S.L. Soled, R.A. Fiato, G.H. Via, *Stud. Surf. Sci. Catal*. 81 (1994) 433.

46 H.Schulz, M. Claeys, *Appl. Catal*. 186 (1999) 91.

Chapter 8

Conclusions

The main objectives of this study were to: (i) evaluate the effect of ethanol on the product selectivity and activity of a titania supported Co catalyst during the FT reaction; (ii) study the effect that could originate from varying the cobalt carboxylate chain length during FT catalyst preparation and (iii) evaluate the effect of Au addition on the structure of a cobalt catalyst supported on titania, alumina and silica respectively. The outcomes of the study are:

1. Ethanol addition (2 and 6%) during the FT reaction over 10%Co/TiO_2 catalyst was found to decrease the catalyst activity and to increase the selectivity to methane and light hydrocarbons. An increase in the light olefin to paraffin ratio was also observed. The effect of ethanol on the catalyst activity was explained by the oxidation of surface Co metal to CoO by ethanol as predicted by thermodynamic calculations and further confirmed by TPR and XRD studies. TPR and XRD studies also revealed that the Co oxidation by ethanol was fast and that the resulting CoO species were easy to reduce. For low conversion runs the catalyst almost recovered its initial performance after the ethanol was switched off from the feed. This was explained by the reduction of the easy to reduce CoO species which resulted from the oxidation of Co by ethanol. The decrease in catalyst activity on ethanol addition was accompanied by an increase in methane selectivity. This suggested that methane selectivity related to the oxidation of

cobalt metal to cobalt oxide species. Some runs, where only ethanol (in nitrogen) was passed on the Co FT catalyst, revealed that ethanol was transformed to some FT products. Thus, the change in product selectivity for runs where ethanol was added to the synthesis gas was a result of changes in the catalyst surface as well as ethanol transformation reactions on the cobalt FT catalyst. The effect of ethanol addition during the FT reaction over Co/TiO_2 was the opposite of the water effect that was discussed in earlier reports. Thus, the effect of the addition of an oxygen containing compound to the feed for the FT reaction depends on the ability of the additive to oxidize cobalt under reaction conditions.

2. The effect of cobalt carboxylate chain length on catalyst preparation was found to depend on the cobalt loading in the catalyst. For low loaded catalysts (10 wt.% Co), the catalyst activity increased after increasing the chain length. Co carboxylates with longer chains led to bigger Co particles, as determined by XRD and H_2 chemisorption studies combined with O_2 titration. These catalysts presented a high extent of reduction and a low metal-support interaction. At higher cobalt contents, the catalyst prepared from the shortest chain length became the most active. The precursor chain length was found to influence the final cobalt particle sizes in the catalyst which in turn influenced the catalyst performance for the FT reaction. The measured Turn Over Frequencies (TOF) were comparable for all the catalysts and the changes in catalyst activities were explained by changes in active site densities as a function of Co reduction extent and dispersion. The olefin to paraffin ratio was almost unchanged for all the

catalysts. The methane selectivity was higher on poorly reduced catalysts, thus suggesting that methane selectivity related to the presence of cobalt oxide species. It was also found interesting to compare the performance of the 10%Co/Al_2O_3 catalysts prepared from Co carboxylates (Table 4.3) with the cobalt nitrate derived 10%Co/Al_2O_3 (Table 6.3). The results are presented in the Table 8.1 below.

Table 8.1 Comparison of 10%Co/Al_2O_3 catalysts derived from Co carboxylates and Co nitrate

Catalyst	CO conv. rate [$\mu mol.(g_{cat}.s)^{-1}$]	CH_4 selectivity [%]	C_{5+} selectivity [%]
Co10-2Al	0.007	60	3
Co10-5Al	0.067	16	64
Co10-9Al	0.077	14	69
*10%Co/Al_2O_3	0.290	11	80

*10%Co/Al_2O_3 prepared using Co nitrate

The catalyst prepared from Co nitrate with the same cobalt loading level (10% Co) as those derived from cobalt carboxylates showed a better performance for the FT reaction as it exhibited a far better activity, lower methane selectivity and a higher selectivity to longer chain products. An unumbigous explanation of this observation was not obvious as the difference in precursor type was coupled with differences in catalyst preparation methods, properties of the support used, operating conditions and type of reactors used for the Co carboxylates and Co nitrate derived catalysts.

3. Most of the Au that was added to supported Co catalysts (titania, alumina, silica supported Co catalysts) existed in metallic form after catalyst calcination as confirmed by XRD and XPS analysis. XPS analysis also showed that most of the Au particles in the calcined supported Co catalysts were located between cobalt oxides species and the support. An improvement in Co reduction was observed by adding Au to the supported Co catalyst. This was explained by a direct contact between Co and Au in the catalyst. The addition of Au also led to a significant improvement of Co dispersion on titania and silica supports. Only a minor effect on Co dispersion on alumina was observed when Au was added to the alumina supported cobalt catalyst. The titania supported catalyst revealed that the activity increased with an increase in Au loading in the catalyst and passed through a maximum around 1 wt.% Au loading. The increase in catalyst activity after the addition of Au to the catalyst was explained by the improvement of catalyst dispersion. However addition of Au above 1 wt.% was believed to negatively

affect the reconstruction phases on the catalyst surface during the early stage of the FT reaction. For silica and alumina supported catalysts the catalyst activity significantly increased after the addition of Au up to 1.5 wt.%.. Further increase in Au led to small increases in catalyst activity. Thus, Au loadings between 1 and 1.5wt.% can be recommended for addition to Co supported catalysts.

The methane selectivity was found to increase after the addition of Au to supported catalysts. This was mainly explained by an Au catalysed water-gas-shift reaction taking place during the FT reaction over Au doped supported Co catalysts. This effect was even more significant on titania supported catalysts. On an Au doped alumina supported Co catalyst, the methane selectivity passed through a maximum at around 0.7 wt.% Au. This maximum in methane selectivity was explained by two parameters which had two opposite effects on methane selectivity: (i) the extent of the WGS reaction which increased with an increase in Au loading in the catalyst and which led to an increase in the local H_2/CO ratio on the catalyst surface and (ii) the CO conversion which increased after Au addition to the catalyst and which led to a decrease of the H_2/CO ratio in the reactor, hence decreasing the methane selectivity.

Au doped silica supported Co catalysts produced the highest selectivity for ethanol. This was explained by the presence of highly dispersed Co metal in these catalysts.

This effect of Au addition was found to be dependent of the type of support used.

Table 8.2 shows the FT activities as well as the methane selectivities of the three supports used, titania, alumina and silica, containing 10% Co, with zero Au as well as the "best case" of each class promoted with Au.

Table 8.2 Comparison of zero Au 10%Co and "best case" of Au 10%Co supported on the three different supports, titania, alumina and silica

Catalyst	[a]Rate of CO converted to hydrocarbons [$\mu mol.(g_{cat}.s)^{-1}$]	[b]CH_4 selectivity [%]
Zero Au		
10%Co/TiO_2	1.262	12
10%Co/Al_2O_3	0.258	11
10%Co/SiO_2	0.165	8
"best case"		
1%Au/10%Co/TiO_2	1.915	18
1.5%Au/10%Co/Al_2O_3	1.452	11
1.5%Au/10%Co/SiO_2	0.534	16

a: calculated as rate of CO conversion – rate of CH_4 formation - rate of CO_2 formation – rate of C_2H_6O formation; b: selectivity based on (CO + CO_2) consumed

The "best case" represented the Au loading above which further increase in Au loading did not result in significant increase in FT products formation rate.

The results presented in table 8.2 showed a clear relationship between the FT activity and the surface area of the supports (TiO_2 = 50 m^2g^{-1}; Al_2O_3 = 150 m^2g^{-1}; SiO_2 = 300 m^2g^{-1}) used for both, the zero Au cases as well as for the best case class of Au promoted 10%Co catalysts. While no overall relationship between methane selectivity and support surface area was evident, the FT activities were found to decrease with an increase in support surface area. Figure 8.1 shows XRD patterns of unpromoted 10%Co on the three different supports. No diffraction peak for Co oxides was detected on the highest surface area support (SiO_2) but Co oxides diffraction peaks were detected on lower surface area supports (TiO_2 and Al_2O_3 around 2 theta = 31° and 57°). This suggested the formation of smaller (more dispersed) Co oxides particles on high surface area supports. Also TPR profiles for unpromoted 10%Co on the three different supports (Figure 8.2) showed better reduction behaviour for Co oxide species on the low surface area support (TiO_2) compared to those supported on Al_2O_3 and SiO_2. This suggests that the low FT activity measured on 10%Co catalysts on high surface area support was due to the formation of highly dispersed and difficult to reduce cobalt oxide species.

The effect of the addition of Au to supported Co catalysts was found to be similar to the effect of other noble metals like Ru, Re and Pt as they also improved the catalyst reducibility and dispersion resulting in more active sites. The negative effect of the addition of Au is the increase in methane selectivity due to the water gas shift reaction that is catalysed by Au particles. However, this increase in

methane selectivity with the increase in Au loading can be overcome by choosing a support on which the addition of Au can significantly increase the Co catalyst activity.

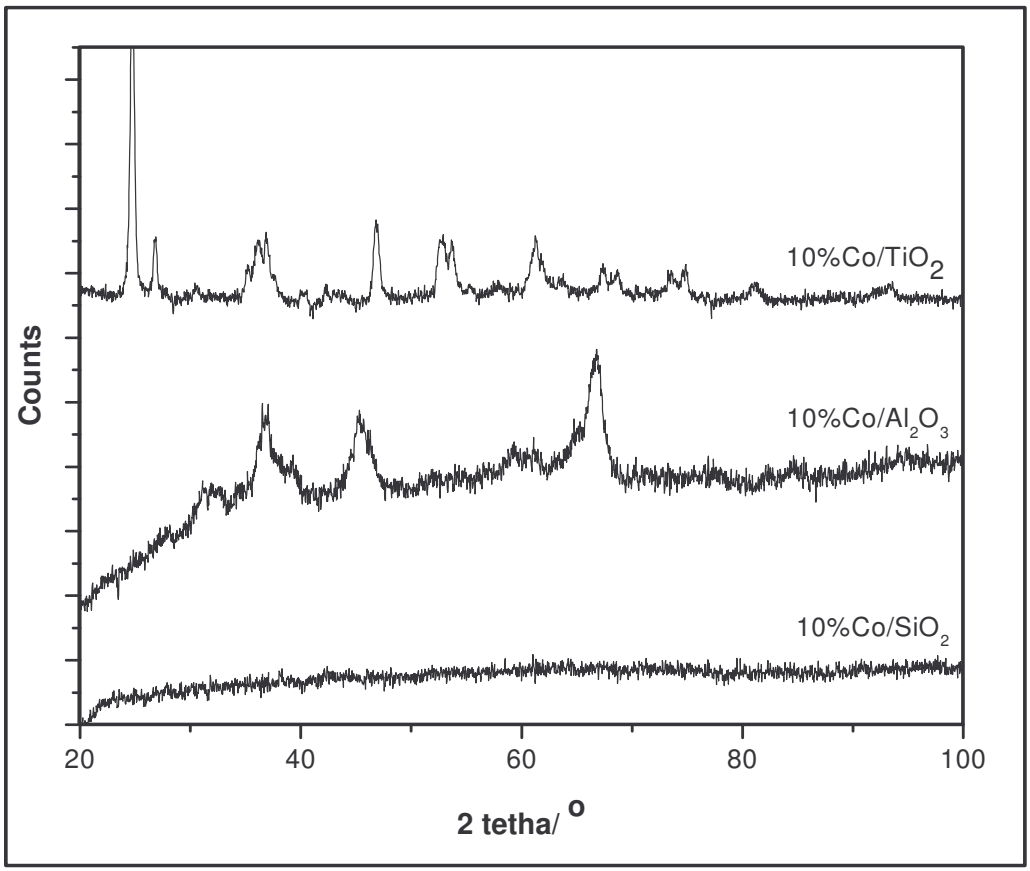

Figure 8.1 *XRD patterns for unpromoted 10%Co on the three different supports: TiO_2, Al_2O_3 and SiO_2.*

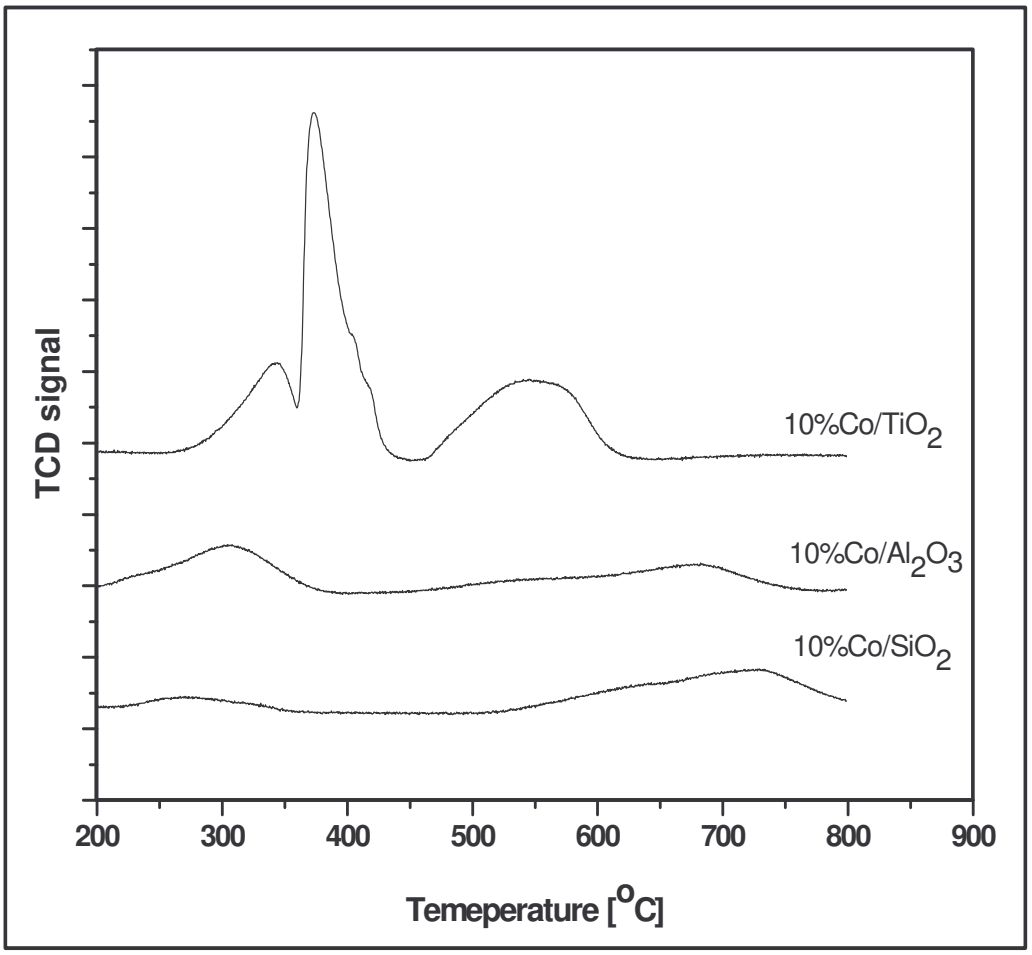

Figure 8.2 *TPR profiles for unpromoted 10%Co on the three different supports: TiO_2, Al_2O_3 and SiO_2.*

In this study the most significant effect of Au addition on the catalyst activity was found on alumina supported Co catalyst where the maximum conversion (on 5%Au/10%Co/Al_2O_3) was more than six times higher compared to the activity of the undoped catalyst (10%Co/Al_2O_3). The increase in CO conversion had a significant impact in decreasing the methane selectivity compared to the opposite contribution effect from the WGS on the methane selectivity.

APPENDIX

EQUILIBRIUM CONDITIONS FOR COBALT OXIDATION BY ETHANOL AND WATER

Figure A1 shows the equilibrium conditions for the cobalt oxidation by water. At typical FT reaction temperatures (200ºC - 300ºC), a hydrogen to water partial pressures ratio around 8/1000, i.e. (P_{H2}/P_{H2O} = 8/1000 or ln (P_{H2}/P_{H2O}) = -4.8) is required for the oxidation of bulk cobalt metal by water to be thermodynamically possible. The above requirement (P_{H2}/P_{H2O} = 8/1000) suggests the addition of a very large amount of water compared to reactants (H_2 and CO). The feed would essentially be water; these conditions are not practical in the FT reaction.

Figure A2 shows the equilibrium conditions for cobalt oxidation by ethanol.

Figure A1

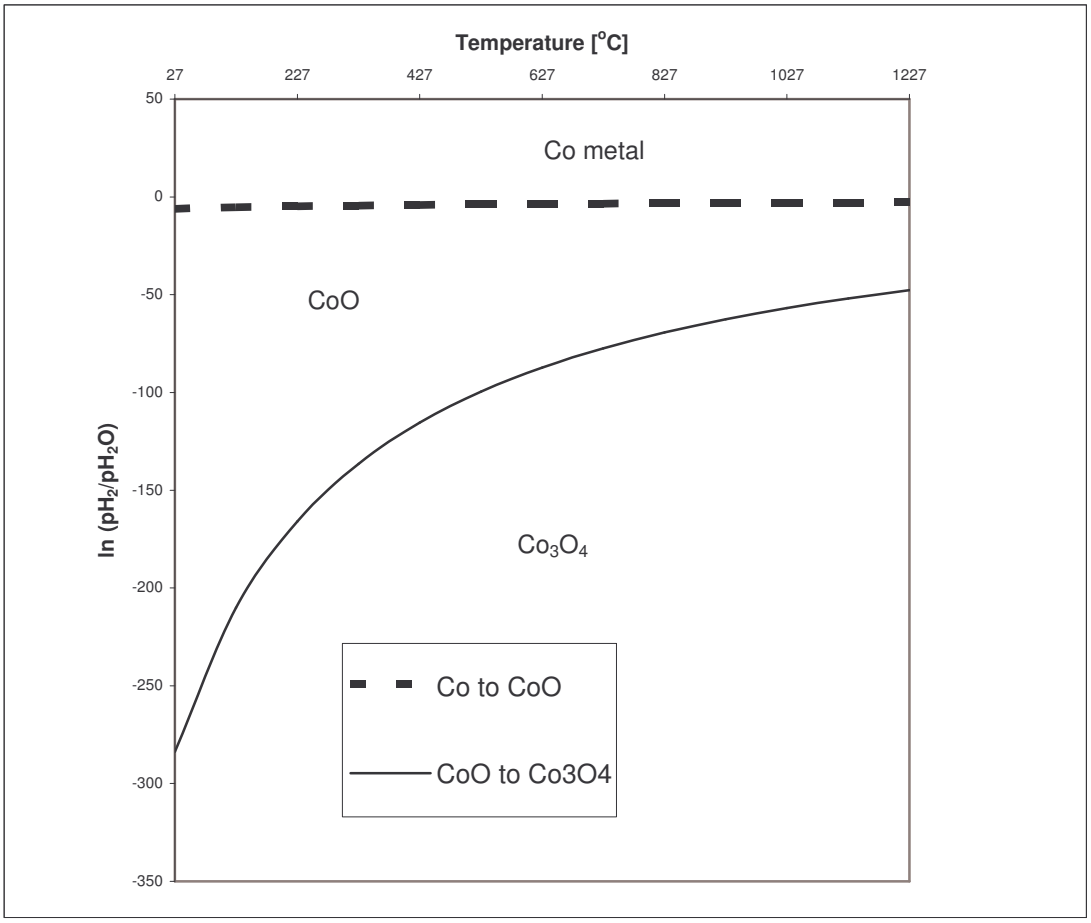
Temperature [°C]
27
227
427
627
827
1027
1227
50
0
-50
-100
-150
-200
-250
-300
-350
ln (pH2/pH2O)
Co metal
CoO
Co3O4
Co to CoO
CoO to Co3O4

Figure A2

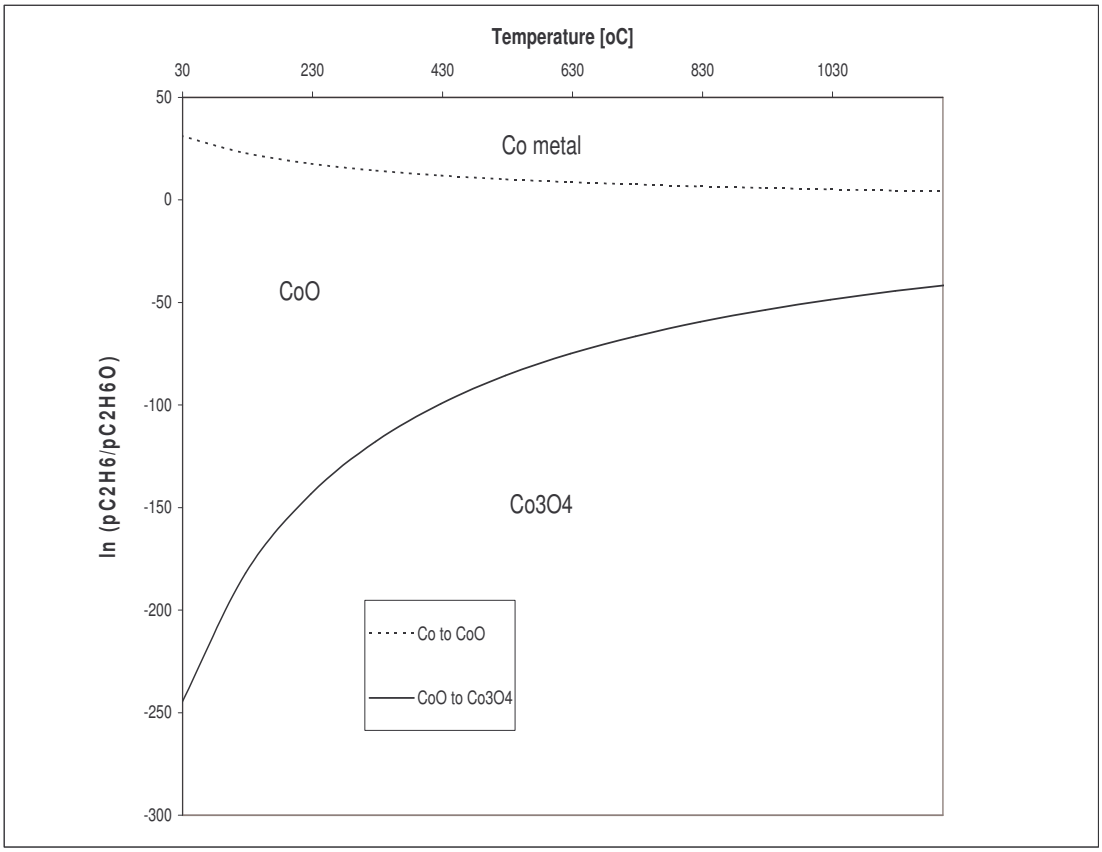
Temperature [oC]
30
230
430
630
830
1030
50
0
-50
-100
-150
-200
-250
-300
ln (pC2H6/pC2H6O)
Co metal
CoO
Co3O4
Co to CoO
CoO to Co3O4